

**GENOMIC, PHYSIOLOGIC, AND KINETIC INVESTIGATIONS
OF MARINE IRON-OXIDIZING BACTERIA**

by

Beverly K. Chiu

A thesis submitted to the Faculty of the University of Delaware in partial fulfillment
of the requirements for the degree of Master of Science in Geological Sciences

Summer 2017

© 2017 Beverly K. Chiu
All Rights Reserved

**GENOMIC, PHYSIOLOGIC, AND KINETIC INVESTIGATIONS
OF MARINE IRON-OXIDIZING BACTERIA**

by

Beverly K. Chiu

Approved: _____
Clara Chan, Ph.D.
Professor in charge of thesis on behalf of the Advisory Committee

Approved: _____
Neil Sturchio, Ph.D.
Chair of the Department of Geological Sciences

Approved: _____
Mohsen Badiy, Ph.D.
Acting Dean of the College of Earth, Ocean, and Environment

Approved: _____
Ann L. Ardis, Ph.D.
Senior Vice Provost for Graduate and Professional Education

ACKNOWLEDGMENTS

Thank you to my advisor Dr. Clara Chan for all of the guidance and opportunities that you've provided me these past two years. As your student, I've learned so much and gained invaluable skills, which have shaped me into a better scientist. Thank you to all of my fellow Chan Lab members past and present, whose expertise, assistance, and humor have helped me through this journey. Thank you to my committee members Dr. Jennifer Biddle and Dr. George Luther, whose knowledge and support helped me to refine my work, and to all members of AT37-11 for a successful and unforgettable cruise.

Thank you to my awesome parents and brother who have been there every step of the way. And finally, to all of the brilliant friends I've made here, thanks for sharing in the laughs and Pizza Today.

My research would not have been possible without NASA Exobiology Program Grant NNX12AG20G, NSF CAREER Geobiology grant EAR-1151682, and NSF Marine Geology and Geophysics OCE-1558712.

TABLE OF CONTENTS

LIST OF TABLES	vii
LIST OF FIGURES	ix
ABSTRACT	xi

Chapter

1	INTRODUCTION	1
2	NOVEL PELAGIC IRON-OXIDIZING ZETAPROTEOBACTERIA FROM THE CHESAPEAKE BAY OXIC-ANOXIC TRANSITION ZONE ...	5
2.1	Introduction	5
2.2	Materials and Methods	8
2.2.1	Sampling, Enrichments, and Isolation	8
2.2.2	Physiological Characterization	9
2.2.3	Microscopy	10
2.2.4	Genome Sequencing and Analysis	11
2.2.5	16S rRNA Gene Analysis	12
2.2.6	Genome Accession Numbers and Culture Availability	13
2.3	Results and Discussion	13
2.3.1	Isolation and Physiological Characterization	13
2.3.2	Phylogenetic Analyses	17
2.3.3	Iron Oxyhydroxide Biomineral Morphology	20
2.3.4	General Genome Features of Strains CP-5 and CP-8	23
2.3.5	Electron Transport Chain Analysis	24
2.3.6	Carbon Metabolism Analysis	28
2.3.7	Unusual Genomic Features for Biofilm Formation	29
2.3.8	Adaptations of Pelagic Zetaproteobacteria in Estuarine Water Columns	33
2.4	Species Descriptions	36
2.4.1	Description of <i>Mariprofundus aestuarium</i> sp. nov.	36
2.4.2	Description of <i>Mariprofundus ferrinatatus</i> sp. nov.	36

3	FE OXIDATION KINETICS OF ZETAPROTEOBACTERIUM <i>MARIPROFUNDUS FERRINATATUS</i> CP-8.....	38
3.1	Introduction	38
3.2	Materials and Methods	39
3.2.1	Fe(II) Oxidation Kinetics Experiments	39
3.2.1.1	Ferrozine Assay	42
3.2.1.2	Calculating Pseudo First-order Rate Constants (k_1)	42
3.2.2	Fe(II) Oxidation Rates From the Strain CP-8 Growth Curve.....	43
3.3	Results and Discussion	44
3.3.1	Fe(II) Oxidation Kinetics Experiments	44
3.3.2	Fe(II) Oxidation Rates From the Strain CP-8 Growth Curve.....	48
3.4	Conclusions	49
4	EAST PACIFIC RISE CRUISE ACTIVITIES	50
4.1	Introduction	50
4.2	Materials and Methods	52
4.2.1	Sample Collection at East Pacific Rise	52
4.2.2	Rusty <i>Riftia</i> Tubes, Rocks, Flocculent Mats, and Seawater Samples.....	55
4.2.2.1	Biomass Concentration and Preservation	55
4.2.2.2	FeOB Enrichment Culturing.....	57
4.2.2.3	Fe Measurements of Slurp Seawater and Flocculent Mat Slurp	58
4.2.3	<i>Riftia</i> Endosymbionts	59
4.2.3.1	<i>Riftia</i> Endosymbiont Purification and Preservation	59
4.2.3.2	FeOB Enrichment Culturing with Purified <i>Riftia</i> Endosymbionts	60
4.2.3.3	Fe(II) Oxidation and Expression Experiment.....	61
4.3	Results and Discussion	63
4.3.1	Rusty <i>Riftia</i> Tubes, Rocks, Flocculent Mats, and Seawater Samples.....	63

4.3.1.1	Biomass Concentration and Preservation	63
4.3.1.2	FeOB Enrichment Culturing.....	65
4.3.1.3	Fe Measurements of Slurp Seawater and Flocculent Mat Slurp	67
4.3.2	<i>Riftia</i> Endosymbionts	67
4.3.2.1	<i>Riftia</i> Endosymbiont Purification and Preservation	67
4.3.2.2	FeOB Enrichment Culturing with Purified <i>Riftia</i> Endosymbionts	69
4.3.2.3	Fe(II) Oxidation and Expression Experiment.....	72
4.4	Conclusions	73
REFERENCES		75
Appendix		
A	SUPPLEMENTARY MATERIAL FOR NOVEL PLANKTONIC IRON- OXIDIZING ZETAPROTEOBACTERIA FROM THE CHESAPEAKE BAY OXIC-ANOXIC TRANSITION ZONE	87
B	SUPPLEMENTARY MATERIAL FOR EAST PACIFIC RISE REPORT	99
B.1	Methods for Trial Fe(II) Oxidation and Expression Experiment with Purified <i>Riftia</i> Endosymbionts	99

LIST OF TABLES

Table 2.1:	Summary of strains CP-5 and CP-8 genomic and physiological characteristics in comparison to other selected Zetaproteobacteria.	16
Table 2.2:	Source environment, 16S rRNA gene similarity, ANI, and AAI comparisons of strains CP-5 and CP-8 to other Zetaproteobacteria.	19
Table 3.1:	Summary of CP-8 kinetics experimental conditions and results. O ₂ , pH, and temperatures are average values of each run.	46
Table 3.2:	Comparison of CP-8 Fe(II) oxidation kinetics data to other neutrophilic FeOB.	47
Table 4.1:	Summary of samples collected and processed from the EPR.	54
Table 4.2:	Summary of preserved biomass subsamples by sample name.	64
Table 4.3:	Number of subsamples preserved from dissected <i>Riftia</i> samples..	68
Table 4.4:	Numbers of preserved subsamples of <i>Riftia</i> endosymbiont enrichment floc biomass.....	72
Table A1:	Geochemical parameters of the Chesapeake Bay water samples from which strains CP-5 and CP-8 were isolated.	91
Table A2:	Comparison of Zetaproteobacteria genome features.....	91
Table A3:	Electron transport genes in the CP strain genomes.	92
Table A4:	Carbon-related genes in the CP strain genomes.....	95
Table A5:	Wsp system subunits in the CP strain genomes.	98
Table A6:	WCI genes in the CP strain genomes.	98
Table B1:	Sample Log of all samples retrieved by Alvin on cruise AT37-11 with selected metadata displayed.	100

Table B2:	Subsample Log of all subsamples preserved for future analyses with selected metadata displayed.	103
Table B3:	Enrichment Log of all enrichments performed aboard the cruise with selected metadata displayed.	108

LIST OF FIGURES

Figure 2.1:	CP strain gradient tube cultures with FeCO ₃ plugs and fluorescence micrographs of CP-5 and CP-8 cells.	14
Figure 2.2:	Strain CP-5 and CP-8 growth curves and corresponding total Fe curves including abiotic controls.....	15
Figure 2.3:	16S rRNA gene phylogenetic tree of <i>Mariprofundus ferrinatatus</i> CP-8 and <i>Mariprofundus aestuarium</i> CP-5 and other Zetaproteobacteria.....	18
Figure 2.4:	CP strain cell and biomineral micrographs.	22
Figure 2.5:	Scanning electron micrograph of extracellular iron oxide biomineral structures.	23
Figure 2.6:	Proposed electron transport system in strains CP-5 and CP-8 based on genomic analysis..	25
Figure 2.7:	The Wsp operon and WCI genes in strains CP-5 and CP-8.....	30
Figure 2.8:	Model of CP strain floc formation and interactions with Fe/S biogeochemical cycling in redox-stratified waters.....	35
Figure 3.1:	Reaction vessel used for strain CP-8 kinetics experiments.	41
Figure 3.2:	Plots of CP-8 kinetics experiment data at 5 and 15 μM O ₂	45
Figure 4.1:	Site map of EPR at 9°N and examples of the sample types collected....	53
Figure 4.2:	Orange paste-like material with a goopy texture caught on the slurp container filter in flocculent_mat_slurp2 and flocculent_mat_slurp5. ...	57
Figure 4.3:	Homogenized <i>Riftia</i> trophosome before and after Percoll centrifugation.....	60
Figure 4.4:	Fe oxidation and expression experiment samples..	63
Figure 4.5:	Corresponding phase and bright-field micrographs of Flocculent_mat_slurp5 displaying a tubular sheath-like structure and a twisted stalk-like structure.....	65

Figure 4.6: Hazy white material overlying the black FeS layers in liquid gradient tubes inoculated with Flocculent_mat_slurp4.....	67
Figure 4.7: Time series of fast floc development in liquid enrichment plate cultures inoculated with purified endosymbionts from Riftia5.	70
Figure 4.8: Time series of slow floc development in liquid enrichment plate cultures inoculated with purified endosymbionts from Riftia8.....	71
Figure 4.9: Plot showing that duplicate biotic samples inoculated with purified Riftia8 endosymbionts accelerated Fe(II) oxidation in comparison to the uninoculated abiotic control	73
Figure A1: 16S rRNA gene maximum likelihood phylogenetic tree showing that the CP strains cluster with sequences from the original Chesapeake Bay FeOB enrichment.	88
Figure A2: EDX analyses of abiotic iron oxides and CP strain dreads confirming iron content.....	89
Figure A3: Scanning electron micrographs of iron oxides from strain CP-5, CP-8, and abiotic control cultures.	90
Figure A4: Transmission electron micrographs of iron oxides from strain CP-5, CP-8, and abiotic control cultures..	90

ABSTRACT

The Zetaproteobacteria are a widespread class of marine iron-oxidizing bacteria (FeOB). Although Zetaproteobacteria inhabit a wide range of environmental settings such as coastal sediment, deep-sea hydrothermal vents, and more recently, stratified water columns, little is known about the adaptations enabling Zetaproteobacteria to inhabit each of these niches. Additionally, the metabolic potential of Zetaproteobacteria has not been well quantified, making it difficult to assess their contributions to environmental Fe-cycling. Here we describe the isolation, characterization, and genomes of two new species from the Chesapeake Bay, *Mariprofundus aestuarius* CP-5 and *Mariprofundus ferrinatatus* CP-8, which are the first Zetaproteobacteria isolated from a pelagic environment. We looked for physiologic and genomic differences between the CP strains and benthic or subsurface Zetaproteobacteria to identify adaptations enabling strains CP-5 and CP-8 to overcome the challenges of living in a low Fe redoxcline with frequent O₂ fluctuations due to tidal mixing. We found that the CP strains produce distinctive dreadlock-like Fe oxyhydroxide structures that are easily shed, which would help cells maintain suspension in the water column. The CP strains also have two gene clusters associated with biofilm formation (Wsp system and the Widespread Colonization Island) that are absent or rare in other Zetaproteobacteria. We propose that biofilm formation enables the CP strains to attach to FeS particles and form flocs, an advantageous strategy for scavenging Fe(II) and developing low [O₂] microenvironments within more oxygenated waters. Besides identifying these adaptations, we measured strain CP-8

Fe(II) oxidation kinetics and show that strain CP-8 is capable of accelerating Fe(II) oxidation compared to abiotic processes alone at low (micromolar) [O₂].

In addition to our work with Chesapeake Bay Zetaproteobacteria, we investigated FeOB at the East Pacific Rise (EPR). To identify Zetaproteobacteria at the EPR, we collected rust-colored *Riftia* tubes, rocks, and mats for FeOB enrichments and future metagenomic analyses. We also sought to examine the Fe(II) oxidation potential of EPR tubeworm endosymbionts that belong to the Gammaproteobacteria, but possess the putative Fe(II) oxidase, *Cyc2*. We purified *Riftia* endosymbionts to attempt FeOB enrichments and Fe(II) oxidation experiments, and our preliminary results suggest that these endosymbionts may be capable of oxidizing Fe(II). Together, our results provide insight on the Zetaproteobacteria living in different environmental settings, reveal niche-specific adaptations for Zetaproteobacteria to inhabit pelagic settings, and suggest other marine bacteria that may be capable of oxidizing Fe(II).

Chapter 1

INTRODUCTION

Neutrophilic iron-oxidizing bacteria (FeOB) live at circumneutral pH, oxidizing Fe(II) to Fe(III) for energy and precipitating Fe oxyhydroxide structures as a byproduct. Some FeOB are known for producing distinctive morphologies of Fe biominerals, including tubular sheaths (van Veen *et al.*, 1978; Emerson and Revsbech, 1994; Fleming *et al.*, 2013) and twisted stalks (Vatter and Wolfe, 1956; Emerson *et al.*, 2007; Chan *et al.*, 2011; Krepski *et al.*, 2012). These elongated Fe oxyhydroxide structures serve as holdfasts and provide the framework for FeOB to form Fe mats and colonize surfaces. These Fe mats are advantageous for neutrophilic FeOB, enabling them to grow toward or maintain a position at Fe(II)/O₂ interfaces where they are known to thrive (Chan *et al.*, 2016). These interfaces are favorable geochemical niches for neutrophilic FeOB because [O₂] is low, allowing FeOB to efficiently compete with abiotic Fe(II) oxidation that quickly consumes Fe(II) at higher [O₂] (Emerson and Revsbech, 1994; James and Ferris, 2004; Singer and Stum, 1970).

The known neutrophilic obligate chemolithotrophic FeOB belong to two classes: the Betaproteobacteria, associated with terrestrial and freshwater environments, and the Zetaproteobacteria, associated with coastal and marine environments. Here we focus investigations on FeOB of the Zetaproteobacteria class. A large portion of our knowledge of Zetaproteobacteria comes from culture-independent studies (Kato *et al.*, 2009; McAllister *et al.*, 2011; Singer *et al.*, 2013; Field *et al.*, 2014) because there are relatively few isolates available. The

Zetaproteobacteria isolates that do exist (e.g., *Mariprofundus ferrooxydans* PV-1, *Mariprofundus micogutta* ET2, *Ghiorsea bivora* TAG-1) are all from benthic or subsurface habitats (Emerson and Moyer, 2002; Makita *et al.*, 2016; Mori *et al.*, in review), but not redox-stratified water columns. This may be due to the challenges that a pelagic lifestyle would pose for Zetaproteobacteria, given low Fe(II) concentrations in modern marine waters and the possibility that Fe oxyhydroxide biominerals could cause cells to sink. However, we have cultivated Zetaproteobacteria from the Chesapeake Bay oxic-anoxic transition zone (MacDonald *et al.*, 2014; Field *et al.*, 2016), suggesting that they can survive and contribute to biogeochemical cycling in a stratified estuary. In Chapter 2, we introduce two new species isolated from the Chesapeake Bay, *Mariprofundus aestuarium* CP-5 and *Mariprofundus ferrinatatus* CP-8, which are the first two pelagic Zetaproteobacteria isolated from a redox-stratified water column. We analyze their physiologic and genomic traits to identify potential adaptations enabling Zetaproteobacteria to survive in the water column.

FeOB isolates are also useful for measuring microbial Fe(II) oxidation rates to quantify FeOB contributions to Fe-cycling. Unlike kinetics studies of environmental FeOB performed in situ, laboratory experiments with FeOB isolates enable control over key geochemical variables that affect Fe(II) oxidation kinetics such as [O₂]. Understanding the relationship between microbial Fe(II) oxidation kinetics and [O₂] provides a measure of how quickly FeOB can oxidize Fe(II) under a given [O₂], which helps us infer the overall impact FeOB have on Fe-cycling. However, only one study (Druschel *et al.*, 2008) has measured the change in microbial Fe(II) oxidation rates by Betaproteobacterium *Sideroxydans lithotrophicus* ES-1 as a function of [O₂]. ES-1 oxidized Fe(II) faster than abiotic Fe(II) oxidation between ~3-50 μM O₂, with fastest

microbial Fe(II) oxidation rates measured at 25 μM O_2 (Druschel *et al.*, 2008). This study provides $[\text{O}_2]$ boundaries for identifying potential environments where ES-1 could be expected and suggests an optimal $[\text{O}_2]$ at which ES-1 can oxidize Fe(II) the fastest. Similar kinetics studies with Zetaproteobacteria have yet to be conducted, but would provide insights into where and how much FeOB can be expected to contribute to marine Fe-cycling. In Chapter 3, I present Fe(II) oxidation kinetics experiments with *M. ferrinatatus* CP-8 at 5 and 10 μM O_2 to begin understanding the effect of varying $[\text{O}_2]$ on Fe(II) oxidation rates of Zetaproteobacteria.

Although neutrophilic microbial Fe(II) oxidation is well documented, the molecular mechanism for this metabolism is still unclear. Cyc2 is an outer membrane cytochrome that has been proven to oxidize Fe(II) in the acidophilic FeOB *Acidithiobacillus ferrooxidans* (Castelle *et al.*, 2008), and is considered as a putative Fe oxidase for neutrophilic FeOB as well. The putative function of Cyc2 in neutrophilic FeOB is supported by its high expression in *M. ferrooxydans* PV-1 (Barco *et al.*, 2015) and its consistent presence in all known neutrophilic FeOB genomes (Chapter 2.3.5; Kato *et al.*, 2015; Mumford *et al.*, 2016). Besides Betaproteobacteria and Zetaproteobacteria, homologs of *cyc2* are also found in Gammaproteobacteria, including the metagenomes of endosymbionts of hydrothermal tubeworms *Riftia pachyptila* and *Tevnia jerichonana* (Gardebrecht *et al.*, 2012). Given the opportunity to participate in a cruise to the East Pacific Rise (EPR; Cruise AT37-11, March-April, 2017), I attempt to test whether the possession of *cyc2* confers Fe(II) oxidation abilities to *Riftia* endosymbionts, described in Chapter 4. I also describe the collection of samples intended for future analyses of the potential Zetaproteobacteria community at the EPR.

In sum, I present genomic and physiologic adaptations for Zetaproteobacteria to inhabit pelagic environments, attempt to quantify the rates of Zetaproteobacteria Fe(II) oxidation at various [O₂] concentrations, and begin to explore whether the putative Fe oxidase gene, *cyc2*, confers Fe(II) oxidation abilities to Gammaproteobacteria at the EPR.

Chapter 2

NOVEL PELAGIC IRON-OXIDIZING ZETAPROTEOBACTERIA FROM THE CHESAPEAKE BAY OXIC-ANOXIC TRANSITION ZONE

This chapter contains a manuscript accepted for publication by *Frontiers in Microbiology*. Beverly Chiu is the first author of this manuscript, and she completed the majority of the analyses and writing except as follows: Dr. Shingo Kato isolated strains CP-5 and CP-8, performed microscopy and physiological growth tests (excluding growth curves), prepared the strains for sequencing, and wrote corresponding results for the manuscript. Sean McAllister helped plan and prepare DNA for sequencing, performed genome quality control, and performed phylogenetic analyses. Dr. Erin Field initiated and advised genomic analysis. Dr. Clara Chan contributed to genome analysis and the writing of this paper. The complete list of authors on this manuscript is as follows: Beverly K. Chiu, Shingo Kato (Japan Agency for Marine-Earth Science and Technology), Sean M. McAllister (University of Delaware), Erin K. Field (East Carolina University), and Clara S. Chan (University of Delaware).

2.1 Introduction

Chemolithotrophic Fe-oxidizing bacteria (FeOB) use Fe(II) oxidation for energy and growth, and are therefore thought to play important roles in Fe cycling. Fe is practically ubiquitous, raising the question of whether FeOB are active in every environment with Fe redox cycling, which would likely require a variety of niche-

specific adaptations. Fe cycling is particularly important at coasts, where Fe transformations affect the chemistry of waters in coastal sediments and estuaries, and ultimately the concentrations of nutrients (e.g. Fe, P) and other metals (e.g. As) transported to the ocean (Charette *et al.*, 2005; Jung *et al.*, 2009). Significant redox activity occurs in stratified marine waters, such as the Chesapeake Bay, which experience seasonal anoxia in bottom waters (Officer *et al.*, 1984). In our previous studies of the Chesapeake, water samples from the oxic-anoxic transition zone always yielded enrichments of chemolithotrophic FeOB (MacDonald *et al.*, 2014; Field *et al.*, 2016). From these enrichments, we isolated two FeOB, which represent the first known marine FeOB from the water column (isolate strain CP-8 previously reported in Field *et al.*, 2016). The presence of FeOB was somewhat surprising given the relatively low (micromolar) concentrations of Fe, and the strong tidal mixing, which may frequently expose FeOB to higher O₂ concentrations, making it harder for them to compete with abiotic Fe(II) oxidation. Further study of these isolates may reveal their distinct adaptations to life in the estuarine water column, while also showing commonalities shared among all marine FeOB across different environments.

The Chesapeake FeOB isolates are members of the Zetaproteobacteria, all of which are marine neutrophilic chemolithotrophic FeOB. The other Zetaproteobacteria isolated to date primarily originate from deep sea hydrothermal microbial mats and sediments (Emerson *et al.*, 2007; McAllister *et al.*, 2011; Field *et al.*, 2015; Makita *et al.*, 2016), with some from coastal sediment (Laufer *et al.*, 2016; Laufer *et al.*, 2017). Zetaproteobacteria sequences have also been found in coastal groundwater and worm burrows (16S rRNA gene analysis; McAllister *et al.*, 2015) and briny terrestrial groundwater (metagenomics; Emerson *et al.*, 2016). Steel coupon incubation

experiments provide sequence and culture-based evidence that Zetaproteobacteria inhabit coastal waters (Dang *et al.*, 2011; McBeth *et al.*, 2011; Mumford *et al.*, 2016), though the Chesapeake isolates are the first Zetaproteobacteria isolated directly from a coastal redox-stratified water column. In total, previous studies show that Zetaproteobacteria grow at oxic-anoxic interfaces where Fe(II) and O₂ are available, typically preferring lower O₂ concentrations (Chan *et al.*, 2016), though *Mariprofundus* sp. DIS-1 is an exception in that it tolerates saturated O₂ conditions (Mumford *et al.*, 2016). The molecular mechanism of neutrophilic Fe(II) oxidation is not well known; comparative analysis of six existing Zetaproteobacteria isolate genomes with freshwater FeOB genomes has resulted in hypothesized pathways (Singer *et al.*, 2011; Liu *et al.*, 2012; Barco *et al.*, 2015), but differences in single amplified genomes (SAGs) and metagenomes suggest that the pathway has some variants (Field *et al.* 2015; Fullerton *et al.*, 2017). Fe(II) oxidation by the Zetaproteobacteria results in Fe(III) oxyhydroxides, typically in the form of twisted ribbon-like stalks, which form the framework of Fe microbial mats (Chan *et al.*, 2016). Such large, dense stalk structures would make it difficult for a pelagic FeOB to maintain buoyancy. In sum, our knowledge of benthic Zetaproteobacteria may not necessarily be representative of FeOB in the water column.

Here we detail the isolation, physiological characterization, and genomic analysis of two new Fe-oxidizing Zetaproteobacteria from the Chesapeake Bay, *Mariprofundus aestuarium* CP-5 and *Mariprofundus ferrinatatus* CP-8. We compare the CP strains to the other Zetaproteobacteria and propose that physiological and genomic distinctions represent adaptive strategies for the Chesapeake

Zetaproteobacteria to scavenge Fe in low Fe(II) waters and to withstand highly variable oxygen conditions associated with physically dynamic redoxclines.

2.2 Materials and Methods

2.2.1 Sampling, Enrichments, and Isolation

The redox-stratified waters of the Chesapeake Bay at Station 858 (38°58.600N, 076°22.080W) were sampled aboard the R/V *Hugh R Sharp* in August, 2014. Details of sampling and the geochemical conditions can be found in Field *et al.* (2016). Water samples collected from the oxic-anoxic transition zone were used to inoculate FeOB enrichment cultures. Agarose-stabilized gradient tube cultures (Emerson and Floyd, 2005) were set up with a FeCO₃ plug (1% w/v high-melt agarose) and simulated estuary medium (0.15% w/v low-melt agarose), which is a 50:50 mixture of modified Wolfe's mineral medium (MWMM) and artificial seawater (ASW). Per liter, estuary medium contains 13.75 g NaCl, 2.69 g MgCl₂·6H₂O, 3.49 g MgSO₄·7H₂O, 0.36 g KCl, 0.75 g CaCl₂·2H₂O, 1 g NH₄Cl, 0.05 g KH₂PO₄, 0.42 g NaHCO₃. After autoclaving, estuary medium was amended with 1 μL/mL Wolfe's trace mineral solution and 1 μL/mL vitamin solution and adjusted to pH 6.2 with CO₂. The headspace of all tube cultures contained a low O₂ gas mixture (N₂/CO₂/O₂; 95:4:1).

Strains CP-5 and CP-8 were isolated by serial dilution-to-extinction from water samples CTD12-5 and IS8-11.3 respectively (water geochemistry in Table A1; further details in Field *et al.*, 2016). Growth was confirmed by the development of colonies or distinct growth bands in agarose-stabilized tubes (Figure 2.1A) and by microscopy. Purity was checked by microscopic observation, absence of heterotrophic growth on

R2A-estuary medium agar plates, and sequencing of the 16S rRNA genes amplified with the bacterial-universal primer sets Bac27F and Uni1492R (Lane, 1991).

2.2.2 Physiological Characterization

To assess alternate substrate usage and optimal growth conditions of strains CP-5 and CP-8, growth tests were carried out in agarose-stabilized gradient tubes as described above, but buffered to pH 7.0 except for pH testing. To test if the strains could use non-Fe(II) substrates, we tested growth on 5 mM sodium thiosulfate, 5 mM sodium sulfide, 10 mM sodium pyruvate, 10 mM glucose, 10 mM sodium acetate, and 0.2% w/v yeast extract. The pH range of growth was determined using several buffers: acetate-acetic acid (pH 5.0 and 5.2, 10 mM), MES (pH 5.5, 6.0, 6.4 and 6.9, 10 mM), and HEPES (pH 7.2, 7.4, 7.7, 8.0, 8.3 and 8.5, 10 mM). pH measurements taken before and after cultivation confirmed minimal (0.1-0.2) decreases during cultivation periods. Preferred growth temperature was determined by incubating cultures at 5, 10, 15, 20, 25, 30, 35, and 40°C, and preferred salinity was determined using different ratios of MWMM (0‰):ASW (35‰): 0:10, 1:9, 2:8, 3:7, 4:6, 5:5, 6:4, 7:3, 8:2, 9:1, and 10:0. All cultures were assessed for growth after two weeks based on the development of growth bands and observation by fluorescent microscopy.

To determine the preferred oxygen concentration for growth, the dissolved oxygen (DO) within strain CP-5 and CP-8 growth bands was measured 48 hours after inoculation using a Firesting optical oxygen probe with a needle-type sensor (PyroScience, Aachen, Germany) mounted on a micromanipulator (Narishige International, Amityville, NY). Attempts to test growth under anoxic conditions were also set up by preparing deoxygenated media (bubbling with N₂ and autoclaving in an N₂-flushed vessel), setting up gradient tubes under a stream of N₂, and using a 100%

N₂ headspace. However, the Firesting optical oxygen probe detected trace O₂ in the gradient tube medium (~250 nM) indicating that this procedure did not yield completely anoxic cultures.

To measure the growth rate of each strain, growth bands from triplicate gradient tube cultures (buffered with PIPES) were harvested daily over the course of the experiment (10 and 9 days for strain CP-5 and CP-8 respectively). Samples were stained with Syto 13 for cell counting using a Petroff-Hausser counting chamber. Aliquots of harvested growth bands were also used to measure total Fe concentrations in cultures over time. Fe concentrations in abiotic control gradient tubes were measured as well, using samples at the same height as biotic growth bands.

We used total Fe measurements to follow Fe(II) oxidation because nearly all Fe accumulated in developing growth bands was shown to be Fe(III) in the strain CP-5 growth experiment (data not shown). Samples for total Fe analysis were reduced with 200 mM hydroxylamine for 22-24 hours and measured using the ferrozine method (modified from Stookey, 1970).

2.2.3 Microscopy

Phase contrast and fluorescent micrographs of cultures (stained with SYBR green I, in the case of fluorescence) were captured on an Olympus BH-2 microscope with 400x total magnification. For these analyses, we used liquid cultures (without agarose) grown for 24 hours. Samples for scanning electron microscopy (SEM) were gently mounted on a 0.2- μ m-pore-size polycarbonate filter, air dried, and coated with gold/palladium for observation, or with carbon for energy dispersive spectroscopy (EDS) analysis. Samples for transmission electron microscopy (TEM) were gently mounted on a Formvar-coated copper grid, air dried, and coated with gold/palladium.

Electron microscopy was performed at the Delaware Biotechnology Institute Bioimaging Center, using a Hitachi S-4700 field emission SEM with an Oxford INCA EDS system and a Zeiss LIBRA 120 TEM.

2.2.4 Genome Sequencing and Analysis

For DNA extraction, strains CP-5 and CP-8 were grown using 25 mL FeCO₃ gradient plates (1 L total volume per culture) under microaerobic conditions (N₂/CO₂/O₂; 95:4:1; Emerson and Floyd, 2005). Genomic DNA was isolated from these cultures using the FastDNA Spin Kit for Soil (MP Biomedicals, Santa Ana, CA). We used the PowerClean Pro DNA kit (MO BIO Laboratories, Carlsbad, CA) to remove remaining inhibitors. The purified DNA (2.5 and 0.5 µg of CP-5 and CP-8, respectively) was size-selected using electrophoresis (BluePippin, Sage Science, Beverly, MA) to a minimum size of 6 kb, resulting in an average size of 12 kb. The genomes were sequenced using PacBio RSII technology at the University of Delaware Sequencing and Genotyping Center. Size-selected DNA was prepared for sequencing using the SMRTbell Template Prep Kit 1.0 (PacBio, Menlo Park, CA) as per the manufacturer's instructions. One SMRT cell per genome was sequenced with P6-C4 chemistry and a 6-hour movie. For strain CP-5, sequencing generated 1.37 Gbp of raw data (mean read length 15,263 bp; N₅₀ 26,034 bp); for strain CP-8, sequencing generated 0.84 Gbp of raw data (mean read length 8,877 bp; N₅₀ 19,311 bp). Assembly was completed on the PacBio SMRT Portal. Subreads were filtered to a minimum length of 1kb (CP-5) or 2kb (CP-8) with a polymerase quality score minimum of 0.8. The hierarchical genome assembly process 3 (HGAP-3) was used to assemble a single high quality contig from each of the sequencing runs. The average coverage over the entire sequenced contigs was 382x for strain CP-5 and 300x for

strain CP-8. Gepard (v.1.40; Krumsiek *et al.*, 2007) was used to compare each genome against itself to check for inverted repeats and to close each contig into a complete circular genome.

The complete genomes of strains CP-5 and CP-8 were annotated using the pipeline of the Integrated Microbial Genome Expert Review (IMG/ER) system (Markowitz *et al.*, 2012). Manual verification of predicted genes of interest was completed using MUSCLE alignments in MEGA (v.7.0.14) against reference gene sequences from UniProt or the RSCB Protein Data Bank (Edgar, 2004; Kumar *et al.*, 2016). The Rapid Annotation using Subsystem Technology (RAST) platform (Aziz *et al.*, 2008; Overbeek *et al.*, 2014) was used to identify possible frameshifts (none were detected) and to help find genes unique to the CP strain genomes, with respect to the other Zetaproteobacteria. Average amino acid identities (AAI) of bidirectional best hit proteins were calculated using a web-based calculator (<http://lycofs01.lycoming.edu/~newman/AAI/>). Reported AAI values are the average of the separate calculations run in both directions for each pair (standard deviation <1.18%). Average nucleotide identities (ANI) were calculated using OrthoANI (Yoon *et al.*, 2017). An AAI heatmap was made using the R package gplots heatmap.2 (v 3.0.1); hierarchical clustering using complete agglomeration was used to calculate the dendrogram.

2.2.5 16S rRNA Gene Analysis

The CP strain 16S rRNA genes were found in their completed genomes and aligned to the arb-SILVA database using the SINA online web tool (v.1.2.11; Pruesse *et al.*, 2012). Aligned sequences were masked to unambiguously aligned base positions and a maximum-likelihood tree was constructed using RAxML with the

GTR-gamma nucleotide substitution model (v.8.2.8; Stamatakis, 2014). Bootstrap values were estimated from 500 replicates. To calculate pairwise percent nucleotide identity, we calculated the Similarity score metric on the Ribosomal Database Project (RDP) website (Cole *et al.*, 2014).

2.2.6 Genome Accession Numbers and Culture Availability

GenBank accession numbers for *Mariprofundus aestuarius* CP-5 and *Mariprofundus ferrinatatus* CP-8 are CP018799 and CP018800 respectively. IMG taxon IDs for strains CP-5 and CP-8 are 267118011 and 267180111 respectively. Both isolates are available on request from C.S. Chan (University of Delaware, USA) and will be available at the Provasoli-Guillard National Center for Marine Algae and Microbiota (NCMA; Bigelow Laboratory for Ocean Sciences, USA).

2.3 Results and Discussion

2.3.1 Isolation and Physiological Characterization

Strains CP-5 and CP-8 were both successfully isolated using Fe(II)/O₂ gradient tubes after 5 transfers of the 10⁻⁵ serial dilutions. Growth consistently appeared as a sharp orange band typical of microaerophilic FeOB (Figure 2.1A) and cells appeared as curved rods under fluorescent microscopy (Figure 2.1B and 2.1C). Strain CP-5 cells are $0.43 \pm 0.05 \mu\text{m} \times 1.01 \pm 0.18 \mu\text{m}$, and strain CP-8 cells are $0.45 \pm 0.04 \mu\text{m} \times 0.91 \pm 0.08 \mu\text{m}$. Purity was demonstrated by the lack of growth on R2A-estuary medium plates (no contaminant oligotrophs) and by a single unambiguous full length 16S rRNA gene sequence amplified from each culture.

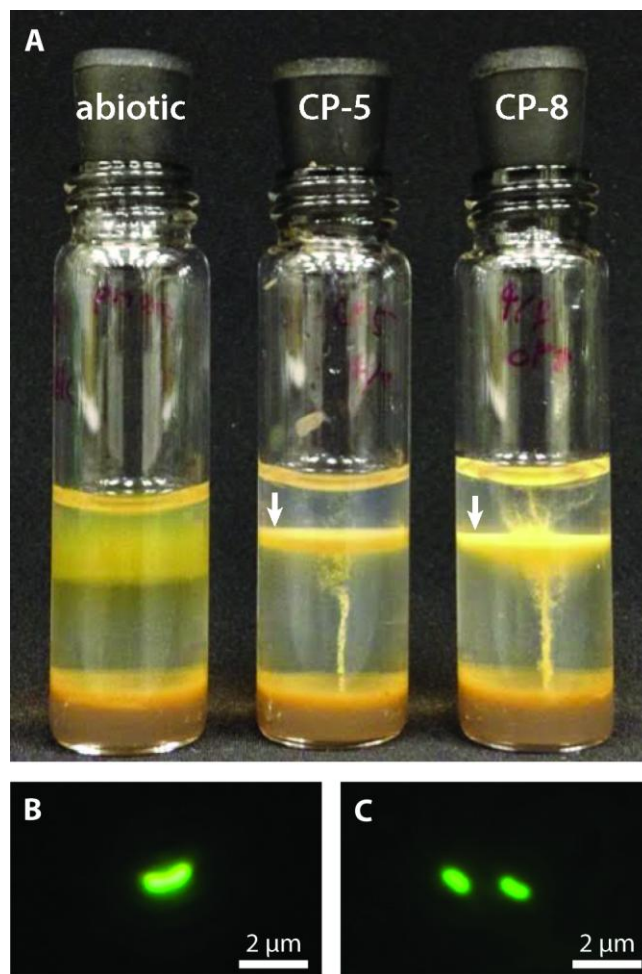


Figure 2.1: A) CP strain gradient tube cultures with FeCO_3 plugs (8 days old). CP strain-inoculated tubes display distinct orange growth bands (indicated by white arrows) in contrast to the diffuse oxide cloud in the abiotic control. The inoculum for the CP strain tubes is visible as thin orange vertical lines. B, C) Fluorescence micrographs of CP-5 (B) and CP-8 (C) cells.

Strains CP-5 and CP-8 have doubling times of 19.5 and 27 hours, respectively. These generation times are slower than *M. ferrooxydans* PV-1 (12 hrs), but similar to the 24 hour doubling time reported for the closely related *Mariprofundus micogutta*. During growth, strains CP-5 and CP-8 both accelerated Fe(II) oxidation, compared to

uninoculated controls (Figure 2.2). The O_2 concentration in the growth bands of inoculated gradient tubes was $<2 \mu\text{M } O_2$, comparable to or lower than *M. ferrooxydans* PV-1 (Krepeski *et al.*, 2013). Strains CP-5 and CP-8 appear to be obligate Fe(II)-oxidizers as neither grew on reduced S or organic carbon substrates (Table 2.1). Overall, our experiments suggest that strains CP-5 and CP-8 are microaerophilic chemolithoautotrophic Fe(II)-oxidizers, consistent with all other Zetaproteobacteria isolates.

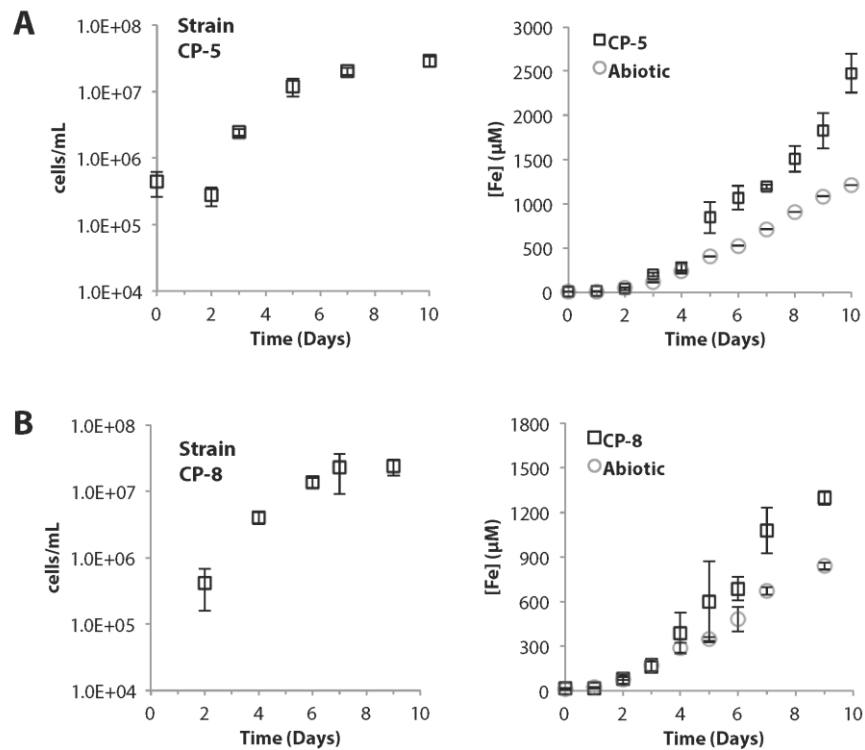


Figure 2.2: A) Strain CP-5 growth curve (left) and corresponding total Fe curve (right) including abiotic controls. B) Strain CP-8 growth curve (left) and corresponding total Fe curve (right) including abiotic controls. All cell concentrations are an average of direct cell counts from triplicate samples per time point. Error bars represent one standard deviation from the mean.

Table 2.1: Summary of strains CP-5 and CP-8 genomic and physiological characteristics in comparison to other selected Zetaproteobacteria.

Name	<i>Mariprofundus aestuarium</i>	<i>Mariprofundus ferrinatatus</i>	<i>Mariprofundus micogutta</i>	<i>Mariprofundus ferrooxydans</i>
Strain	CP-5	CP-8	ET2	PV-1
Genome size (Mbp)	2.54	2.30	2.50	2.87
GC content	51%	54%	49%	54%
Protein coding gene count	2427	2237	2417	2866
tRNA count	50	45	49	48
Doubling time (h)	19.5	27	24	12
Growth salinity (‰)				
Range	7–31.5	7–31.5	10-40	3.5–35***
Optimum	14–17.5	14–17.5	27.5	28–31.5***
Growth temp. (°C)				
Range	10–30	15–35	15-30	10–30
Optimum	20–25	25–30	25	30
Growth pH				
Range	5.5–8.3	5.5–8.3	5.8-7.0	5.5–7.2
Optimum	6.9-7.2	6.9-7.2	6.4	6.2–6.5
Energy source				
Fe(II)	+	+	+	+
S*	-	-	-	-
Organics**	-	-	-	-
Iron biomineral morphology	Dreads	Dreads	Filaments	Stalk
Reference	This study	This study	Makita <i>et al.</i> , 2016	Emerson <i>et al.</i> , 2007; Singer <i>et al.</i> , 2011

*Sulfide, thiosulfate; **Glucose, Acetate, Pyruvate, Yeast extract, ***This study

ND = Not determined

To optimize culturing of the CP strains, growth was tested over a range of salinity and pH. The preferred salinity was brackish, 14-17.5‰, with no growth at 0‰ (freshwater) or 35‰ (normal seawater). The preferred pH range was 6.9-7.2, and

both strains grew at pH up to 8.3, unusually high for neutrophilic FeOB isolates, which typically prefer pH between 6.0-6.5 (e.g., *M. ferrooxydans* PV-1 and *M. micogutta*, Table 2.1; freshwater FeOB *Gallionella capsiferriformans* ES-2, *Sideroxydans lithotrophicus* ES-1, and *Ferriphaseelus amnicola* OYT-1; Emerson and Moyer, 1997; Kato *et al.*, 2014). One exception is *Mariprofundus* sp. DIS-1, which can grow at pH 8.0 (Mumford *et al.*, 2016). The CP strain salinity and pH preferences reflect the brackish seawater from which they were sampled.

2.3.2 Phylogenetic Analyses

Strains CP-5 and CP-8 are representative of the Chesapeake Bay environment, as their 16S rRNA gene sequences match the dominant 16S rRNA sequences of the original FeOB enrichment cultures from which each strain was isolated (Figure A1). Phylogenetic analysis of 16S rRNA gene sequences shows that strains CP-5 and CP-8 are Zetaproteobacteria within OTUs 18 and 37 respectively (as defined by McAllister *et al.* (2011) and determined using ZetaHunter, <https://github.com/mooreryan/ZetaHunter>) and cluster with nearly all other isolated Zetaproteobacteria (Figure 2.3). Among the Zetaproteobacteria isolates and SAGs, strains CP-5 and CP-8 are most similar to each other based on average nucleotide identity (ANI), average amino acid identity (AAI), and 16S rRNA gene identity (Table 2.2). Because both strains share less than 97% 16S rRNA gene identity (Stackebrandt and Goebel, 1994) and have less than 95% ANI (Konstantinidis and Tiedje, 2005) with all other Zetaproteobacteria isolates and SAGs, including each other, strains CP-5 and CP-8 are two new species, with proposed names *Mariprofundus aestuarium* CP-5 and *Mariprofundus ferrinatatus* CP-8.

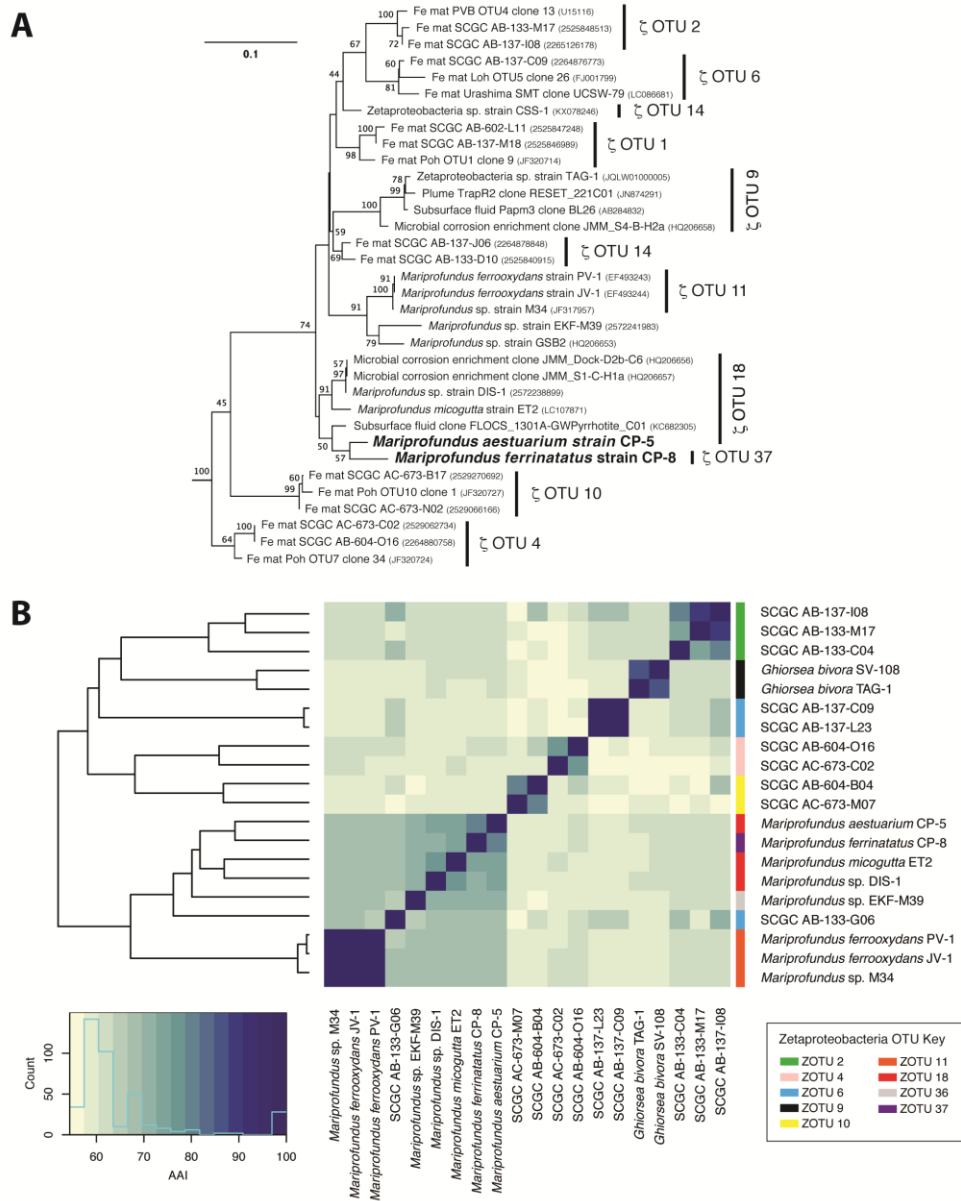


Figure 2.3: A) 16S rRNA gene phylogenetic tree of *Mariprofundus ferrinatatus* CP-8 and *Mariprofundus aestuarium* CP-5 and other Zetaproteobacteria. *Thermotoga maritima* (AJ401021) and *Aquifex pyrophilus* (M83548) were used as outgroups (not shown). All sequences were masked to 1275 bp. B) Heatmap showing pairwise comparisons of AAI between all Zetaproteobacteria isolates and the most complete SAGs.

Table 2.2: Source environment, 16S rRNA gene identity, ANI, and AAI comparisons of strains CP-5 and CP-8 to other Zetaproteobacteria.

Name	Source environment	Zeta OTU*	Contigs	complete-ness** (%)	16S rRNA gene identity (%) (RDP)				ANI (%)		AAI (%)		Reference
					Strain CP-5	Strain CP-8	Strain CP-5	Strain CP-8	Strain CP-5	Strain CP-8	Strain CP-5	Strain CP-8	
<i>Mariprofundus aestuarii</i> CP-5	Estuarine water column	18	1	100	100.0	96.36	100.0	77.40	100.0	80.42	100.0	80.42	This study
<i>Mariprofundus ferrinatatus</i> CP-8	Estuarine water column	37	1	100	96.36	100.0	77.40	100.0	80.42	100.0	80.42	100.0	This study
<i>Mariprofundus micogutta</i> ET2	Deep-sea hydrothermal sediment	18	59	100	93.74	93.95	73.93	73.07	74.18	73.25	74.18	73.25	Makita <i>et al.</i> , 2016
<i>Mariprofundus</i> sp. DIS-1	Steel coupon incubation in coastal bay	18	57	100	94.39	94.60	73.85	72.67	72.93	71.74	72.93	71.74	Mumford <i>et al.</i> , 2016
<i>Mariprofundus</i> sp. EKF-M39	Deep-sea hydrothermal Fe mat	36	45	98.3	93.42	95.01	72.19	72.51	70.01	70.27	70.01	70.27	Field <i>et al.</i> , 2015
<i>Mariprofundus</i> sp. M34	Deep-sea hydrothermal Fe mat	11	36	100	94.42	95.77	72.54	72.00	69.58	68.90	69.58	68.90	McAllister <i>et al.</i> , 2011
<i>Mariprofundus ferrooxydans</i> PV-1	Deep-sea hydrothermal Fe mat	11	32	100	94.59	95.94	72.62	72.17	69.56	69.11	69.56	69.11	Emerson and Mover, 2002
<i>Mariprofundus ferrooxydans</i> JV-1	Deep-sea hydrothermal Fe mat	11	39	100	94.59	95.94	72.34	72.09	69.52	69.09	69.52	69.09	Emerson and Mover, 2002
Zetaproteobacteria SAG I08	Deep-sea hydrothermal Fe mat	2	233	81.6	93.04	91.55	68.97	68.63	62.78	62.41	62.78	62.41	Field <i>et al.</i> , 2015
Zetaproteobacteria SAG C09	Deep-sea hydrothermal Fe mat	6	225	83.3	92.20	92.42	68.20	68.14	59.00	58.88	59.00	58.88	Field <i>et al.</i> , 2015
<i>Gliorsea bivora</i> TAG-1	Deep-sea hydrothermal Fe mat	9	13	100	92.48	92.48	68.18	67.50	60.50	60.27	60.50	60.27	Mori <i>et al.</i> , in review
<i>Gliorsea bivora</i> SV108	Deep-sea hydrothermal Fe mat	9	54	100	92.29	91.01	68.57	67.90	60.76	60.56	60.76	60.56	Mori <i>et al.</i> , in review

*Defined by McAllister *et al.* (2011) and determined using ZetaHunter, <https://github.com/mooreyan/ZetaHunter>

** Estimated by CheckM (v1.0.6; Parks *et al.*, 2015), and manual correction where Zetaproteobacteria *recO* gene sequences were not recognized. Because the CP strain genomes are known to be 100% complete, we re-examined the genomes and found that CheckM failed to recognize *recO* gene sequences in numerous Zetaproteobacteria genomes (strains CP-5, CP-8, ET2, DIS-1, EKF-M39, TAG-1, and SV108, and SAG C09), thereby underestimating % completeness of these genomes.

Comparisons of 16S rRNA sequences and %AAI among Zetaproteobacteria show that most of the isolates fall within a closely-related group, i.e. the genus *Mariprofundus* (Figure 2.3). By 16S rRNA gene identity and %AAI, the CP strains are most closely related to *Mariprofundus* sp. DIS-1, isolated from a steel coupon incubated in a coastal bay (Mumford *et al.*, 2016), and *M. micogutta*, isolated from marine hydrothermal sediment (Table 2.2; Figure 2.3; Makita *et al.*, 2016). These close relationships show that *Mariprofundus* is a cosmopolitan genus that inhabits a variety of environments, coastal and deep sea, as well as planktonic, benthic, and subsurface.

2.3.3 Iron Oxyhydroxide Biomineral Morphology

To investigate how suspended FeOB manage Fe oxyhydroxide precipitation to avoid sinking, we examined the Fe biominerals produced by strains CP-5 and CP-8. Both strains produce bundles of stubby rod-shaped extracellular structures (Figure 2.4), confirmed to be Fe-rich by SEM-EDX (Figure A2) and morphologically distinct from abiotic mineral precipitates (Figures A3 and A4). This morphology has previously been identified in freshwater FeOB and referred to as dreadlocks (or dreads) given their resemblance to the dreadlock hairstyle (Figure 2.5; Kato *et al.*, 2015). Dreads are somewhat similar to the fibrillar twisted Fe stalks produced by other microaerophilic FeOB (Figure 2.5B; Chan *et al.*, 2011; Kato *et al.*, 2014), in that they are bundles of elongated Fe oxyhydroxides (referred to as oxides from here on). However, dreads are short, never exceeding 10 μm in length, and many dreads can radiate from, and surround a single cell. In contrast, Fe oxide stalks range in length from 10's of μm to cm, extend from one side of the cell, and are used by mat-forming

FeOB to anchor themselves to surfaces (Chan *et al.*, 2011; Chan *et al.*, 2016). Dreads were closely associated with CP cells observed by fluorescent microscopy (Figure 2.4A) while the radiating arrangement observed under SEM made it apparent that CP strain cells were once attached (Figure 2.5A). In fact, the lack of cell-attached dreads under SEM suggests they are easily shed. In total, these observations suggest that the CP strains produce short Fe oxide dreads as an adaptation to shed their biominerals to maintain suspension within the water column.

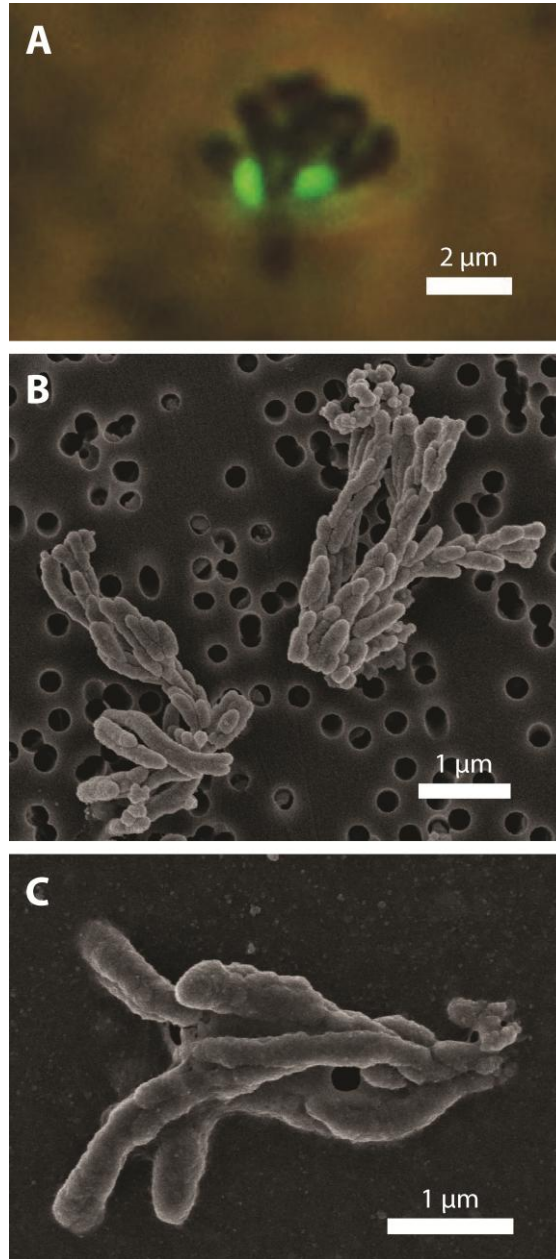


Figure 2.4: CP strain cell and biomineral micrographs. A) Phase contrast and fluorescence micrograph (overlay) of strain CP-5 showing bean-shaped cells (green), stained with SYBR Green I, and iron oxide dreads. B) Scanning electron micrograph of bundles of iron oxide dreads produced by strain CP-8. C) Scanning electron micrograph of bundles of iron oxide dreads produced by strain CP-5.

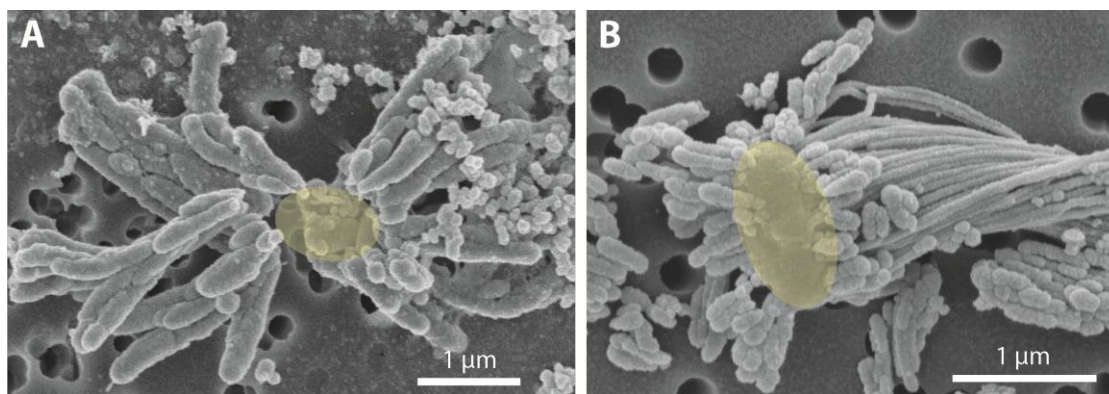


Figure 2.5: Scanning electron micrograph of extracellular iron oxide biomineral structures. A) Dreads produced by strain CP-8, with likely location of missing cell denoted as a yellow oval. B) Dreads surrounding a freshwater FeOB *Ferriphaseus* R-1 cell, highlighted in yellow (modified from Kato *et al.*, 2015). To the right of the cell, a longer iron oxide stalk produced by R-1 is also visible.

2.3.4 General Genome Features of Strains CP-5 and CP-8

The CP-5 and CP-8 strain genomes are both single circular chromosomes, which make them the first and only closed Zetaproteobacteria genomes. High consensus read coverage (382x for strain CP-5; 300x for strain CP-8) led to significant overlap of the ends of each CP strain genome assembly (15 and 9 kb, respectively), overall providing confidence in genome accuracy and completion. The CP-5 and CP-8 strain genomes are 2.54 Mbp and 2.30 Mbp respectively; sizes, GC contents, and COG distributions are comparable to the other sequenced Zetaproteobacteria isolates (Tables 2.1 and A2). The COG distribution of the two CP strains is highly similar and there are no obvious major metabolic or physiological differences apparent in the genes distinguishing the two strains from one another. The CP-5 and CP-8 strain genomes contain 258 and 211 genes without homologs in other Zetaproteobacteria isolates. As described below, the CP strains share several genes that are absent or rare

in the other sequenced Zetaproteobacteria and may represent adaptations to life in the water column.

2.3.5 Electron Transport Chain Analysis

Based on the electron transport-related genes identified in the genomes (Table A3), strains CP-5 and CP-8 appear to have an electron transport system similar to other Zetaproteobacteria (Figure 2.6), with some key differences, described below. Like all microaerophilic FeOB, including Zetaproteobacteria, the CP strains have the putative Fe oxidase, outer membrane cytochrome *Cyc2* (e.g., Barco *et al.*, 2015; Kato *et al.*, 2015; Mumford *et al.*, 2016), which has been proven to oxidize Fe(II) in *Acidithiobacillus ferrooxidans* (Castelle *et al.*, 2008). The CP strain *cyc2* gene sequences are homologous to characterized *cyc2* sequences from PV-1 (e-values: 10^{-72} - 10^{-73} ; Table A3; Barco *et al.*, 2015) and each contain a predicted signal sequence, one CXXCH heme-binding motif, and an outer membrane beta barrel domain as with other *cyc2* gene sequences (White *et al.*, 2016). The CP strains both lack the putative outer membrane Fe oxidase MtoA (Liu *et al.*, 2012), consistent with our observation that *Cyc2* is common amongst microaerophilic and other FeOB, while MtoA is rare (Kato *et al.*, 2015).

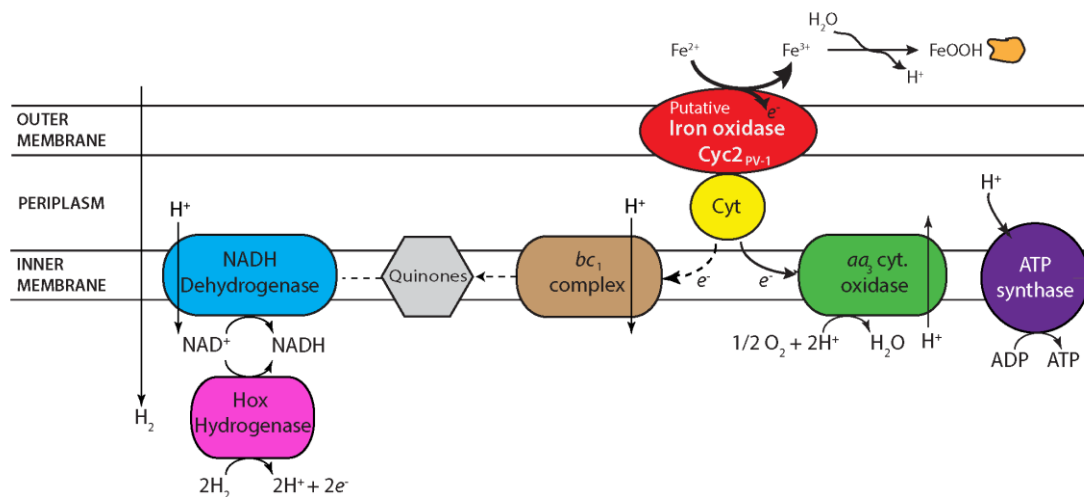


Figure 2.6: Proposed electron transport system in strains CP-5 and CP-8 based on genomic analysis. See text for further description.

One unusual feature in the CP strain genomes is the possession of aa_3 -type cytochrome *c* oxidases (Table A3) in place of the cbb_3 -type cytochrome *c* oxidases present in all other Zetaproteobacteria genomes to date. Several SAGs and isolate *M. micogutta* have both aa_3 and cbb_3 -type oxidases (Field *et al.*, 2015), but no other Zetaproteobacteria has only the aa_3 -type. Between the aa_3 and cbb_3 -type oxidases, the cbb_3 -type oxidase is considered to be better adapted for low O_2 conditions given its higher affinity for oxygen (Arai *et al.*, 2014), consistent with the association of Zetaproteobacteria with low O_2 habitats. Conversely, the lower oxygen affinity of the aa_3 -type oxidase suggests adaptation to somewhat higher O_2 conditions. Though the K_m values of both oxidases would be considered low O_2 (K_{m-cbb_3} on the order of nanomolar and K_{m-aa_3} on the scale of micromolar O_2 ; Arai *et al.*, 2014), the difference suggests that the CP strains may have a higher O_2 niche. Curiously, the single Zetaproteobacteria isolate shown capable of growing in O_2 -saturated waters, DIS-1,

possesses only the *cbb*₃-type oxidase, suggesting other genetic adaptations contribute to its O₂ tolerance. Still, the uncommon possession of only *aa*₃-type oxidases in the CP strains likely represents an adaptation to frequent exposure to high O₂ waters.

Periplasmic electron carriers are required for electron transport between Cyc2 and the terminal oxidase. Because of the high redox potential of Fe(II)/Fe(III)OOH (24 mV for ferrihydrite; Majzlan, 2012), these electron carriers are most likely cytochromes. In *A. ferrooxidans*, the cytochrome Cyc1 is one of these intermediate electron carriers (Malarte *et al.*, 2005; Castelle *et al.*, 2008). While there are homologs to *cyc1* in several Zetaproteobacteria isolate genomes, the CP strain genomes lack homologs. However, Cyc1 is suggested to interact specifically with the *cbb*₃-type oxidase in *M. ferrooxydans* PV-1 (Barco *et al.*, 2015), making the lack of *cyc1* homologs in the CP strains consistent with the absence of the *cbb*₃-type oxidase. There is a different predicted periplasmic cytochrome found in the CP strains, which may transfer electrons between Cyc2 and the *aa*₃-type terminal oxidase. This potential periplasmic cytochrome gene in both strains CP-5 and CP-8 codes for a 127aa protein, with a signal sequence and one CXXCH heme-binding motif (Table A3). In the strain CP-8 genome, this gene is located near the genes encoding the terminal *aa*₃-type oxidase, but it is in a different genomic neighborhood in strain CP-5. Homologs of this periplasmic cytochrome are found in several Zetaproteobacteria isolates (PV-1, JV-1, M34, and EKF-M39; e-values 10⁻²³–10⁻²¹) and are also near terminal oxidases. The genomic context and presence in several Zetaproteobacteria (including 7 SAGs) suggests that this predicted cytochrome plays a role in Fe(II) oxidation and energy conservation.

The high potential of Fe(II)/Fe(III)OOH requires FeOB to regenerate NADH using either reverse electron transport, or an alternate reductant. Like other Zetaproteobacteria, the CP strains have the components for reverse electron transport: a *bc1* complex, ubiquinone synthesis genes, and NADH dehydrogenase (Figure 2.6). However, the CP strains are the only Zetaproteobacteria isolates that definitively lack an alternative complex III, indicating that it is not a necessary component for neutrophilic Fe(II) oxidation, despite its conservation in other FeOB (Kato *et al.*, 2015; Singer *et al.*, 2011). Both CP strains have a cytochrome *b*/diheme cytochrome *c* gene cluster (Table A3) that likely also plays an electron transport role. Present in all Zetaproteobacteria isolates and several SAGs, these two genes in each of the CP strains are also homologous to the fused *cytbc* gene in the Fe-oxidizing KS culture *Gallionellaceae*, which was proposed to pass electrons from periplasmic cytochromes to quinones and on toward denitrification (He *et al.*, 2016). The CP strains lack a dissimilatory nitrate reductase, but this novel *bc* complex may still function to reduce quinones for reverse electron transport. Both CP strains have genes coding sulfide quinone oxidoreductases (Table A3), which would allow them to take advantage of the high sulfide concentrations in the Chesapeake Bay to reduce quinones. The CP strains also have *hoxWHYUF* genes, which could allow them to use H₂ to reduce NAD⁺ to NADH (Tran-Betcke *et al.*, 1990; Thiemermann *et al.*, 1996), relieving at least some of the need for reverse electron transport. In sum, the CP strain genomes show multiple options for regenerating NADH for carbon fixation and biosynthetic pathways.

2.3.6 Carbon Metabolism Analysis

The CP strain genomes are consistent with autotrophy in these organisms. The CP strains each possess complete gene sets for the Calvin–Benson–Bassham (CBB) cycle, including form II ribulose 1,5-bisphosphate carboxylase (*RuBisCO*) for fixing inorganic carbon (Table A4). Also present are the genes to convert the chief product of the CBB cycle, glycerate 3P, to pyruvate, which can then be utilized in the predicted, complete tricarboxylic acid (TCA) cycle to generate energy and biosynthetic precursors (Table A4).

The CP strain genomes each contain form II *RuBisCO* and lack form I *RuBisCO*, as observed in several other Zetaproteobacteria (e.g., EKF-M39, SV108 *M. micogutta*, Zetaproteobacteria SAGs). CO₂ concentrations were ~70-80 μM in the waters from which the CP strains were isolated (Cai *et al.*, in review). These concentrations are within the K_{m,CO_2} ranges for both Form I and Form II *RuBisCO* (Badger and Bek, 2008), so either should be functional in this environment. However, the absence of form I *RuBisCO* is somewhat unexpected in the CP strains given that form I is considered to be better adapted to higher O₂ conditions than form II (Badger and Bek, 2008) and would provide a potential adaptation for more efficient carbon fixation during exposure to higher O₂ waters. Indeed, Mumford *et al.* suggest that the presence of both forms of *RuBisCO* in DIS-1 helps adapt this strain to a larger range of oxygenated environments (2016). In any case, the form II *RuBisCO* genes in the CP strain genomes support Fe(II) oxidation chemolithoautotrophy, consistent with all other Zetaproteobacteria.

Support for strict autotrophy comes from the apparent lack of transporters for organic carbon substrates. Close analysis of a cluster of genes annotated as phosphotransferase (PTS) system genes in each CP strain genome suggests they do not

make up a complete system for carbohydrate uptake, but may instead play a role in nitrogen regulation (Table A4). The CP strain genomes also lack complete ABC transport systems for sugars, peptides, and amino acids, making heterotrophy unlikely.

2.3.7 Unusual Genomic Features for Biofilm Formation

We surveyed the CP genomes for genes that could represent adaptations to life in the Chesapeake Bay redoxcline, focusing on ones that were rare or absent in other Zetaproteobacteria. We found two gene clusters related to biofilm formation: the Wsp system, a chemosensory system that produces the biofilm-inducing signal molecule cyclic dimeric guanosine monophosphate (c-di-GMP), and the widespread colonization island (WCI), a pilus assembly system that enables surface attachment.

Each CP strain genome includes a complete *wsp* gene cluster (*wspABCDEFR*), which encodes the Wsp chemosensory system (Figure 2.7; Table A5). Genetic and protein functional studies have demonstrated the role of these genes in biofilm formation in *Pseudomonas*, the model organism for the Wsp system (D'Argenio *et al.*, 2002; Hickman *et al.*, 2005). The Wsp system is homologous to the Che chemotaxis system; both contain a methyl-accepting chemotaxis protein (MCP) chemoreceptor and a complex of signal transduction proteins (Bantinaki *et al.*, 2007). However, the Wsp system regulates biofilm formation rather than flagellar motor switching as in the Che system. The major distinguishing feature of the Wsp system is subunit WspR, a diguanylate cyclase response regulator required for Wsp system-induced biofilm production. Phosphorylation stimulates WspR to synthesize the signal molecule cyclic di-GMP (c-di-GMP), which induces biofilm formation pathways, including the production of extracellular polymeric substances (EPS; D'Argenio *et al.*, 2002; Hickman *et al.*, 2005; Malone *et al.*, 2007). The signal activating the Wsp system

MCP, WspA, remains unclear, but has been shown to be related to physical and/or chemical signals associated with growth on surfaces (Güvener and Harwood, 2007; O'Connor *et al.*, 2012). This suggests that given a mechanism for initial surface attachment, the Wsp system could enable the CP strains to form biofilms to colonize particles in the water column.

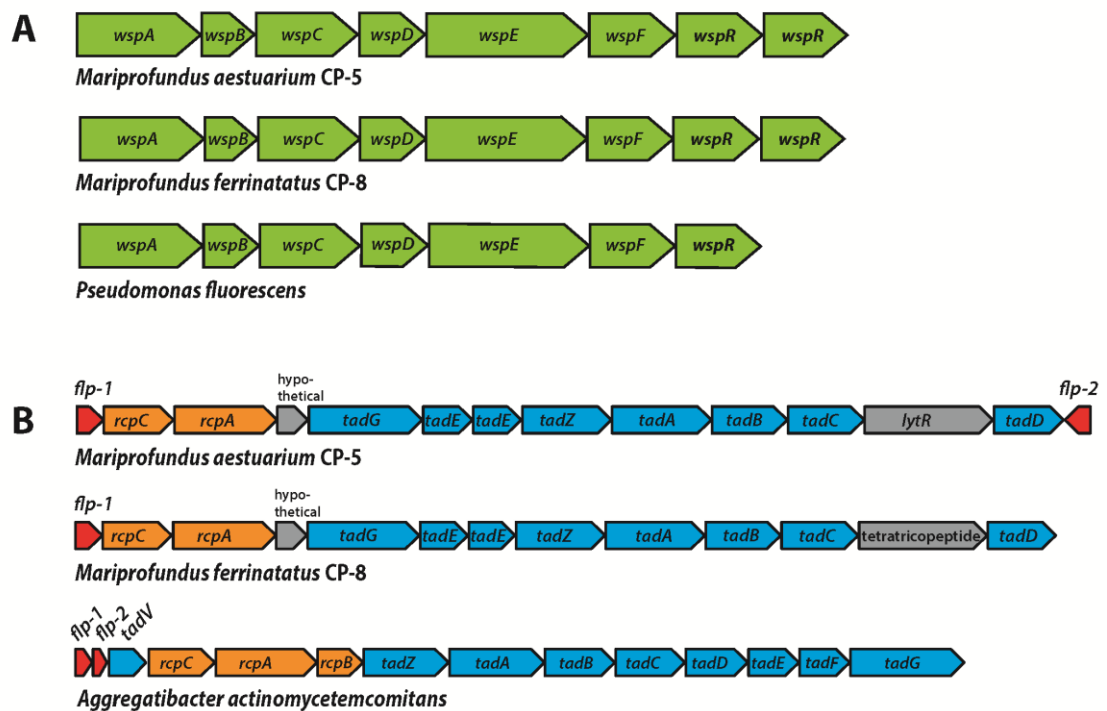


Figure 2.7: A) The Wsp operon in strains CP-5 and CP-8, showing synteny with the well-studied *Pseudomonas fluorescens* Wsp operon. B) The WCI genes in strains CP-5 and CP-8, showing similar gene content, but somewhat different gene order compared to *Aggregatibacter actinomycetemcomitans*.

Each CP strain genome contains two predicted copies of *wspR* that are homologs of the gene sequences of the functionally and structurally characterized WspR of *Pseudomonas aeruginosa* (e-values: $10^{-111} - 10^{-93}$; Table A5; De *et al.*, 2008). Like *Pseudomonas wspR*, all CP strain *wspR* sequences contain the conserved C-terminal diguanylate cyclase domain GGEEF in the active site loop and the RxxD motif making up the conserved inhibitory site in GGEEF domain-containing proteins (De *et al.*, 2008; De *et al.*, 2009). The remaining Wsp system subunit genes (*wspABCDEF*) are also present in the CP strain genomes and homologous to the *wsp* counterparts in *Pseudomonas* species (e-values $0 - 10^{-35}$; Table A5). Other Zetaproteobacteria genomes either lack *wsp* gene homologs or only contain single subunits (TAG-1, *wspR*; SV108, *wspR*; M34, *wspE*). The exception is Zetaproteobacteria SAG C09, a Loihi Seamount Fe mat single cell genome (2.45 Mb; Field *et al.*, 2015), which contains *wspABCDEF*, but clearly lacks *wspR*, with the gene cluster in the middle of a contig. Instead, the immediately adjacent features are a pseudouridine synthase and a tRNA, which are not obviously related to biofilm formation, though further downstream in the cluster (6 ORFs away from *wspF*), there is an adenylate cyclase gene. Adenylate cyclase forms the signal molecule cAMP, which is associated with many processes (Gancedo, 2013), one of which may be initial cell attachment to surfaces (O'Toole and Wong, 2016). Nevertheless, the lack of *wspR* in Zetaproteobacteria C09 genome suggests that the *wspABCDEF* homologs in C09 have a different role and output than in the CP strains. The absence of complete Wsp systems in Zetaproteobacteria genomes other than the CP strains suggests that Wsp-related biofilm formation may be an adaptation specific to pelagic Zetaproteobacteria for particle colonization.

The second genomic feature of the CP strains that is rare among Zetaproteobacteria is the widespread colonization island (WCI), a gene cluster responsible for tight attachment to surfaces (Figure 2.7; Table A6). The WCI includes *flp-1*, a gene encoding for the major structural component of the type IV Flp (fimbrial low-molecular-weight protein) pili, as well as the *tad* (tight adherence) genes, and *rcp* pilus assembly genes (Planet *et al.*, 2003). First characterized in *Aggregatibacter actinomycetemcomitans*, but studied in numerous other organisms including *Caulobacter* and *Pseudomonas* (Skerker and Shapiro, 2000; Bentzmann *et al.*, 2006), the WCI genes assemble adhesive Flp pili that mediate tenacious surface adherence and biofilm formation (Kachlany *et al.*, 2000; Kachlany *et al.*, 2001; Planet *et al.*, 2003). The CP strain genomes each contain *flp-1* gene sequences that were confirmed to contain the conserved processing site motif GXXXXEY (Inoue *et al.* 1998; Kachlany *et al.*, 2001), as well as *tadABCDEFGHIJ* and *rcpAC* (Table A6). Both CP strain genomes have two predicted copies of *tadE*, one of which is likely *tadF* given the high sequence similarity of these two subunits (Tomich *et al.*, 2006). Two WCI genes, *tadV* and *rcpB*, are not present in the CP genomes, which may be due to the general variability of WCI organization across bacteria or the potential for individual species to possess novel genes in place of individual WCI components (Tomich *et al.*, 2007). For example, *P. aeruginosa* was demonstrated to encode a novel prepilin peptidase, FppA, instead of TadV (Bentzmann *et al.*, 2006), suggesting that the CP strains could possess different versions of TadV and RcpB that would not be recognized by genomic analysis alone. The set of WCI genes in the CP strain genomes is also found in EKF-M39, but entirely absent from all other Zetaproteobacteria isolates, suggesting that only a small subset of Zetaproteobacteria can produce Flp pili.

The mechanisms thought to regulate WCI Flp pilus production vary across species (Tomich *et al.*, 2007) and could be controlled by c-di-GMP signaling in the CP strains. In each CP strain genome, predicted WCI components are adjacent to *pilZ* domain-containing genes (Table A6), which have been linked to c-di-GMP-regulated fimbriae production (Johnson *et al.*, 2011; Wilksch *et al.*, 2011). The CP strain *pilZ* sequences contain the c-di-GMP binding motifs RxxxR-(D/ N)x(S/A)xxG (Ryjenkov *et al.*, 2006; Christen *et al.*, 2007), and thus may connect Wsp system c-di-GMP synthesis to WCI Flp pilus production to promote a surface-attached biofilm lifestyle.

2.3.8 Adaptations of Pelagic Zetaproteobacteria in Estuarine Water Columns

In many ways, the Chesapeake strains are like other Zetaproteobacteria isolates: they are autotrophic, obligate Fe(II)-oxidizers, with similar electron transport and carbon fixation mechanisms. However, the CP strains differ in that they produce distinctive dreadlock-shaped oxides that are much smaller than the twisted stalks common to other Zetaproteobacteria. This is likely a key difference between pelagic and benthic FeOB. Our previous work has shown that iron biomineral stalks are the building blocks of Fe microbial mats (Chan *et al.*, 2016). Millimeters-long stalks create a highly porous framework unlike any other biofilm or mat, in that the bulk is made of mineral, without much interstitial EPS. This architecture allows Fe(II)-bearing fluids to flow through mats, enabling FeOB to biomineralize and position themselves at a benthic Fe(II)/O₂ interface (e.g. hydrothermal vent on the seafloor). In contrast, for FeOB that need to maintain position in a water column, large stalk structures would be undesirable because of their weight. Instead, the CP strains make smaller dreads that can be constantly shed, thereby eliminating the heavy oxide byproducts to avoid sinking out of the oxic-anoxic transition zone.

Instead of making Fe mats, it appears that the CP strains have the genes to form standard, EPS-bound biofilms, as is typical of organisms possessing the WCI and Wsp system. EPS production enables marine bacteria to colonize suspended particle surfaces (Decho, 1990), and is likely key for CP strains to attach to and access nutrients from Fe(II)-bearing minerals such as FeS. In seasonally stratified Chesapeake Bay waters, particulate FeS is formed by an O₂-Fe-H₂S catalytic cycle where sulfidic (H₂S) bottom waters reduce solid Fe(III) oxyhydroxides to dissolved Fe(II) and react further to precipitate solid FeS particles (Figure 2.8A; MacDonald *et al.*, 2014; Hansel *et al.*, 2015; Field *et al.*, 2016). Indeed, a majority of the Fe(II) in the Chesapeake Bay oxic-anoxic transition zone was found to be particulate (Field *et al.*, 2016), likely as FeS. Still, FeS particles are likely to be sparse given the low overall Fe(II) concentration, necessitating strategies for the CP strains to recognize and firmly attach to these Fe(II)-bearing particles. The c-di-GMP produced by the Wsp system could stimulate WCI Flp pilus production and other pathways involved in biofilm production to facilitate tight cell attachment to suspended FeS particles (Figure 2.8B). These small cell-mineral aggregates could further assemble and grow into larger flocs, incorporating other suspended particles and cells (Figure 2.8C). These flocs could trap more FeS for consumption (Figure 2.8D), and any trapped flocs could be recycled back to FeS if flocs settle into sulfidic bottom waters (Figure 2.8E). Floc formation can further benefit the CP strains by effectively increasing their O₂ tolerance, as previously described for freshwater floc-dwelling FeOB (Elliot *et al.*, 2014). Diffusion of O₂ into flocs is slowed by the EPS matrix (Brezonik, 1993). If floc-dwelling bacteria consume O₂ faster than it can diffuse in, low oxic or anoxic microenvironments develop within the floc structure (Flemming and Wingender,

2001; Han *et al.*, 2012). Should a CP strain floc be mixed into oxic layers of the water column, low $[O_2]$ microenvironments would provide a niche where the CP strains could still compete with abiotic oxidation for matrix-bound Fe(II). In all, biofilm-related genes would give the CP Zetaproteobacteria multiple advantages for persisting in the water column despite low Fe(II) and fluctuating O_2 conditions.

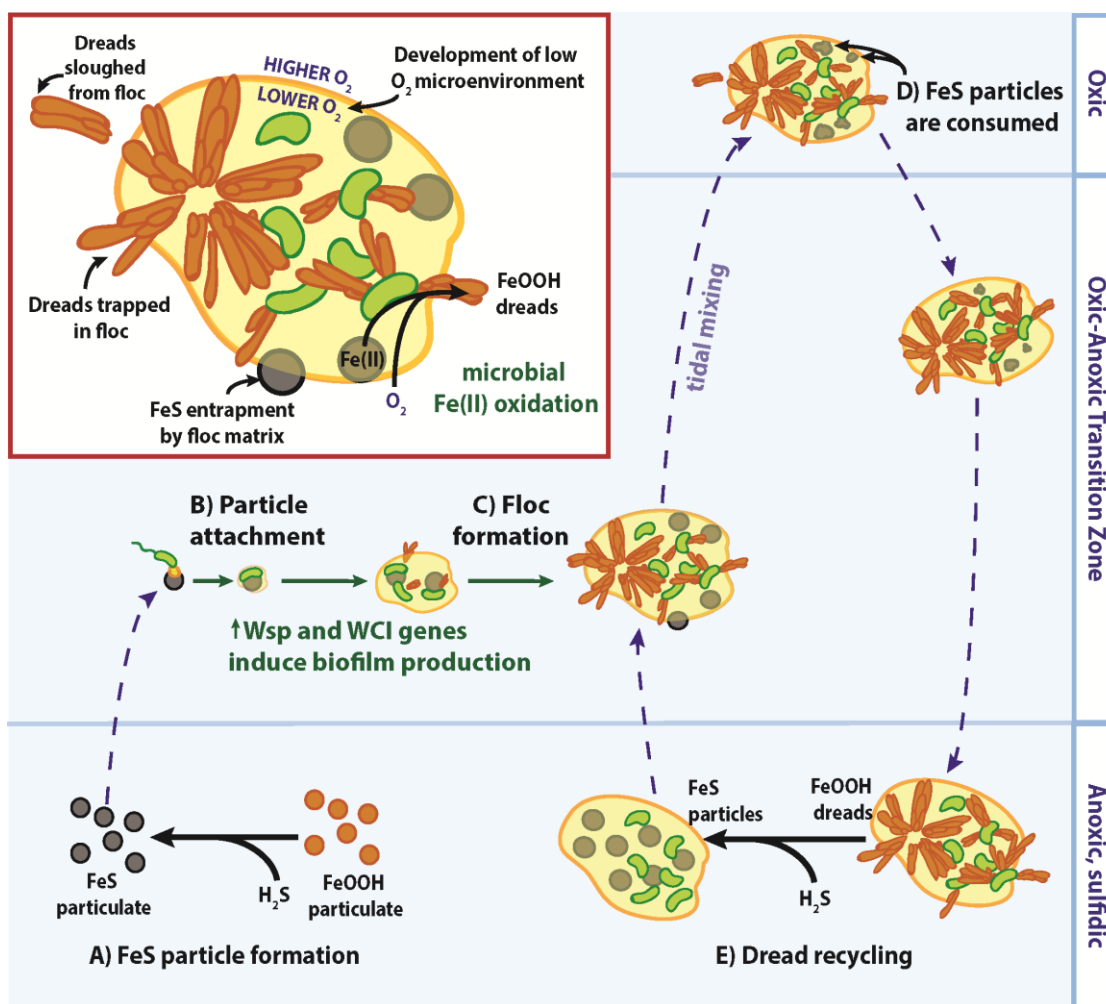


Figure 2.8: Model of CP strain floc formation and interactions with Fe/S biogeochemical cycling in redox-stratified waters. See text for detailed description.

Mariprofundus aestuarium CP-5 and *Mariprofundus ferrinatatus* CP-8 add to the growing number of Zetaproteobacteria isolates that form a closely related phylogenetic cluster despite differing environmental origins and lifestyles. Our analyses suggest that key genes can confer specialized strategies for these organisms to live in diverse environmental niches. If broadly true, the Fe-oxidizing Zetaproteobacteria would be expected to live anywhere that Fe(II) and O₂ are available, and thereby be a widespread driver of marine Fe cycling.

2.4 Species Descriptions

2.4.1 Description of *Mariprofundus aestuarium* sp. nov.

Mariprofundus aestuarium [aes.tu.a'ri.um. L. n. *aestuarium* an estuary].

Cells are slightly curved, short rods ($0.43 \pm 0.05 \mu\text{m} \times 1.01 \pm 0.18 \mu\text{m}$). Does not form spores. Mesophilic and neutrophilic. Microaerobic, growing with opposing gradients of Fe(II) and O₂. Autotrophic. Grows at 10–30°C (optimally at 20–25°C), pH 5.5–8.3 (optimally at pH 6.9–7.2), and 7–31.5‰ salinity (optimally at 14–17.5‰ salinity). Utilizes ferrous iron as an energy source for lithotrophic growth. Does not utilize thiosulfate, sulfide, pyruvate, glucose or acetate as an energy source. Produces extracellular dreadlock-like iron oxides around the cell. The doubling time under optimal conditions is 19.5 h. The type strain is CP-5^T, isolated from redox-stratified waters in the Chesapeake Bay, USA. The total DNA G+C content of the type strain is 51.5 mol%.

2.4.2 Description of *Mariprofundus ferrinatatus* sp. nov.

Mariprofundus ferrinatatus [fer.ri.na'ta.tus. L. neut. n. *ferrum* iron; L. masc. n. *natatus* floating; N.L. masc. n. *ferrinatatus* floating iron].

Cells are slightly curved, short rods ($0.45 \pm 0.04 \mu\text{m} \times 0.91 \pm 0.08 \mu\text{m}$). Does not form spores. Mesophilic and neutrophilic. Microaerobic, growing with opposing gradients of Fe(II) and O₂. Autotrophic. Grows at 15–35°C (optimally at 25–30°C), pH 5.5–8.3 (optimally at pH 6.9–7.2), and 7–31.5‰ salinity (optimally at 14–17.5‰ salinity). Utilizes ferrous iron as an energy source for lithotrophic growth. Does not utilize thiosulfate, sulfide, pyruvate, glucose or acetate as an energy source. Produces extracellular dreadlock-like iron oxides around the cell. The doubling time under optimal conditions is 27 h. The type strain is CP-8^T, isolated from redox-stratified waters in the Chesapeake Bay, USA. The total DNA G+C content of the type strain is 53.7 mol%.

Chapter 3

FE OXIDATION KINETICS OF ZETAPROTEOBACTERIUM *MARIPROFUNDUS FERRINATATUS* CP-8

3.1 Introduction

Studying microbial Fe(II) oxidation kinetics quantifies the potential influence of FeOB on Fe-cycling in the environment. The rate law of Fe(II) oxidation kinetics is as follows:

$$-\frac{d[\text{Fe(II)}]}{dt} = k[\text{Fe(II)}][\text{O}_2][\text{OH}^-]^2 \quad (3.1)$$

where $k = 8.0 \times 10^{13} \text{ L}^2 \text{ mol}^{-2} \text{ atm}^{-1} \text{ min}^{-1}$ at 25°C for abiotic oxidation (Singer and Stumm, 1970). The rate law indicates that abiotic Fe(II) oxidation occurs extremely quickly at circumneutral pH and saturated $[\text{O}_2]$, leading neutrophilic FeOB to occupy low $[\text{O}_2]$ niches where they can efficiently compete against abiotic oxidation for Fe(II). However, little has been done to quantify the effect of different $[\text{O}_2]$ concentrations on microbial Fe(II) oxidation rates, and the upper and lower $[\text{O}_2]$ boundaries that can support FeOB activity are still being studied. Indeed, only one study (Druschel *et al.*, 2008), has measured Fe(II) oxidation rates of a chemolithoautotrophic FeOB, Betaproteobacterium *Sideroxydans lithotrophicus* ES-1, as a function of $[\text{O}_2]$. ES-1 oxidized Fe(II) faster than abiotic Fe(II) oxidation between ~3-50 $\mu\text{M O}_2$, with the fastest microbial Fe(II) oxidation rates measured at 25 $\mu\text{M O}_2$. Such studies help resolve the $[\text{O}_2]$ conditions that support efficient neutrophilic FeOB

activity and also provide insight into the optimal $[O_2]$ for a given FeOB, i.e. the $[O_2]$ yielding the fastest biotic Fe(II) oxidation rates.

Here we investigate the Fe(II) oxidation rates of Zetaproteobacteria *Mariprofundus ferrinatatus* CP-8 through a series of 1 hour-long kinetics experiments conducted in reaction vessels maintained at 5 and 15 $\mu M O_2$. We also estimate Fe(II) oxidation rates based on the rate of iron oxyhydroxide mineral formation during a 9-day growth curve of strain CP-8. Results from the growth curve method were published as part of a study by Field *et al.*, (2016).

3.2 Materials and Methods

3.2.1 Fe(II) Oxidation Kinetics Experiments

To measure the dependence of strain CP-8 Fe(II) oxidation rates on $[O_2]$, kinetics experiments were performed at 5 and 15 $\mu M O_2$. Each experiment included a separate live-cell run to measure biotic rates and an azide-killed-cell run to measure abiotic rates. The purpose of conducting a killed-cell run instead of an uninoculated control to measure abiotic rates was to take into account autocatalysis of Fe(II) oxidation by the Fe oxyhydroxide biominerals associated with the CP-8 cultures being tested.

Strain CP-8 was cultured in petri plates containing sterilized zero valent iron (ZVI; Alfa Aesar CAS# 7439-89-6) and 25 mL liquid estuary medium (composition described in 2.2.1). Estuary medium was buffered with 10 mM MOPS or PIPES and adjusted to pH 6.9-7.2. Plates were incubated under a low O_2 gas mixture ($N_2/CO_2/O_2$; 95:4:1) atmosphere. Strain CP-8 cultures were incubated at room temperature for 2-3 days before use. For each kinetics experiment, 12 plate cultures (300 mL total volume)

were combined, washed with fresh estuary medium, and concentrated by centrifugation to a volume of 84 mL. Any remaining ZVI in the concentrated CP-8 culture was removed using a sterilized magnetic stir bar.

The concentrated CP-8 culture was divided into two aliquots for live-cell and killed-cell runs. The killed-cell aliquot was amended with 3 mM sodium azide. A 2-mL subsample was taken from the live-cell aliquot and used to count cell concentrations. A 2-mL subsample was also removed from the killed-cell aliquot to maintain consistent cell densities between the two aliquots. If cells were not counted immediately, the live-cell subsample was fixed with 4% formaldehyde and stored at 4°C until counting. Subsamples were stained with Syto 13 and directly counted in triplicate using a Petroff-Hausser counting chamber.

Live-cell and killed-cell runs were performed in succession, with live-cell runs first and killed-cell aliquots stored at 4°C until use. Kinetics experiments were conducted at room temperature (~20-25°C) in a reaction vessel consisting of a small glass jar with a plastic screw-top (Figure 3.1). The vessel was designed such that FeOB samples could be continuously stirred and monitored for pH, [O₂], and temperature (Figure 3.1). Holes were drilled in the screw-top of the vessel to allow for reagent addition, a pH meter, and the robust trace oxygen probe and temperature sensor of a Firesting optical oxygen meter (PyroScience, Aachen, Germany). Tubing was also fit through the screw-top, one for gas inlet and one for sampling from the vessel. The pH of experiments was maintained at ~7.25 (MOPS) or 7.02 (PIPES).

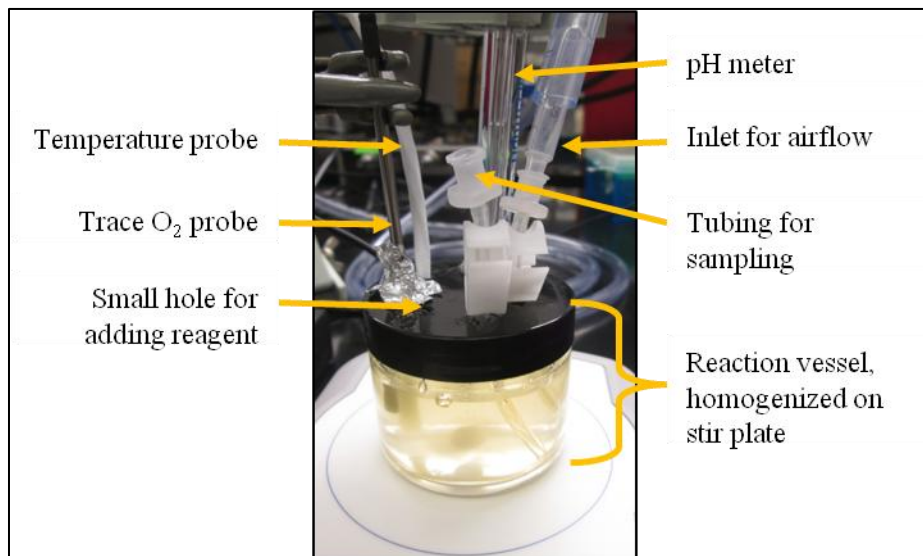


Figure 3.1: Reaction vessel used for strain CP-8 kinetics experiments.

For each kinetics run, the concentrated CP-8 culture (live-cell or killed-cell aliquot) was transferred to the reaction vessel and continuously bubbled with a N_2/O_2 gas mixture to maintain dissolved oxygen concentrations at 5 or 15 $\mu M O_2$. One 0.5 mL syringe-filtered aliquot (0.22 μm nylon membrane syringe filters; Sartorius, Göttingen, Germany) and one 0.5 mL unfiltered aliquot, were sampled from the reaction vessel. These aliquots were immediately acidified 1:1 (V:V) with 40 mM sulfamic acid to stabilize them for later Fe measurements. Though initial concentrations of dissolved Fe(II) in samples for each run were expected to be negligible, initial total Fe concentrations ($[Fe\ total]_{initial}$) were of interest to quantify the amount of iron oxyhydroxide biominerals associated with the CP-8 cultures used for each experiment.

Each kinetics experiment run was begun by spiking the reaction vessel with 150-250 $\mu M FeCl_2$ to induce Fe(II) oxidation. The reaction vessel was sampled, as

described above, just after the Fe(II) spike and then every 7-10 minutes for 60 minutes to measure Fe(II) consumption (oxidation) over time.

3.2.1.1 Ferrozine Assay

Fe(II) concentrations of kinetics experiment samples were measured using a modified version of the ferrozine assay (Stookey *et al.*, 1970). Reduction of unfiltered samples in hydroxylamine (0.12 M final concentration) provided measurements of total Fe, including Fe(II) and Fe(III), the latter likely in the form of solid iron oxyhydroxide minerals. Filtered samples were measured without reduction by hydroxylamine, providing measurements of dissolved Fe(II) concentrations. Analyses were performed in 96-well plates and measured using a Victor 3V 1420 Multilabel Counter (Perkin Elmer, Waltham, MA).

3.2.1.2 Calculating Pseudo First-order Rate Constants (k_1)

Dissolved Fe(II) concentrations over time were used to calculate biotic and abiotic rate constants for Fe(II) oxidation. When O₂ and pH conditions are constant, the Fe(II) oxidation rate law (Equation 3.1) becomes pseudo first-order:

$$-\frac{d[\text{Fe(II)}]}{dt} = k_1 [\text{Fe(II)}] \quad (3.2)$$

Integration of Equation 3.2 yields a linear equation where the pseudo first-order rate constant, k_1 , is the slope:

$$\ln[\text{Fe(II)}] = k_1 t + \ln[\text{Fe(II)}]_0 \quad (3.3)$$

We solved for the rate constants of each kinetics experiment by plotting the natural log of Fe(II) concentrations over time and measuring the slopes of these linear plots. As abiotic Fe(II) oxidation of the killed-cell runs reflects the effects of autocatalysis by

the starting Fe oxyhydroxide biominerals associated with CP-8 cultures, we correct biotic rate constants ($k_{1\text{biotic}}$) measured in live-cell runs by subtracting the abiotic rate constants ($k_{1\text{abiotic}}$) measured in corresponding killed-cell runs. The corrected biotic rate constants ($k_{1\text{biotic}^*}$) are assumed to represent the enzymatic Fe(II) oxidation by strain CP-8.

3.2.2 Fe(II) Oxidation Rates From the Strain CP-8 Growth Curve

A strain CP-8 growth curve was carried out (detailed in 2.2.2), where cell counts and total Fe concentrations were measured in agarose-stabilized gradient tube cultures over 9 days. We plotted biotic and abiotic Fe concentrations from the exponential growth phase (3-7 days after inoculation) and fit second-order polynomial functions to the data. These second-order polynomial functions describe how Fe(II) oxidation rates changed over the course of the exponential growth phase. Using the derivative of each function, we extrapolated instantaneous rates, i.e., the Fe(II) oxidation rate of a single time point. We correct biotic Fe(II) oxidation rates to exclude the contribution of abiotic and autocatalyzed Fe(II) oxidation by subtracting abiotic rates from the biotic rates at each time point.

To convert biotic Fe(II) oxidation rates to per cell rates, we first extrapolated cell numbers based on the calculated growth rate of strain CP-8:

$$N(t) = 4.03 \times 10^6 e^{0.617 * t} \quad (3.4)$$

where N is number of cells at time t . We divided corrected biotic Fe(II) oxidation rates by number of cells for time points 4-6 days after inoculation, yielding a range of maximum per cell Fe(II) oxidation rates by strain CP-8.

3.3 Results and Discussion

3.3.1 Fe(II) Oxidation Kinetics Experiments

A total of five kinetics experiments with strain CP-8 were performed: triplicate experiments at 5 $\mu\text{M O}_2$ (Experiments 1-3) and duplicate experiments at 15 $\mu\text{M O}_2$ (Experiments 4-5). Plots of kinetics experiment data (Figure 3.2) and calculated rate constants (Table 3.1) show that CP-8 accelerates Fe(II) oxidation relative to abiotic processes alone at 5 $\mu\text{M O}_2$, but does not significantly accelerate Fe(II) oxidation at 15 $\mu\text{M O}_2$. Corrected biotic rate constants (k_{biotic^*}) at 5 $\mu\text{M O}_2$ were variable, ranging from 0.001 to 0.007 min^{-1} , and this variation persists even when Fe(II) oxidation rates are normalized per cell (Table 3.1). Variability could be caused by differences in culture activity and/or the inconsistent $[\text{Fe total}]_{\text{initial}}$ in the triplicate experiments. The inconsistencies in $[\text{Fe total}]_{\text{initial}}$ are likely contributors to the variable Fe oxidation rates as the highest $[\text{Fe total}]_{\text{initial}}$, in Experiment 2, corresponds with the highest rate constant values.

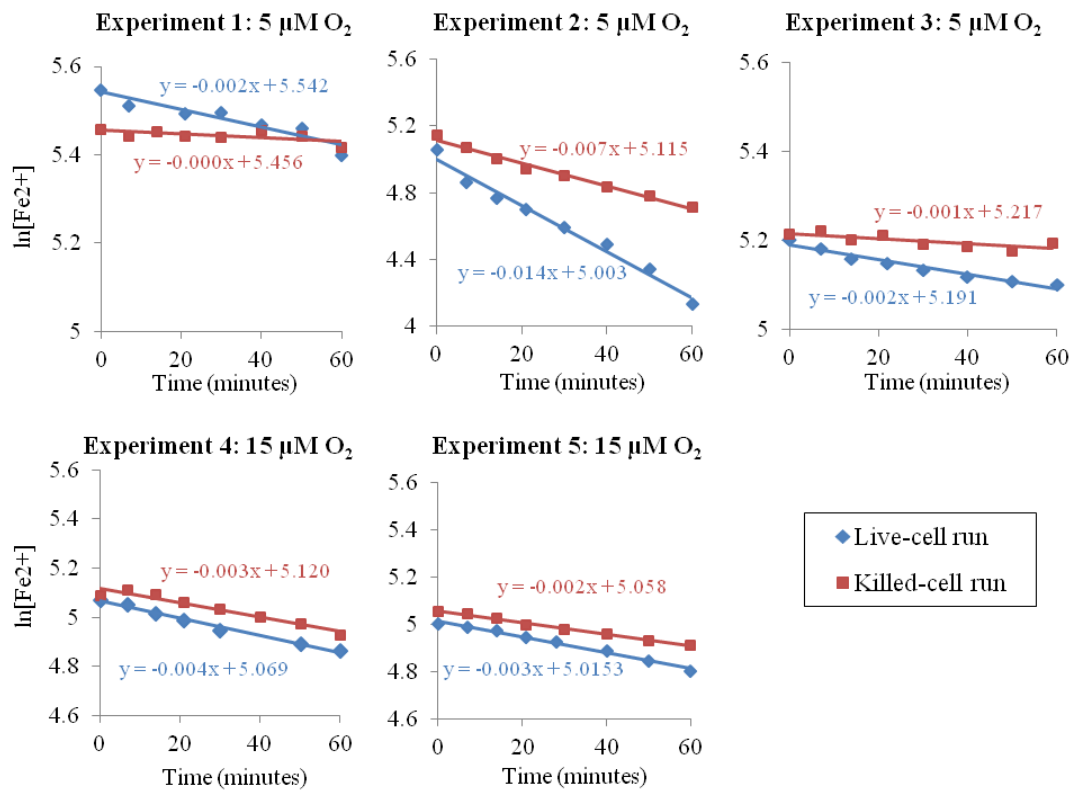


Figure 3.2: Plots of CP-8 kinetics experiment data at 5 and 15 μM O₂. Slopes live-cell run data provide $k_{1\text{biotic}}$ (before correction). Slopes of killed-cell run data provide $k_{1\text{abiotic}}$.

Table 3.1: Summary of CP-8 kinetics experimental conditions and results. O₂, pH, and temperatures are average values of each run.

Exp. #	Run	O ₂ (μM)	pH	Temp. (°C)	[Fe(II)] ₀ (μM)	Cell density (cells/mL)	[Fe total] _{initial} (μM)	k ₁ (min ⁻¹)	k _{1biotic*} (min ⁻¹)	per cell Fe oxidation rate (mol Fe cell ⁻¹ hr ⁻¹)
1	live	5.4	7.2	20.0	256	4.24E+06	411	0.0020	0.0016	5.77E-15
1	killed	5.2	7.2	20.2	235		422	0.0004		
2	live	5.4	7.3	19.8	157	8.73E+06	1666	0.0139	0.0070	7.59E-15
2	killed	5.4	7.3	19.7	172		1618	0.0068		
3	live	5.1	7.0	21.6	182	2.89E+06	223	0.0017	0.0011	4.07E-15
3	killed	5.1	7.0	21.9	184		205	0.0006		
4	live	15.1	7.0	24.7	160	2.46E+06	216	0.0035	0.0006	2.21E-15
4	killed	15.1	7.0	25.4	162		182	0.0030		
5	live	15.2	7.0	25.0	149	3.16E+06	215	0.0033	0.0009	2.43E-15
5	killed	15.2	7.0	25.2	157		199	0.0025		

We compared our strain CP-8 kinetics experiment results to two other FeOB kinetics studies that systematically compared microbial Fe(II) oxidation rates as a function of [O₂]. These studies focused on freshwater Betaproteobacterium *Sideroxydans lithotrophicus* ES-1 (Druschel *et al.*, 2008) and marine Zetaproteobacteria *Mariprofundus ferrooxydans* PV-1 (Gartman *et al.*, unpublished data). Although pH and [O₂] conditions differed among the studies, all experiments were consistent in controlling [O₂], quantifying cell densities, and using azide-killed samples for abiotic controls. Comparing strain CP-8 results to ES-1 and PV-1 contextualizes how quickly CP-8 can oxidize Fe(II) relative to other neutrophilic obligate FeOB.

The values of CP-8 $k_{1biotic*}$ at 5 μM O₂ are lower than those of ES-1 at 9 and 10 μM O₂, the closest tested O₂ concentrations for ES-1 (Table 3.2). Despite the differences in $k_{1biotic*}$ values, CP-8 and ES-1 have similar cell-normalized Fe(II)

oxidation rates, both on the order of 10^{-15} mol Fe cell⁻¹ hr⁻¹ (Table 3.2). The difference in biotic rate constants, yet similarity in per cell Fe(II) oxidation rates may be the result of lower CP-8 cell densities used for kinetics experiments and/or the higher pH of CP-8 experiments, which would accelerate abiotic Fe(II). Per cell Fe(II) oxidation rates suggest that under 5 μ M O₂ conditions, CP-8 can oxidize Fe(II) at a rate similar to ES-1 under 9-10 μ M O₂.

Table 3.2: Comparison of CP-8 Fe(II) oxidation kinetics data to other neutrophilic FeOB.

Organism	<i>Mariprofundus ferrinatatus</i> CP-8		<i>Sideroxydans lithotrophicus</i> ES-1		<i>Mariprofundus ferrooxydans</i> PV-1	
	$k_{1\text{biotic}}^*$ (min ⁻¹)	per-cell rate (mol Fe cell ⁻¹ hr ⁻¹)	$k_{1\text{biotic}}^*$ (min ⁻¹)	per-cell rate (mol Fe cell ⁻¹ hr ⁻¹)	$k_{1\text{biotic}}^*$ (min ⁻¹)	per-cell rate (mol Fe cell ⁻¹ hr ⁻¹)
O₂ (μM)						
5	0.002	5.77×10^{-15}				
5	0.007	7.59×10^{-15}				
5	0.001	4.07×10^{-15}				
9			0.018	5.14×10^{-15}		
10			0.020	5.71×10^{-15}	0.002	5.50×10^{-13}
10					0.002	5.83×10^{-13}
15	0.001	2.21×10^{-15}				
15	0.001	2.43×10^{-15}	0.026	7.43×10^{-15}		
16			0.021	6.00×10^{-15}		
pH		7.0-7.3		6.2		6.6-6.7
Cell density (cell/mL)		$3-9 \times 10^6$		2×10^7		$1-2 \times 10^5$
Reference		This study		Druschel <i>et al.</i> , 2008		Gartman <i>et al.</i> , Unpublished data

The range of biotic rate constants measured at 5 $\mu\text{M O}_2$ for CP-8 includes the biotic rate constants measured for PV-1 in duplicate kinetics experiments at 10 $\mu\text{M O}_2$ (Table 3.2). However, cell-normalized Fe(II) oxidation rates indicate that CP-8 oxidizes Fe(II) at a rate two orders of magnitude slower than PV-1. Here, the difference in per cell rates suggests that PV-1 is metabolically faster or more active than CP-8, which agrees with the difference in doubling time of CP-8 and PV-1: 27 and 12 hours respectively (2.3.1; Emerson *et al.*, 2007). It is also possible that the availability of gaseous CO_2 may have affected the Fe(II) oxidation rates of CP-8 and PV-1. The gas mixture used to maintain $[\text{O}_2]$ in PV-1 kinetics experiments contained CO_2 , while the gas mixture used for CP-8 experiments lacked CO_2 . Though the medium used for CP-8 kinetics experiments contained sodium bicarbonate as an inorganic carbon source, a constant infusion of gaseous CO_2 could have increased strain CP-8 Fe(II) oxidation rates.

3.3.2 Fe(II) Oxidation Rates From the Strain CP-8 Growth Curve

Strain CP-8 was shown to accelerate Fe(II) oxidation in agarose-stabilized gradient tubes compared to uninoculated controls over a 9-day growth curve (Figure 2.2B). From exponential growth phase data, we estimate maximum enzymatic Fe(II) oxidation rates by strain CP-8 to be $1.91\text{-}6.64 \times 10^{-16} \text{ mol Fe cell}^{-1} \text{ hr}^{-1}$. These rates are one order of magnitude slower than those measured by kinetics experiments with strain CP-8 at both 5 and 15 $\mu\text{M O}_2$ (Table 3.1).

The slower biotic Fe(II) oxidation rates from the CP-8 growth curve data may be due to the relatively high amount of abiotic Fe(II) oxidation in the growth experiment compared to the kinetics experiments. Calculations of the biotic contribution to total Fe(II) oxidized in the growth curve experiment indicates that

strain CP-8 only accounted for 26-35% of total Fe(II) oxidation. This range is less than the 51-80% biotic contribution by strain CP-8 during the kinetics experiments at 5 μM O_2 . The discrepancy in abiotic contributions to total Fe(II) oxidation between the growth curve experiment and the kinetics experiments is likely due to the difference in experimental run times. The duration of the growth curve experiment was 9 days, which is much longer than the 1-hour duration of each kinetics experiment. The higher abiotic Fe(II) oxidation in the growth curve experiment likely reflects a much greater autocatalytic effect due to accumulating Fe oxyhydroxides over the 9-day period. In sum, we were able to estimate strain CP-8 Fe(II) oxidation rates from growth curve data, but this method underestimates the Fe(II) oxidation potential of strain CP-8 Fe(II) when compared to kinetics experiment results.

3.4 Conclusions

Overall, CP-8 Fe(II) oxidation rate data indicate that CP-8 accelerates Fe(II) oxidation under microaerophilic conditions compared to abiotic Fe(II) oxidation alone. Of the two methods used to determine Fe(II) oxidation rates, growth curve experiments seemed to underestimate the potential of CP-8 based on the much higher rates measured by kinetics experiments. Considering only the kinetics experiment results, we showed that strain CP-8 significantly increased Fe(II) oxidation at 5 μM O_2 , but not at 15 μM O_2 , suggesting a preference for the lower $[\text{O}_2]$, which agrees with the general preference of neutrophilic FeOB for inhabiting lower O_2 niches.

Chapter 4

EAST PACIFIC RISE CRUISE ACTIVITIES

4.1 Introduction

In hydrothermal settings, anoxic Fe(II)-bearing vent fluids meet oxygenated seawater, forming Fe(II)/O₂ interfaces where neutrophilic FeOB can thrive. Indeed, the first recognized Zetaproteobacteria were isolated from Loihi Seamount (Emerson and Moyer, 2002; Emerson *et al.*, 2007), a hydrothermal site with abundant Fe microbial mats that have provided much insight into the diversity and genetic potential of Zetaproteobacteria (e.g., McAllister *et al.*, 2011; Singer *et al.*, 2013; Field *et al.*, 2015). Besides Loihi, Zetaproteobacteria have also been detected and isolated from rust-colored mats growing at diffuse flow vents proximal to the black smokers of the Mid-Atlantic Ridge (MAR; Scott *et al.*, 2015; Mori *et al.*, in review).

The East Pacific Rise (EPR) at 9°N is another hydrothermal setting with Fe(II)-bearing vent fluids that should theoretically support FeOB. However, the current evidence for Zetaproteobacteria at the EPR is limited to several sequences from metagenomic datasets (Sylvan *et al.*, 2012; Singer *et al.*, 2015). Culturing and further molecular analyses is required for more thorough assessment of Zetaproteobacteria diversity and microbial Fe(II) oxidation potential at the EPR.

The Fe oxidase is still unknown in the Zetaproteobacteria, and neutrophilic FeOB as a whole, but mounting evidence points to Cyc2, an outer membrane cytochrome. Cyc2 has been proven to oxidize Fe(II) in the acidophilic FeOB *Acidithiobacillus ferrooxidans* (Castelle *et al.*, 2008). Support for Cyc2 as the Fe(II)

oxidase in neutrophilic bacteria comes from high expression in Zetaproteobacteria *Mariprofundus ferrooxydans* PV-1 (Barco *et al.*, 2015), as well as its consistent presence in neutrophilic FeOB genomes (e.g., Barco *et al.*, 2015; Kato *et al.*, 2015; Mumford *et al.*, 2016).

If Cyc2 is indeed the neutrophilic Fe(II) oxidase, it could confer Fe(II) oxidation abilities to any bacteria that possess it. Homologs of *cyc2* sequences are found in the genomes of Gammaproteobacteria endosymbionts of two EPR tubeworms, *Riftia pachyptila* and *Tevnia jerichonana* (Gardebrecht *et al.*, 2012), suggesting that these endosymbionts may be capable of Fe(II) oxidation. The endosymbionts of *Riftia pachyptila* and *Tevnia jerichonana* have been found to be of a single phylotype of Gammaproteobacteria known as “*Candidatus* Endoriftia persephone,” (Di Meo *et al.*, 2000). “*Ca.* Endoriftia persephone” is known to oxidize sulfide to fix carbon for its hosts, but these endosymbionts can also assume a free-living state during which their metabolic pathway is less clear (Harmer *et al.* 2008; Klose *et al.*, 2015). Given the presence of *cyc2* sequences in the metagenomes of *Riftia pachyptila* and *Tevnia jerichonana* endosymbionts, we propose that Fe(II) oxidation by Cyc2 may be a metabolic strategy for “*Ca.* Endoriftia persephone” to produce energy in its free-living state.

Given the opportunity to participate in cruise AT37-11 to the East Pacific Rise, we were able to conduct work toward two major objectives. 1) To prove the presence of Zetaproteobacteria at the EPR, we collected samples for enrichment culturing and molecular analysis. 2) To investigate the function of Cyc2 in “*Ca.* Endoriftia persephone,” samples of purified *Riftia* endosymbionts were also used to perform a Fe(II) oxidation and expression experiment.

4.2 Materials and Methods

4.2.1 Sample Collection at East Pacific Rise

Sampling occurred on cruise AT37-11 (March 27 – April 18, 2017) aboard the R/V *Atlantis*. Samples were collected from various East Pacific Rise vent sites between 9°50'N and 9°51'N (Figure 4.1) using DSV Alvin (dives 4877-4892). Samples included *Riftia* tubeworms, rocks covered in rust-colored mats or crusts, flocculent rust-colored mats, and seawater from *Riftia* fields (Table 4.1, Figure 4.1). Different collection vessels were used to transport each sample type to the surface: *Riftia* samples in large bioboxes, rock samples in bioboxes or crates, flocculent mat material in slurp gun containers, and seawater in slurp gun containers or major samplers.

Four sample logs, were compiled to organize details and metadata related to the different samples retrieved, processed, and preserved: 1) Sample Log (Table B1)- records of the samples retrieved by Alvin, 2) Sub-sample Log (Table B2)- records of the subsamples that were preserved for future analyses, 3) Enrichment Log (Table B3)- records of all enrichments performed aboard the cruise, 4) CTD Sample Log- records of CTD water samples used for culturing and experiments.

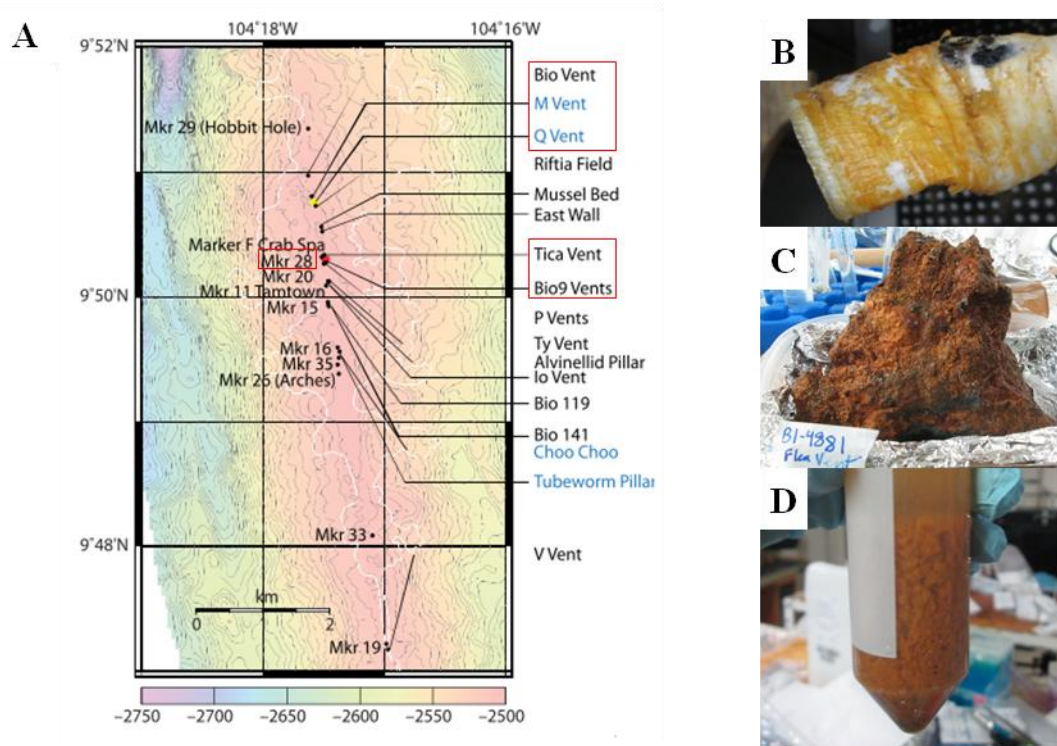


Figure 4.1: A) Site map of EPR at 9°N with sampled vent sites boxed in red (modified from Fornari *et al.*, 2012). Examples of the sample types collected and processed: B) rusty *Riftia* tube, C) rock covered in rust-colored mat and crust, D) flocculent rust-colored mats collected by slurp sampling.

Table 4.1: Summary of samples collected and processed from the EPR.

Sample type	Sample name	Dive #	Site	E-chem scans
<i>Riftia</i>	Riftia1	4877	Bio9	--
	Riftia2	4877	Bio9	--
	Riftia3	4878	Tica	36-44
	Riftia4	4880	Bio9	--
	Riftia5	4880	Biovent	--
	Riftia6	4883	Q Vent	278
	Riftia7	4884	Tica	341-344
	Riftia8	4889	Tica	488-493
Rocks with rust-colored mats and crusts	rock1	4880	Q vent	--
	rock2	4881	Q Vent	225-227
	rock3	4883	Q Vent	275-277
	rock4	4884	Q-vent	321-325
	rock5	4884	Q-vent	321-325
Rust-colored flocculent mats	Flocculent_mat_slurp1	4883	Q vent	275-277
	Flocculent_mat_slurp2	4888	M-Vent	445-447
	Flocculent_mat_slurp3	4889	P-Vent	485-487
	Flocculent_mat_slurp4	4890	M Vent	540
	Flocculent_mat_slurp5	4891	Mkr 28	561-565
Seawater	seawater1	4880	Biovent	--
	seawater2	4887	Tica	--
	seawater3	4888	Biovent	440

Electrochemical (e-chem) scans were taken by an AIS ISEA-IV *in situ* electrochemical analyzer (Analytical Instrument Systems, Inc.) controlled by an operator with a computer in DSV Alvin. E-chem scans provide measurements of *in situ* geochemical conditions (O₂, H₂S, Fe(II), Mn(II), FeS) to accompany collected

samples (Table 4.1). Samples collected on dives 4878, 4887, and 4880 lack accompanying in situ e-chem scans (Table 4.1), but alternate scans, i.e. scans of the same vent site from a different dive, can be used to infer geochemical conditions. For example, e-chem was not performed near the Biovent *Riftia* fields sampled on dive 4880, but e-chem scans of Biovent *Riftia* fields from dive 4878 can be analyzed to provide relevant geochemistry. Although e-chem scans taken at the same time as sampling are preferred for interpreting in situ geochemistry, any single scan may not be entirely representative of overall geochemical conditions as flow geochemistry can fluctuate greatly on the timescale of minutes (Luther *et al.*, 2008). This chemical variability suggests that using alternate e-chem scans for the samples from dives 4878, 4887, and 4880 can provide comparable representation of in situ geochemistry.

Video was recorded on all Alvin dives to provide visual records of sampling. Starboard and portside observers each controlled separate video recording systems yielding two sets of videos per dive. Thus, each sample taken should have two corresponding video files, though only one video file per sample is currently included in my sample log (Table B1). Still frames from the video recording were captured every 30 seconds and compiled in the DSV Alvin Frame-Grabber System. Frame-Grabber data (<http://4dgeo.who.edu/alvin>) provide a convenient visual summary of dive videos.

4.2.2 Rusty *Riftia* Tubes, Rocks, Flocculent Mats, and Seawater Samples

4.2.2.1 Biomass Concentration and Preservation

Samples were processed to obtain biomass for FeOB enrichment cultures and/or molecular analysis as follows: Rusty *Riftia* tubes and rock samples were first

rinsed with 0.22 μm filter-sterilized seawater (except sample rock1), then scraped with a sterile metal spatula to collect visibly rusty-colored material. Sections of two rusty *Riftia* tubes, ~5 cm length each, were also frozen for future Fe extractions. Rust-colored flocculent mat material was allowed to settle out of suspension and then concentrated by removing the seawater supernatant. The fine mesh filter of the slurp container from Flocculent_mat_slurp2 and Flocculent_mat_slurp5 samples was covered with an orange paste-like substance (Figure 4.2), which was collected by scraping with a sterile metal spatula. Seawater samples were filtered using Millipore stericup vacuum filter units (EMD Millipore, Billerica, MA) to collect biomass on the 0.22 μm PES Stericup filter membranes. Filter membranes were cut out of each unit using sterile scalpel blades. Collected biomass was preserved at -70°C for DNA extractions. 12% glycerol or 1:1 (V:V) 2x RNA preservation medium was added to additional subsamples of Flocculent mat slurp2 through 5 before freezing to preserve for culturing or RNA extractions respectively. RNA preservation medium (0.02M EDTA; 0.025M $\text{Na}_3\text{C}_6\text{H}_5\text{O}_7$; 5.30M $(\text{NH}_4)_2\text{SO}_4$; pH 5.2) was prepared, 0.22 μm filter-sterilized, and used like commercially available RNA Later.



Figure 4.2: Orange paste-like material with a goopy texture caught on the slurp container filter in flocculent_mat_slurp2 and flocculent_mat_slurp5.

4.2.2.2 FeOB Enrichment Culturing

Subsamples of all sample types were also used to inoculate FeOB enrichment cultures aboard the ship. Two enrichment culture methods were used: liquid plates with zero valent iron (ZVI; Alfa Aesar CAS# 7439-89-6) and liquid FeS gradient tube cultures (Emerson and Floyd, 2005). Medium for both culture types was 0.22 μm filter-sterilized seawater sampled by CTD. We lacked containers to store >1L seawater at a time, forcing us to use different seawater samples for enrichment media over the course of the cruise. The CTD seawater samples were collected from the oxygen minimum zone (500 and 615 m depth) or bottom waters (2500 m depth) to avoid relatively high organic carbon concentrations of the photic zone that could have preferentially enriched heterotrophs. We chose to adjust seawater to a lower pH to

slow abiotic Fe(II) oxidation rates and provide a kinetic advantage for potential FeOB. Thus seawater medium was buffered with 2 mM NaHCO₃ and 10 mM MES and adjusted to pH 6.0-6.6, with the exception of Flocculent_mat_slurp5 enrichments in which no additional buffer was used and medium pH was 7.5. In some cases, medium was also supplemented with vitamins and trace minerals (1 µL/mL each). See Table B3 for specific culture conditions of individual enrichments.

Liquid plate enrichment cultures consisted of petri plates containing 25-mL seawater medium and sterilized ZVI. One uninoculated abiotic control plate was made for all sets of FeOB enrichments. Plates were incubated at room temperature in GasPak EZ Campy Pouch Systems or GasPak EZ Anaerobe Pouch Systems (BD, Franklin Lakes, NJ). Anaerobic pouches were pricked with a needle to allow O₂ to slowly enter the pouch and create microaerophilic conditions.

Liquid gradient tube cultures consisted of a layer of sterile FeS overlain by ~4-6 mL seawater medium in glass tubes with screw-top caps. One uninoculated abiotic control tube was made for each set of liquid gradient tubes. Tubes were incubated at room temperature.

4.2.2.3 Fe Measurements of Slurp Seawater and Flocculent Mat Slurp

Fe concentrations were measured in two samples: seawater1 and flocculent_mat_slurp_5. Filtered (0.22 µm) and unfiltered aliquots from each sample were acidified with concentrated HCl until Fe measurements. Total Fe(II) concentrations of samples were measured using the ferrozine assay (Stookey *et al.*, 1970). Dissolved Fe(II) concentrations were measured by a modified ferrozine assay, in which samples were not reduced with hydroxylamine before analysis.

Spectrophotometry was performed in 1 cm quartz cells on a Hewlett Packard 8452A Diode Array Spectrophotometer.

4.2.3 *Riftia* Endosymbionts

4.2.3.1 *Riftia* Endosymbiont Purification and Preservation

Once aboard the ship, *Riftia* samples were stored at 4°C until trophosome dissections for endosymbiont purification. Trophosome dissections were performed the same day *Riftia* samples were retrieved except for sample Riftia2, which was processed the morning after collection (less than 24 hrs). All *Riftia* were inspected prior to dissection to exclude worms that were physically damaged during sampling. All but one *Riftia* samples were also confirmed to be alive based on responsiveness to touch. The exception was sample Riftia3, where the worm fell out of its tube when removed from the biobox, but remained undamaged.

Purification of endosymbionts from dissected *Riftia* trophosomes was carried out by Percoll density centrifugation (Distel and Felbeck, 1988) in microcentrifuge tubes. A dounce homogenizer was used to homogenize trophosome tissue in imidazole buffered saline (IBS; 0.49 M NaCl; 0.03 M MgSO₄; 0.011 M CaCl₂; 0.003 M KCl; 0.05 M imidazole; pH 7.0) supplemented with 30% *Riftia* blood. Percoll (GE Healthcare Life Sciences) was diluted with 2.5x concentrated IBS 6:4 (V:V). In microcentrifuge tubes, 500 µL of diluted Percoll was dispensed and overlaid with 500 µL trophosome homogenate (Figure 4.3). Tubes were centrifuged (Eppendorf Centrifuge 5415 C) for 5 minutes at 12,500 rpm (12,752 x g) for Riftia8 and 13,000 rpm (13,793 x g) for all other *Riftia* samples, resulting in dense white pellets of endosymbionts forming at the bottom of tubes. The dark-colored supernatant was

removed from each tube using a pipet or needle syringe, and pellets were washed by re-suspension in IBS and centrifugation at 6000 rpm (2938 x g) for 5 minutes. Endosymbiont samples designated for future proteomics work were further washed in TE buffer. After washing, subsamples of purified endosymbionts were either refrigerated for use as enrichment culture inoculum or frozen at -70°C for future DNA and protein extractions. To minimize oxidative stress on the endosymbionts, trophosome homogenization and endosymbiont purification were carried out in a glove bag flushed with N_2 .

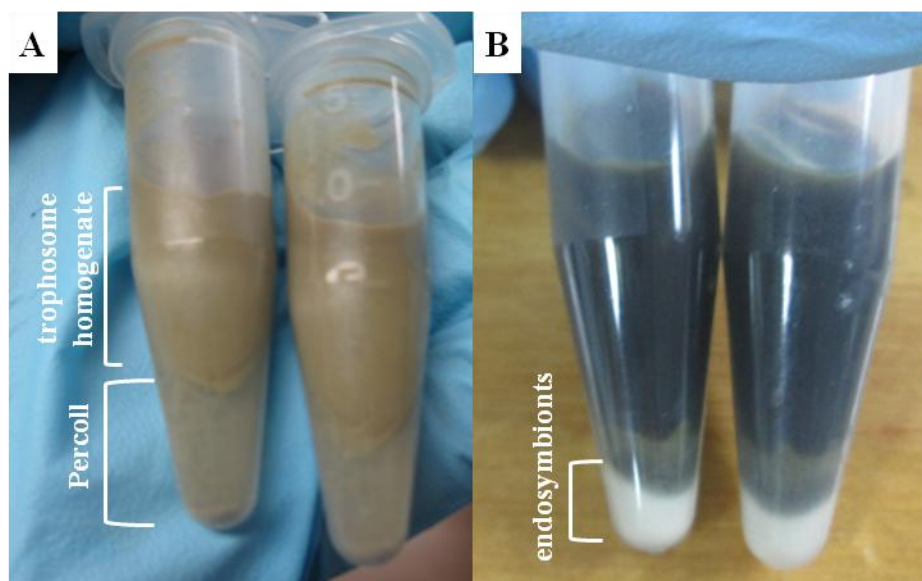


Figure 4.3: Homogenized *Riftia* trophosome before (A) and after (B) Percoll centrifugation.

4.2.3.2 FeOB Enrichment Culturing with Purified *Riftia* Endosymbionts

FeOB enrichment cultures to test *Riftia* endosymbiont growth by Fe(II) oxidation were carried out in liquid plate cultures as described in 3.3.2. For sets of *Riftia* endosymbiont enrichments, additional inoculated control cultures were tested:

killed controls (4% formaldehyde or 3 mM sodium azide) to test if growth was caused by abiotic reactions and plates without ZVI to test usage of non-Fe(II) substrates present in the seawater medium.

4.2.3.3 Fe(II) Oxidation and Expression Experiment

We further investigated potential Fe(II) oxidation metabolism of *Riftia* endosymbionts by conducting a 2 time point kinetics experiment where Fe(II) oxidation was induced by a Fe(II) spike and measured over time. Samples from this experiment were also preserved for future analysis of the expression profiles of *Riftia* endosymbionts before and during Fe(II) oxidation.

The experiment was conducted in seawater medium consisting of CTD seawater (615 m depth), supplemented with 2 mM sodium bicarbonate, 1 $\mu\text{L}/\text{mL}$ of both vitamins and trace minerals, and buffered with 10 mM MES to pH 6.4. Seawater medium was deoxygenated before use by purging with N_2 gas. Five sterile, N_2 -purged 100-mL serum bottles were injected with 40-mL filter-sterilized deoxygenated seawater medium. Four serum bottles were inoculated with 400 μL purified *Riftia* endosymbionts from Riftia8, which had been purified three days before the experiment and stored at 4°C until use. The fifth serum bottle was amended with 400 μL additional seawater medium to serve as an uninoculated abiotic control. O_2 was introduced into all five bottles by injecting each with 5 mL filter-sterilized air. Two inoculated bottles were then spiked 1:1 (V:V) with RNA preservation medium to preserve duplicate endosymbiont expression profiles prior to Fe(II) oxidation.

The remaining three serum bottles, duplicate inoculated biotic samples and one uninoculated abiotic control (Figure 4.4), were spiked with $\sim 150 \mu\text{M}$ FeCl_2 . Each bottle was immediately sampled as follows: 2-mL aliquots of filtered (0.22 μm) and

unfiltered sample were acidified with 100 μ L concentrated HCl to be used for dissolved Fe(II) and total Fe measurements respectively. For 110 minutes, 5 mL filter-sterilized air was injected into all three bottles every ~10-20 minutes (45 mL air total after 110 minutes). After 130 minutes, 2-mL aliquots of filtered (0.22 μ m) sample were taken from all three bottles and acidified with 100 μ L concentrated HCl for measuring final Fe(II) concentrations. The duplicate inoculated biotic samples were then spiked 1:1 (V:V) with RNA preservation medium for preserving duplicate expression profiles during potential Fe(II) oxidation. Fe concentrations of acidified samples were measured using ferrozine as described in 4.2.2.3.

A trial Fe(II) oxidation and expression experiment was performed just before the above procedure was carried out. Details of the experimental procedure can be found in B.1. Although Fe concentrations were not measured for this trial experiment, a biotic sample inoculated with *Riftia* endosymbionts was preserved with RNA preservation medium and can provide an additional expression profile corresponding to potential Fe(II) oxidation.



Figure 4.4: Fe oxidation and expression experiment samples. Uninoculated abiotic control at left and duplicate live samples inoculated with purified endosymbionts from *Riftia*8 at right.

4.3 Results and Discussion

4.3.1 Rusty *Riftia* Tubes, Rocks, Flocculent Mats, and Seawater Samples

4.3.1.1 Biomass Concentration and Preservation

The different biomass samples preserved from rusty *Riftia* tubes, rocks, flocculent mats, and seawater samples are summarized in Table 4.2. Biomass subsamples frozen for DNA extraction are intended for 16S rRNA gene analysis or metagenomics to identify FeOB, namely Zetaproteobacteria, present at the EPR. Detection of free-living *Riftia* endosymbionts in any samples dominated by FeOB

communities would also be of interest to indicate the plausibility of horizontal *cyc2* gene transfer from FeOB to endosymbionts.

Table 4.2: Summary of preserved biomass subsamples by sample name.

Sample name	<i>Riftia</i> tube scraping	seawater biomass filter	mat scraping from rock	flocculent mat	flocculent mat	flocculent mat	slurp filter orange paste
	For DNA extraction	For DNA extraction	For DNA extraction	For DNA extraction	For RNA extraction	For enrichment	For DNA extraction
Riftia4	1	0	0	0	0	0	0
Riftia5	1	0	0	0	0	0	0
Riftia6	2	0	0	0	0	0	0
rock1	0	0	2	0	0	0	0
rock2	0	0	2	0	0	0	0
rock3	0	0	2	0	0	0	0
rock4	0	0	1	0	0	0	0
rock5	0	0	1	0	0	0	0
Flocculent_mat_slurp1	0	0	0	2	0	0	0
Flocculent_mat_slurp2	0	0	0	3	3	2	1
Flocculent_mat_slurp3	0	0	0	2	2	2	0
Flocculent_mat_slurp4	0	0	0	2	2	2	0
Flocculent_mat_slurp5	0	0	0	2	2	2	2
seawater1	0	1	0	0	0	0	0
seawater2	0	1	0	0	0	0	0
seawater3	0	1	0	0	0	0	0

DNA-based analyses will likely show the rust-colored flocculent mat subsamples to be comprised of FeOB-dominated communities given the resemblance of these mats to typical Fe mats produced by FeOB (Chan *et al.*, 2016). Indeed, post-cruise light microscopy of Flocculent_mat_slurp5 revealed that the flocculent mat

material contained structures similar to the tubular sheaths and distinctive twisted iron stalks produced by some Zetaproteobacteria (Figure 4.5; Chan *et al.*, 2016). Though genetic analyses have yet to be performed, macroscopic and microscopic observations of flocculent slurp samples provide strong evidence for the presence of FeOB communities at the EPR. Transcriptome analyses of FeOB-dominated mat samples have the potential to provide Fe(II) oxidation expression profiles, and samples frozen in glycerol can be used for further laboratory enrichment trials.

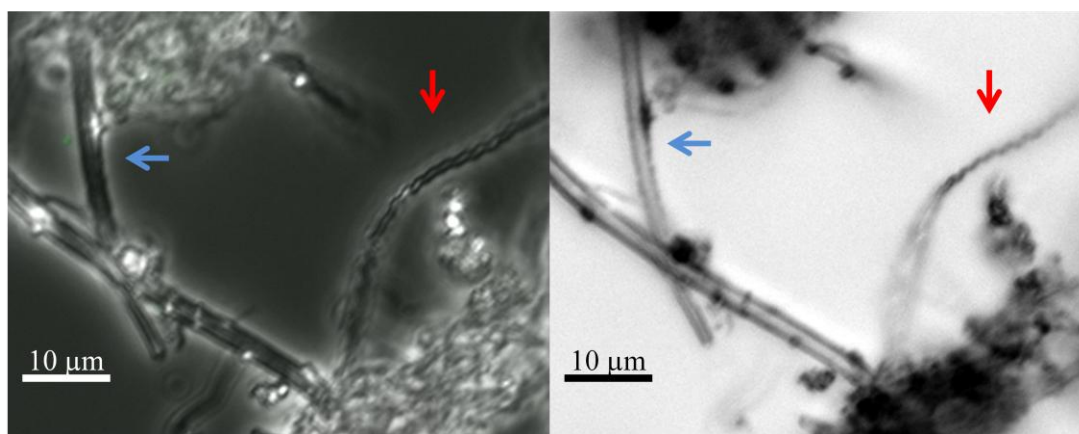


Figure 4.5: Corresponding phase and bright-field micrographs of Flocculent_mat_slurp5, with blue arrows indicating a tubular sheath-like structure and red arrows indicating a twisted stalk-like structure.

4.3.1.2 FeOB Enrichment Culturing

Judgments of growth in enrichment cultures were based on qualitative observations and comparisons to uninoculated abiotic controls, as no microscope was available on the cruise. Of all enrichment cultures inoculated with rusty *Riftia* tube scrapings, rock scrapings, flocculent mats, or seawater, only two FeS gradient tubes inoculated with flocculent_mat_slurp4 displayed conspicuous signs of potential

growth. Potential growth appeared as hazy white material above the FeS layer 4 days after inoculation (Figure 4.6). The hazy white material was harvested and frozen at -70°C, and can be used for 16S rRNA analysis to identify the enriched bacteria. This white material may be composed of FeOB that had not yet oxidized sufficient Fe to display a rusty coloration at the time of preservation. However, given that FeS releases both Fe(II) and sulfide, it is also possible that we enriched sulfur-oxidizing bacteria.

No liquid enrichment plates appeared to yield FeOB growth based on the lack of visual differences between inoculated and uninoculated plates. In cases where the inoculating material was perceptible in liquid plates (rust-colored *Riftia* tube scrapings, rock scrapings, or flocculent mats), inoculum coloration was observed to darken to reddish brown as abiotic oxidation progressed. Overall, the apparent lack of growth in the majority of enrichment cultures may suggest that the samples used as inoculum did not contain active FeOB, enrichment culture conditions were not conducive to robust FeOB growth, or FeOB growth was not apparent by macroscopic observations, i.e. the FeOB did not form flocs. The latter can be analyzed by comparing 16S rRNA analyses between the original sample used as inoculum and the enrichment culture. Therefore, some volume from a representative array of the enrichment cultures was subsampled and frozen despite the lack of conspicuous growth.

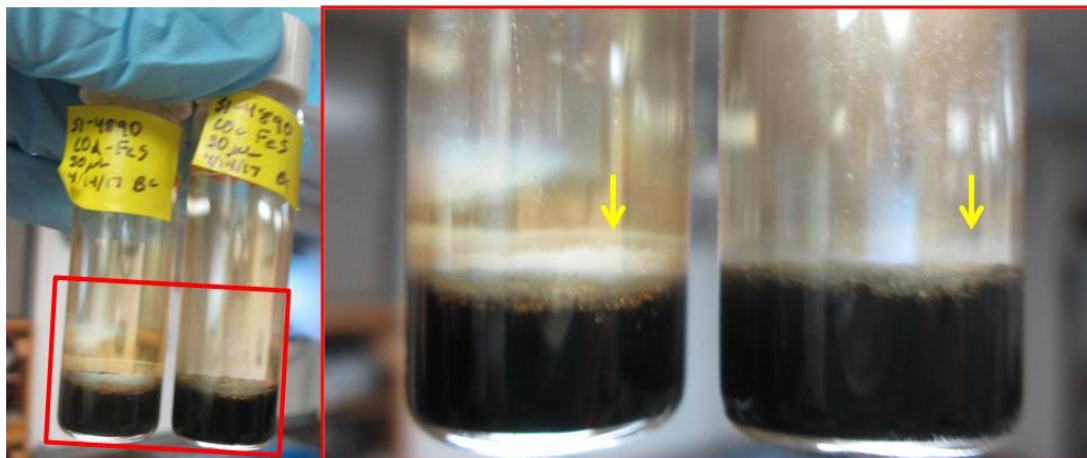


Figure 4.6: Hazy white material (yellow arrows) overlying the black FeS layers in liquid gradient tubes inoculated with Flocculent_mat_slurp4. Image was taken four days after inoculation.

4.3.1.3 Fe Measurements of Slurp Seawater and Flocculent Mat Slurp

For seawater1, concentrations of dissolved Fe(II) and total Fe were 1.6 and 2.4 μM respectively. Dissolved Fe(II) of Flocculent_mat_slurp5 was measured to be 0.8 μM . These Fe concentrations are extremely low, but given the circumneutral pH of the samples (pH 7.3-7.7), the time it took for samples to return to surface, and the fact that these samples were collected in the slurp container rather than a well-sealed water sampler (i.e. major sampler or niskin bottle), it is likely that these Fe measurements are a poor reflection of in situ Fe concentrations. Referring to Fe data from the ferrozine analyses of waters collected by major samplers is recommended.

4.3.2 *Riftia* Endosymbionts

4.3.2.1 *Riftia* Endosymbiont Purification and Preservation

Endosymbionts (white pellets) were successfully purified from five *Riftia*: Riftia1, Riftia2, Riftia3, Riftia5 and Riftia8 (Table 4.3). Riftia7 was dissected, but

trophosome tissue was black and Percoll centrifugation yielded brown pellets instead of white pellets. The black trophosome and brown pellets suggest that these endosymbionts lacked sulfur inclusions and may not have been optimal for further use, so purification of Riftia7 was aborted. Biomass preserved from other *Riftia* worms and potential uses include: whole trophosome tissue for elemental extractions or endosymbiont purification, *Riftia* blood for supplementing medium or other solutions, and *Riftia vestimentum* tissue for extracting *Riftia* DNA (Table 4.3).

Table 4.3: Number of subsamples preserved from dissected *Riftia* samples. Riftia4 and Riftia6 are not included here as they were only sampled for their rusty chitin tubes.

Sample	Whole trophosome	Blood	Vestimentum in 95% ethanol	Purified endosymbionts for DNA extraction	Purified endosymbionts for protein extraction*
Riftia1	2	0	0	1	0
Riftia2	2	1	0	1	0
Riftia3	1	1	0	0	2
Riftia5	1	0	0	0	2
Riftia7	1	0	0	0	0
Riftia8	1	1	1	2	0

*washed in TE buffer before freezing

We plan to perform metagenomic sequencing of the purified *Riftia* endosymbionts to confirm that we successfully purified the endosymbionts, to confirm that these endosymbionts possess *cyc2* sequences, and to assess the genomic neighborhood containing *cyc2* for other genes potentially involved in Fe(II) oxidation. Proteomic analysis of *Riftia* endosymbiont samples may indicate whether or not these organisms were expressing Cyc2 in situ.

4.3.2.2 FeOB Enrichment Culturing with Purified *Riftia* Endosymbionts

Liquid plate cultures inoculated with purified endosymbiont fractions from *Riftia*3 (Tica), *Riftia*5 (Biovent), and *Riftia*8 (Tica), all displayed floc formation, which we interpret as potential signs of growth. These small flocs initially appeared yellowish-white and oxidized to rusty orange with time. Enrichment plates inoculated with purified endosymbionts from *Riftia*3 and *Riftia*5 displayed floc formation within 6-14 hours (Figure 4.7A). The amount of floc did not seem to increase in these plates after 2 days. 4% formaldehyde controls with the purified endosymbionts of *Riftia*3 and *Riftia*5 developed some flocs, but at a slower rate and with less total floc mass compared to the live samples (Figure 4.7B). No-ZVI controls developed some small white flocs, but the total floc mass developed was much less than the live plates. Attempts to transfer flocs from live plates did not yield any apparent floc growth.

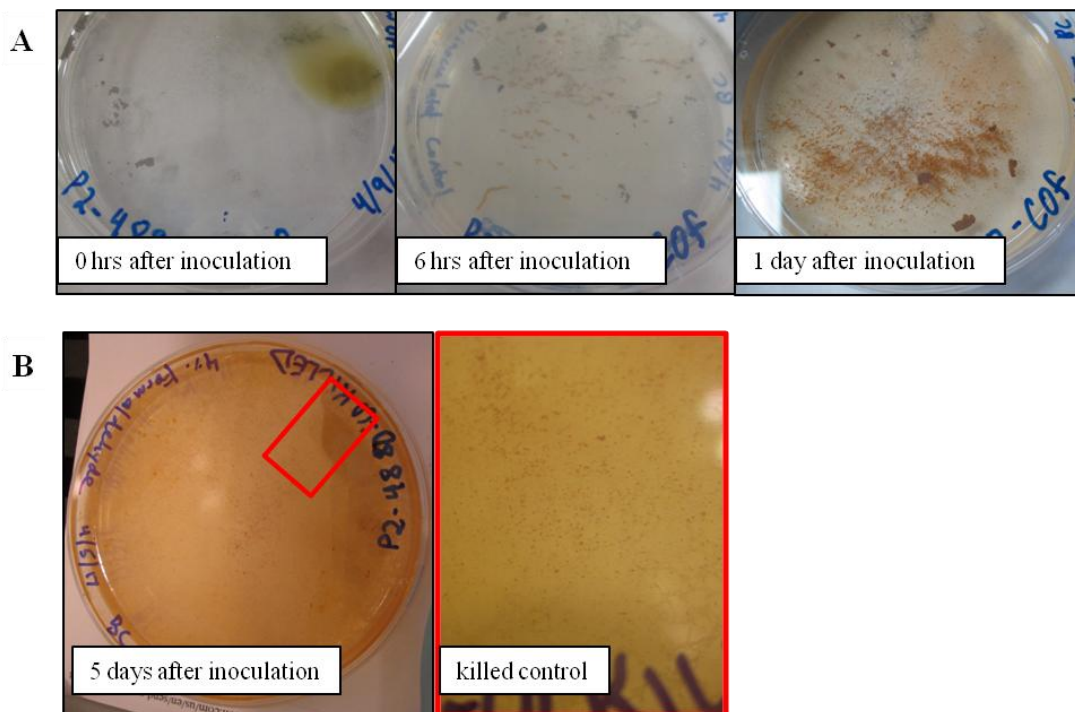


Figure 4.7: Time series of fast floc development in liquid enrichment plate cultures inoculated with purified endosymbionts from Riftia5. B) Only sparse floc development was observed in a corresponding Riftia5 4% formaldehyde-killed control plate.

The floc formation in enrichment plates inoculated with the purified endosymbionts from Riftia8 was different compared to Riftia3 and Riftia5. Floc formation in Riftia8 plates was slower, developing perceptible flocs 2 days after inoculation instead of on the time scale of hours (Figure 4.8A). The flocs themselves seemed to be finer than those developed in the plates of other two endosymbiont samples. Additionally the Riftia8 killed-controls, both 4% formaldehyde and 3 mM sodium azide (Figure 4.8B), seemed to develop flocs at the same pace as live cultures. No-ZVI controls developed some small white floc, but the total floc mass developed was much less than the live samples.

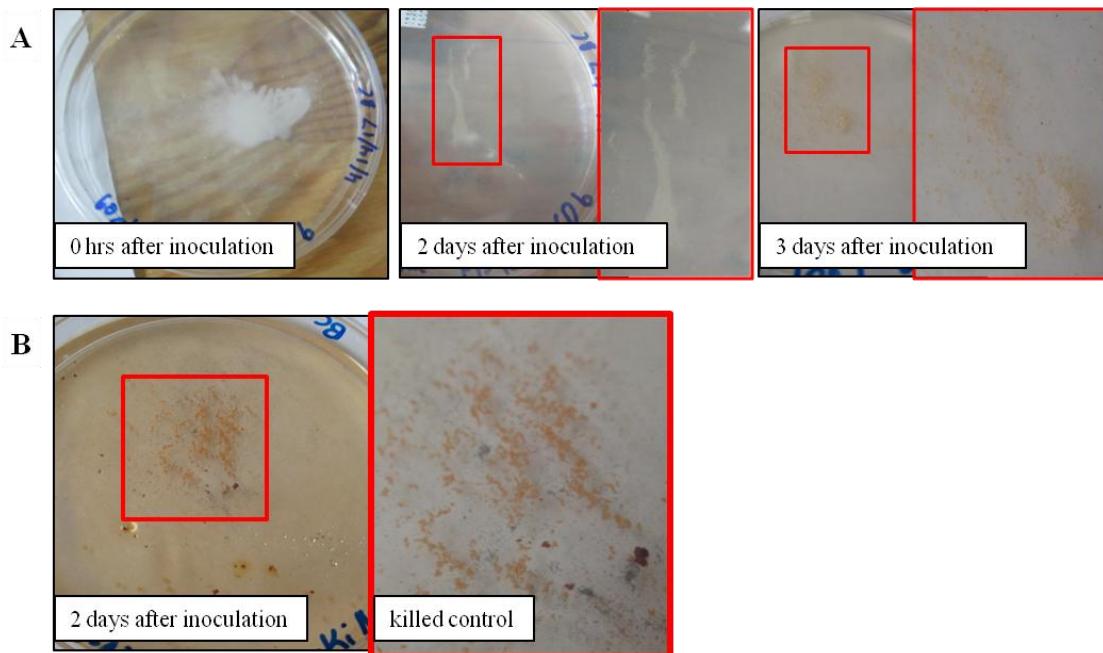


Figure 4.8: A) Time series of slow floc development in liquid enrichment plate cultures inoculated with purified endosymbionts from *Riftia*8. B) Floc development observed in a corresponding *Riftia*8 azide-killed control plate appears similar to the live samples.

Potential reasons for the inconsistent floc formation among the different *Riftia* samples include observed differences in the density gradient produced when processing *Riftia*8, a difference in fitness/activity of the *Riftia*8 endosymbionts, contamination in the endosymbionts used for inoculation, composition differences between the seawater media, or variable amounts of ZVI in the enrichment plates. Regardless, the inconsistent floc formation among different *Riftia* samples, and the observation of floc formation in killed controls of *Riftia*8 cultures prevent us from concluding that these flocs were formed solely by biotic growth. Though it is possible that abiotic processes contributed to floc formation observed in the enrichment plates, it remains likely that biotic growth played a part as well, suggesting that *Riftia* endosymbionts were able to use Cys2 to oxidize Fe(II) for growth.

Subsamples of enriched floc from *Riftia* endosymbiont plates were frozen at -70°C for future DNA extraction (Table 4.4), which can be used for 16S rRNA sequencing to confirm that flocs contain the endosymbionts, or alternately, reveal contamination. Several subsamples of floc were also amended with 12% glycerol or 1:1 (V:V) RNA preservation medium before freezing for future enrichment culturing and RNA extraction respectively (Table 4.4).

Table 4.4: Numbers of preserved subsamples of *Riftia* endosymbiont enrichment floc biomass.

Sample	enrichment floc biomass for DNA	enrichment floc biomass for RNA	enrichment floc biomass for enrichment
Riftia3	2	0	2
Riftia5	4	0	2
Riftia8	0	2	0

4.3.2.3 Fe(II) Oxidation and Expression Experiment

Results from the Fe(II) oxidation kinetics experiment show that Fe(II) concentrations decreased, indicating Fe(II) oxidation, over the experimental duration in the uninoculated abiotic sample and the duplicate biotic samples inoculated with purified endosymbionts from Riftia8. The total amount of Fe(II) oxidized in the duplicate inoculated bottles was nearly 2x greater than in the uninoculated control (Figure 4.9), demonstrating that *Riftia* endosymbionts accelerate the rate of Fe(II) oxidation compared to abiotic processes alone. However, a killed *Riftia* endosymbiont control would be needed to verify that the acceleration of Fe(II) oxidation by inoculated samples was due to enzymatic catalysis rather than abiotic catalysis of Fe(II) oxidation by unknown properties of the seawater medium or the endosymbionts themselves. RNA extractions and expression profiling have yet to be completed, though ideally, they will demonstrate upregulation of *cyc2* in the samples from the second time point, taken during Fe(II) oxidation. A correlation between increased *cyc2* expression and accelerated Fe(II) oxidation in our inoculated samples would suggest that Cyc2 in the *Riftia* endosymbionts is involved in enzymatic catalysis of Fe(II) oxidation.

Fe(II) oxidation and expression experiment

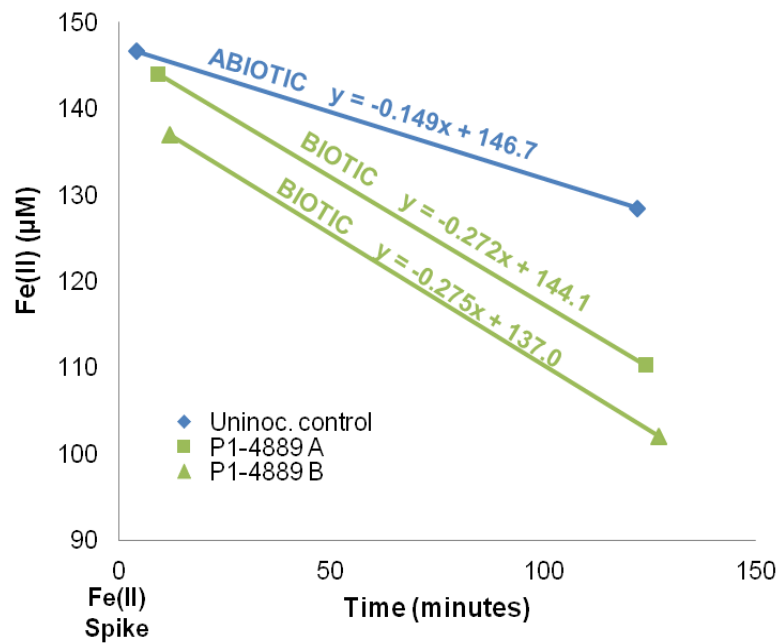


Figure 4.9: Duplicate biotic samples inoculated with purified *Riftia*8 endosymbionts (green) accelerated Fe(II) oxidation in comparison to the uninoculated abiotic control (blue). The times corresponding to each data point reflects the time in minutes after the Fe(II) spike (time 0) that samples were taken.

4.4 Conclusions

The samples collected on cruise AT37-11 provide valuable resources for studying FeOB at the EPR. Microscopy showed that rust-colored flocculent mats from the EPR contained stalk-like structures characteristic of some neutrophilic FeOB, suggesting that we will be able to identify and characterize EPR Zetaproteobacterial communities with DNA-based analyses. Additionally, we observed floc formation in FeOB enrichment cultures of purified *Riftia* endosymbionts and quantitatively showed that these Gammaproteobacteria accelerate Fe(II) oxidation compared to abiotic

oxidation alone. While these results are suggestive that *Riftia* endosymbionts possessing Cyc2 may be capable of Fe(II) oxidation, we plan to further examine this prospect using genomic and transcriptomic analyses. In sum, we expect that these results combined with future analyses will enable identification and characterization of the FeOB present at the EPR.

REFERENCES

- Arai, H., Kawakami, T., Osamura, T., Hirai, T., Sakai, Y., and Ishii, M. (2014). Enzymatic characterization and in vivo function of five terminal oxidases in *Pseudomonas aeruginosa*. *J. Bacteriol.*, 196(24), 4206–4215. doi: 10.1128/JB.02176-14
- Aziz, R. K., Bartels, D., Best, A. A., DeJongh, M., Disz, T., Edwards, R. A., Formsma, K., Gerdes, S., Glass, E. M., Kubal M., Meyer, F., Olsen, G. J., Olson, R., Osterman, A. L., Overbeek, R. A., McNeil, L. K., Paarmann, D., Paczian, T., Parrello, B., Pusch, G. D., Reich, C., Stevens, R., Vassieva, O., Vonstein, V., Wilke, A., and Zagnitko, O. (2008). The RAST Server: rapid annotations using subsystems technology. *BMC Genom.*, 9(75). doi: 10.1186/1471-2164-9-75
- Badger, M. R., and Bek, E. J. (2008). Multiple Rubisco forms in proteobacteria: Their functional significance in relation to CO₂ acquisition by the CBB cycle. *J. Exp. Bot.*, 59(7), 1525–1541. doi: 10.1093/jxb/erm297
- Barco, R. A., Emerson, D., Sylvan, J. B., Orcutt, B. N., Jacobson Meyers, M. E., Ramírez, G. A., Zhong, J. D., and Edwards, K. J. (2015). New insight into microbial iron oxidation as revealed by the proteomic profile of an obligate iron-oxidizing chemolithoautotroph. *Appl. Environ. Microbiol.*, 81(17), 5927–5937. doi: 10.1128/AEM.01374-15
- Bantinaki, E., Kassen, R., Knight, C. G., Robinson, Z., Spiers, A. J., and Rainey, P. B. (2007). Adaptive divergence in experimental populations of *Pseudomonas fluorescens*. III. Mutational origins of wrinkly spreader diversity. *Genetics*, 176(1), 441–453. doi: 10.1534/genetics.106.069906
- Bentzmann, S., Aurouze, M., Ball, G., and Filloux, A. (2006). FppA, a novel *Pseudomonas aeruginosa* prepilin peptidase involved in assembly of type IVb pili. *J. Bacteriol.*, 188(13), 4851–4860. doi: 10.1128/JB.00345-06
- Brezonik, P.L. (1993). *Chemical Kinetics and Process Dynamics in Aquatic Systems*. Boca Raton, FL: CRC Press.

- Cai, W.J., Huang, W.J., Luther, G.W., Pierrot, D., Li, M., Testa, J., Xue, M., Joesoef, A., Mann, R., Brodeur, J., Chen, B., Waldbusser, G.G., Cornwell, J., and Kemp, W.M. Redox reactions and weak buffer capacity lead to acidification in the Chesapeake Bay, *in review*.
- Castelle, C., Guiral, M., Malarte, G., Ledgham, F., Leroy, G., Brugna, M., and Giudici-Ortoni, M.-T. (2008). A new iron-oxidizing/O₂-reducing supercomplex spanning both inner and outer membranes, isolated from the extreme acidophile *Acidithiobacillus ferrooxidans*. *J. Biol. Chem.*, 283(38), 25803–11. doi: org/10.1074/jbc.M802496200
- Chan, C. S., Fakra, S. C., Emerson, D., Fleming, E. J., and Edwards, K. J. (2011). Lithotrophic iron-oxidizing bacteria produce organic stalks to control mineral growth: implications for biosignature formation. *ISME J.* 5(4), 717–727. doi: 10.1038/ismej.2010.173
- Chan, C. S., McAllister, S. M., Leavitt, A. H., Glazer, B. T., Krepski, S. T., and Emerson, D. (2016). The architecture of iron microbial mats reflects the adaptation of chemolithotrophic iron oxidation in freshwater and marine environments. *Front. Microbiol.*, 7, 1–18. doi:10.3389/fmicb.2016.00796
- Charette, M.A., Sholkovitz, E.R., and Hansel, C.M. (2005). Trace element cycling in a subterranean estuary: Part 1. Geochemistry of the permeable sediments. *Geochim. Cosmochim. Acta*, 69(8), 2095–2109. doi: 10.1016/j.gca.2004.10.024
- Christen, M., Christen, B., Allan, M.G., Folcher, M., Jenö, P., Grzesiek, S., Jenal, U. (2007). DgrA is a member of a new family of cyclic diguanosine monophosphate receptors and controls flagellar motor function in *Caulobacter crescentus*. *Proc. Natl. Acad. Sci. U. S. A.*, 104(10), 4112–4117. doi: 10.1073/pnas.0607738104
- Cole, J. R., Wang, Q., Fish, J.A., Chai, B., McGarrell, D.M., Sun, Y., Brown, C.T., Porras-Alfaro, A., Kuske, C.R., and Tiedje, J.M. (2014). Ribosomal Database Project: data and tools for high throughput rRNA analysis. *Nucl. Acids Res.* 42(Database issue), D633–D642. doi: 10.1093/nar/gkt1244
- D'Argenio, D. A., Worth Calfee, M., Rainey, P. B., and Pesci, E. C. (2002). Autolysis and Autoaggregation in *Pseudomonas aeruginosa* Colony Morphology Mutants. *J. Bacteriol.*, 184(23), 6481–6489. doi: 10.1128/JB.184.23.6481

- Dang, H., Chen, R., Wang, L., Shao, S., Dai, L., Ye, Y., Guo, L., Huang, G., and Klotz, M. G. (2011). Molecular characterization of putative biocorroding microbiota with a novel niche detection of Epsilon- and Zetaproteobacteria in Pacific Ocean coastal seawaters. *Environ. Microbiol.*, 13(11), 3059–3074. doi: 10.1111/j.1462-2920.2011.02583.x
- De, N., Navarro, M. V. A. S., Raghavan, R. V., and Sondermann, H. (2009). Determinants for the activation and autoinhibition of the diguanylate cyclase response regulator WspR. *J.Mol. Biol.*, 393(3), 619–633. doi: 10.1016/j.jmb.2009.08.030
- De, N., Pirruccello, M., Krasteva, P. V., Bae, N., Raghavan, R. V., and Sondermann, H. (2008). Phosphorylation-independent regulation of the diguanylate cyclase WspR. *PLoS Biol.*, 6(3), 0601–0617. doi: 10.1371/journal.pbio.0060067
- Decho, A. W. (1990). “Microbial exopolymer secretions in ocean environments: Their role(s) in food webs and marine processes,” in *Oceanography and Marine Biology An Annual Review*, Vol 28, eds H. Barnes and M. Barnes (Aberdeen: Aberdeen University Press), 73-153.
- Di Meo, C. A., Wilbur, A. E., Holben, W. E., Feldman, R. A., Vrijenhoek, R. C., & Cary, S. C. (2000). Genetic Variation among Endosymbionts of Widely Distributed Vestimentiferan Tubeworms. *Appl. Environ. Microbiol.*, 66(2), 651–658.
- Distel, D. L., and Felbeck, H. (1988). Pathways of inorganic carbon fixation in the endosymbiont-bearing lucinid clam *Lucinoma aequizonata* part 1. purification and characterization of the endosymbiotic bacteria. *J. Exp. Zool.*, 247(1), 1–10.
- Druschel, G. K., Emerson, D., Sutka, R., Suchecki, P., & Luther, G. W. (2008). Low-oxygen and chemical kinetic constraints on the geochemical niche of neutrophilic iron(II) oxidizing microorganisms. *Geochim. Cosmochim. Acta*, 72(14), 3358–3370. doi: 10.1016/j.gca.2008.04.035
- Edgar, R. C. (2004). MUSCLE: a multiple sequence alignment method with reduced time and space complexity. *BMC Bioinformatics*, 5(113). doi: 10.1186/1471-2105-5-113.
- Elliott, A. V. C., Plach, J. M., Droppo, I. G., and Warren, L. A. (2014). Collaborative microbial Fe-redox cycling by pelagic floc bacteria across wide ranging oxygenated aquatic systems. *Chem. Geo.*, 366, 90–102. doi: 10.1016/j.chemgeo.2013.11.017

- Emerson D. and Floyd M.M. (2005). Enrichment and isolation of iron-oxidizing bacteria at neutral pH. *Methods Enzymol.*, 397, 112–123. doi: 10.1016/S0076-6879(05)97006-7
- Emerson, D. and Moyer, C. (1997). Isolation and characterization of novel iron-oxidizing bacteria that grow at circumneutral pH. *Appl. Environ. Microbiol.*, 63(12), 4784–4792.
- Emerson, D., and Moyer, C. L. (2002). Neutrophilic Fe-oxidizing bacteria are abundant at the Loihi Seamount hydrothermal vents and play a major role in Fe oxide deposition. *Appl. Environ. Microbiol.*, 68(6), 3085–3093. doi: 10.1128/AEM.68.6.3085-3093.2002
- Emerson, D., Rentz, J. A., Lilburn, T. G., Davis, R. E., Aldrich, H., Chan, C., and Moyer, C. L. (2007). A novel lineage of proteobacteria involved in formation of marine Fe-oxidizing microbial mat communities. *PloS One*, 2(7), e667. doi: 10.1371/journal.pone.0000667
- Emerson, D., and Revsbech, N. P. (1994). Investigation of an iron-oxidizing microbial mat community located near Aarhus, Denmark: Field studies. *Appl. Environ. Microbiol.*, 60(11), 4022–4031.
- Emerson, J. B., Thomas, B. C., Alvarez, W., and Banfield, J. F. (2016). Metagenomic analysis of a high carbon dioxide subsurface microbial community populated by chemolithoautotrophs and bacteria and archaea from candidate phyla. *Environ. Microbiol.*, 18(6), 1686–1703. doi: 10.1111/1462-2920.12817
- Field, E. K., Sczyrba, A., Lyman, A. E., Harris, C. C., Woyke, T., Stepanauskas, R., and Emerson, D. (2015). Genomic insights into the uncultivated marine Zetaproteobacteria at Loihi Seamount. *ISME*, 9(4), 857–870. doi: 10.1038/ismej.2014.183
- Field, E. K., Kato, S., Findlay, A. J., MacDonald, D. J., Chiu, B. K., Luther, G. W., and Chan, C. S. (2016). Planktonic marine iron oxidizers drive iron mineralization under low-oxygen conditions. *Geobiology*, 14(5), 499–508. doi: 10.1111/gbi.12189
- Fleming, E. J., Davis, R. E., Mcallister, S. M., Chan, C. S., Moyer, C. L., Tebo, B. M., and Emerson, D. (2013). Hidden in plain sight: Discovery of sheath-forming, iron-oxidizing Zetaproteobacteria at Loihi Seamount, Hawaii, USA. *FEMS Microbiol. Ecol.*, 85, 116–127. doi: 10.1111/1574-6941.12104

- Flemming, H. C., and Wingender, J. (2001). Relevance of microbial extrapolymeric substances (EPSs)- Part I: structural and ecological aspects. *Water Sci. Technol.*, 43, 1–8.
- Fullerton, H., Hager, K.W., McAllister, S.M., and Moyer, C.L. (2017). Hidden diversity revealed by genome-resolved metagenomics of iron-oxidizing microbial mats from Loihi Seamount, Hawaii. *ISME*, 1-17. doi: 10.1038/ismej.2017.40.
- Gancedo J. M. (2013). Biological roles of cAMP: variations on a theme in the different kingdoms of life. *Biological Reviews*, 88, 645–668.
- Gardebrecht, A., Markert, S., Sievert, S. M., Felbeck, H., Thürmer, A., Albrecht, D., Wollherr, A., Kabisch, J., Le Bris, N., Lehmann, R., Daniel, R., Liesegang, H., Hecker, M., and Schweder, T. (2012). Physiological homogeneity among the endosymbionts of *Riftia pachytila* and *Tevnia jerichonana* revealed by proteogenomics. *ISME J.*, 6(4), 766–76. doi: 10.1038/ismej.2011.137
- Güvener, Z. T., and Harwood, C. S. (2007). Subcellular location characteristics of the *Pseudomonas aeruginosa* GGDEF protein, WspR, indicate that it produces cyclic-di-GMP in response to growth on surfaces. *Mol. Microbiol.*, 66(6), 1459–1473. doi: 10.1111/j.1365-2958.2007.06008.x
- Han, Y., Liu, J., Guo, X., and Li, L. (2012). Micro-environment characteristics and microbial communities in activated sludge flocs of different particle size. *Bioresour. Technol.*, 124(3), 252–258. doi: 10.1016/j.biortech.2012.08.008
- Hansel, C. M., Lentini, C. J., Tang, Y., Johnston, D. T., Wankel, S. D., and Jardine, P. M. (2015). Dominance of sulfur-fueled iron oxide reduction in low-sulfate freshwater sediments. *ISME*, 9(11), 1–13. doi: 10.1038/ismej.2015.50
- Harmer, T. L., Rotjan, R. D., Nussbaumer, A. D., Bright, M., Ng, A. W., DeChaine, E. G., & Cavanaugh, C. M. (2008). Free-living tube worm endosymbionts found at deep-sea vents. *Appl. Environ. Microbiol.*, 74(12), 3895–3898. doi: 10.1128/AEM.02470-07
- He, S., Tominski, C., Kappler, A., Behrens, S., and Roden, E. E. (2016). Metagenomic analyses of the autotrophic Fe(II)-oxidizing, nitrate-reducing enrichment culture KS. *Appl. Environ. Microbiol.*, 82(9), AEM.03493-15. doi: 10.1128/AEM.03493-15
- Hickman, J. W., Tifrea, D. F., and Harwood, C. S. (2005). A chemosensory system that regulates biofilm formation through modulation of cyclic diguanylate levels. *PNAS*, 102(40), 14422–7. doi: 10.1073/pnas.0507170102

- Inoue, T., Tanimoto, I., Ohta, H., Kato, K., Murayama, Y., and Fukui, K. (1998). Molecular characterization of low-molecular-weight component protein, Flp, in *Actinobacillus actinomycescomitans* fimbriae. *Microbiol. Immunol.*, 42(4), 253–258. doi: 10.1111/j.1348-0421.1998.tb02280.x
- James, R. E., and Ferris, F. G. (2004). Evidence for microbial-mediated iron oxidation at a neutrophilic groundwater spring. *Chem. Geol.*, 212, 301–311. doi: 10.1016/j.chemgeo.2004.08.020
- Johnson, J.G., Murphy, C.N., Sippy, J., Johnson, T.J., and Clegg, S. 2011. Type 3 fimbriae and biofilm formation are regulated by the transcriptional regulators MrkHI in *Klebsiella pneumoniae*. *J. Bacteriol.*, 193(14), 3453–3460. doi: 10.1128/JB.00286-11
- Jung, H.B., Charette, M.A., and Zheng, Y. (2009). Field, laboratory, and modeling study of reactive transport of groundwater arsenic in a coastal aquifer. *Environ. Sci. Technol.*, 43(14), 5333–5338. doi: 10.1021/es900080q
- Kachlany, S. C., Planet, P. J., Bhattacharjee, M. K., Kollia, E., DeSalle, R., Fine, D. H., and Figurski, D. H. (2000). Nonspecific adherence by *Actinobacillus actinomycescomitans* requires genes widespread in *Bacteria* and *Archaea*. *J. Bacteriol.*, 182(21), 6169–6176. doi: 10.1128/JB.182.21.6169-6176.2000
- Kachlany, S. C., Planet, P. J., DeSalle, R., Fine, D. H., Figurski, D. H., and Kaplan, J. B. (2001). Flp-1, the first representative of a new pilin gene subfamily, is required for non-specific adherence of *Actinobacillus actinomycescomitans*. *Mol. Microbiol.*, 40(3), 542–554. doi: 10.1046/j.1365-2958.2001.02422.x
- Kato, S., Krepski, S., Chan, C., Itoh, T., and Ohkuma, M. (2014). *Ferriphaselus amnicola* gen. nov., sp. nov., a neutrophilic, stalk-forming, iron-oxidizing bacterium isolated from an iron-rich groundwater seep. *Int. J. Syst. Evol. Microbiol.*, 64, 921–925. doi: 10.1099/ijso.0.058487-0
- Kato, S., Ohkuma, M., Powell, D. H., Krepski, S. T., Oshima, K., Hattori, M., Shapiro, N., Woyke, T., and Chan, C. S. (2015). Comparative genomic insights into ecophysiology of neutrophilic, microaerophilic iron oxidizing bacteria. *Front. Microbiol.*, 6, 1–16. doi: 10.3389/fmicb.2015.01265
- Kato, S., Yanagawa, K., Sunamura, M., Takano, Y., Ishibashi, J. I., Kakegawa, T., Utsumi, M., Yamanaka, T., Toki, T., Noguchi, T., Kobayashi, K., Moroi, A., Kimura, H., Kawarabayashi, Y., Marumo, K., Urabe, T., and Yamagishi, A. (2009). Abundance of Zetaproteobacteria within crustal fluids in back-arc hydrothermal fields of the Southern Mariana Trough. *Environ. Microbiol.*, 11(12), 3210–3222. doi: 10.1111/j.1462-2920.2009.02031.x

- Klose, J., Polz, M. F., Wagner, M., Schimak, M. P., Gollner, S., & Bright, M. (2015). Endosymbionts escape dead hydrothermal vent tubeworms to enrich the free-living population. *Proc. Natl. Acad. Sci.*, *112*(36), 1–6. doi: 10.1073/pnas.1501160112
- Konstantinidis, K. T., and Tiedje, J. M. (2005). Towards a Genome-Based Taxonomy for Prokaryotes. *J. Bacteriol.*, *187*(18), 6258–6264. <http://doi.org/10.1128/JB.187.18.6258>
- Krepski, S. T., Emerson, D., Hredzak-Showalter, P. L., Luther, G. W., and Chan, C. S. (2013). Morphology of biogenic iron oxides records microbial physiology and environmental conditions: toward interpreting iron microfossils. *Geobiology*, *11*(5), 457–71. doi: 10.1111/gbi.12043
- Krepski, S. T., Hanson, T. E., and Chan, C. S. (2012). Isolation and characterization of a novel biomineral stalk-forming iron-oxidizing bacterium from a circumneutral groundwater seep. *Environ. Microbiol.*, *14*, 1671–1680. doi: 10.1111/j.1462-2920.2011.02652.x
- Krumsiek, J., Arnold, R., Rattei, T. (2007). Gepard: a rapid and sensitive tool for creating dotplots on genome scale. *Bioinformatics*, *23*(8), 1026-1028. doi: 10.1093/bioinformatics/btm039
- Kumar, S., Stecher, G., and Tamura, K. (2016). MEGA7: Molecular Evolutionary Genetics Analysis version 7.0 for bigger datasets. *Mol. Biol. Evol.*, *33*(7), 1870-1874. doi: 10.1093/molbev/msw054
- Lane, D. J. (1991). 16S/23S rRNA sequencing. In E. Stackebrandt and M. Goodfellow (Eds.) *Nucleic Acid Techniques in Bacterial Systematics* (115-117). Chichester: Wiley.
- Laufer, K., Nordhoff, M., Halama, M., Martinez, R. E., Obst, M., Nowak, M., Stryhanyuk, H., Richnow, H.H., and Kappler, A. (2017). Microaerophilic Fe(II)-oxidizing Zetaproteobacteria isolated from low-Fe marine coastal sediments – physiology and characterization of their twisted stalks. *Appl. Environ. Microbiol.*, Advance online publication. doi:10.1128/AEM.03118-16
- Laufer, K., Nordhoff, M., Schmidt, C., Behrens, S., Jørgensen, B. B., and Kappler, A. (2016). Co-existence of microaerophilic, nitrate-reducing, and phototrophic Fe(II)-oxidizers and Fe(III)-reducers in coastal marine sediment. *Appl. Environ. Microbiol.*, *82*(5), 1433–1447. doi: 10.1128/AEM.03527-15.Editor

- Liu, J., Wang, Z., Belchik, S. M., Edwards, M. J., Liu, C., Kennedy, D. W., Merkley, E. D., Lipton, M. S., Butt, J. N., Richardson, D. J., Zachara, J. M., Fredrickson, J. K., Rosso, K. M., and Shi, L. (2012). Identification and characterization of M to A: A decaheme *c*-type cytochrome of the neutrophilic Fe(II)-oxidizing bacterium *Sideroxydans lithotrophicus* ES-1. *Front. Microbiol.*, 3(37), 1–11. doi: 10.3389/fmicb.2012.00037
- Luther, G. W., Glazer, B. T., Ma, S., Trouwborst, R. E., Moore, T. S., Metzger, E., Kraiya, C., Waite, T.J., Druschel, G., Sundby, B., Taillefert, M., Nuzzio, D.B., Shank, T.M., Lewis, B.L., and Brendel, P. J. (2008). Use of voltammetric solid-state (micro)electrodes for studying biogeochemical processes: Laboratory measurements to real time measurements with an in situ electrochemical analyzer (ISEA). *Mar. Chem.*, 108, 221–235. doi: 10.1016/j.marchem.2007.03.002
- MacDonald, D. J., Findlay, A. J., McAllister, S. M., Barnett, J. M., Hredzak-Showalter, P., Krepski, S. T., Cone, S. G., Scott, J., Bennett, S. K., Chan, C. S., Emerson, D., and Luther III, G. W. (2014). Using in situ voltammetry as a tool to identify and characterize habitats of iron-oxidizing bacteria: from fresh water wetlands to hydrothermal vent sites. *Environ. Sci. Processes Impacts*, 16(9), 2117–2126. doi: 10.1039/c4em00073k
- Majzlan, J. (2012). "Minerals and aqueous species of iron and manganese as reactants and products of microbial metal respiration," in *Microbial Metal Respiration: From Geochemistry to Potential Applications*, 1st ed., eds. J. Gescher and A. Kappler (Berlin Heidelberg: Springer-Verlag), 1-28.
- Malarte, G., Leroy, G., Lojou, E., Abergel, C., Bruschi, M., and Giudici-Ortoni, M. T. (2005). Insight into molecular stability and physiological properties of the diheme cytochrome CYC41 from the acidophilic bacterium *Acidithiobacillus ferrooxidans*. *Biochemistry* 44(17), 6471–6481
- Malone, J. G., Williams, R., Christen, M., Jenal, U., Spiers, A. J., and Rainey, P. B. (2007). The structure-function relationship of WspR, a *Pseudomonas fluorescens* response regulator with a GGDEF output domain. *Microbiology*, 153(4), 980–994. doi: 10.1099/mic.0.2006/002824-0
- Makita, H., Tanaka, E., Mitsunobu, S., Miyazaki, M., Nunoura, T., Uematsu, K., Takaki, Y., Nishi, S., Shimamura, S., and Takai, K. (2016). *Mariprofundus micogutta* sp. nov., a novel iron-oxidizing zetaproteobacterium isolated from a deep-sea hydrothermal field at the Bayonnaise knoll of the Izu-Ogasawara arc, and a description of *Mariprofundales* ord. nov. and *Zetaproteobacteria* classis nov. *Arch. Microbiol.*, 199(2), 1-12. doi: 10.1007/s00203-016-1307-4

- Markowitz, V. M., Chen, I. M. A., Palaniappan, K., Chu, K., Szeto, E., Grechkin, Y., Ratner, A., Jacob, B., Huang, J., Williams, P., Huntemann, M., Anderson, I., Mavromatis, K., Ivanova, N. N., and Kyrpides, N. C. (2012). IMG: The integrated microbial genomes database and comparative analysis system. *Nucleic Acids Res.*, 40, 115–122. doi: 10.1093/nar/gkr1044
- McAllister, S. M., Davis, R. E., McBeth, J. M., Tebo, B. M., Emerson, D., and Moyer, C. L. (2011). Biodiversity and emerging biogeography of the neutrophilic iron-oxidizing *Zetaproteobacteria*. *Appl. Environ. Microbiol.*, 77(15), 5445–5457. doi: 10.1128/AEM.00533-11
- McAllister, S. M., Barnett, J. M., Heiss, J. W., Findlay, A. J., Macdonald, D. J., Dow, C. L., Luther III, G. W., Michael, H. A., and Chan, C. S. (2015). Dynamic hydrologic and biogeochemical processes drive microbially enhanced iron and sulfur cycling within the intertidal mixing zone of a beach aquifer. *Limnol. Oceanogr.*, 60(1), 329–345. doi: 10.1111/lno.10029
- McBeth, J. M., Little, B. J., Ray, R. I., Farrar, K. M., and Emerson, D. (2011). Neutrophilic iron-oxidizing “Zetaproteobacteria” and mild steel corrosion in nearshore marine environments. *Appl. Environ. Microbiol.*, 77(4), 1405–1412. doi: 10.1128/AEM.02095-10
- Mori, J. F., Scott, J. J., Hager, K. W., Moyer, C. L., Küsel, K., and Emerson, D. Physiological and ecological implications of an iron- or hydrogen-oxidizing member of the Zetaproteobacteria, *Ghiorsea bivora*, gen. nov., sp. nov., *in review*.
- Mumford, A.C., Adaktylou, I.J., and Emerson, D. (2016). Peeking under the Iron Curtain: Development of a microcosm for imaging colonization of steel surfaces by *Mariprofundus* sp. DIS-1, an oxygen tolerant Fe-oxidizing bacterium. *Appl. Environ. Microbiol.*. Advance online publication. doi: 10.1128/AEM.01990-16
- O’Connor, J. R., Kuwada, N. J., Huangyutitham, V., Wiggins, P. A., and Harwood, C. S. (2012). Surface sensing and lateral subcellular localization of WspA, the receptor in a chemosensory-like system leading to c-di-GMP production. *Mol. Microbiol.*, 86(3), 720–729. doi: 10.1111/mmi.12013s
- Officer, C. B., Biggs, R. B., Taft, J. L., Cronin, L. E., Tyler, M. A., and Boynton, W. R. (1984). Chesapeake bay anoxia: origin, development , and significance. *Science*, 223(4631), 22–27.

- Overbeek, R., Olson, R., Pusch, G. D., Olsen, G. J., Davis, J. J., Disz, T., Edwards, R. A., Gerdes, S., Parrello, B., Shukla, M., Vonstein, V., Wattam, A. R., Xia, F., and Stevens, R. (2014). The SEED and the Rapid Annotation of microbial genomes using Subsystems Technology (RAST). *Nucleic Acids Res.*, 42, 206–214. doi: 10.1093/nar/gkt1226
- O'Toole G. A. and Wong G. C. (2016). Sensational biofilms: surface sensing in bacteria. *Curr Opin Microbiol.*, 30, 139–146.
- Parks, D. H., Imelfort, M., Skennerton, C. T., Hugenholtz, P., & Tyson, G. W. (2015). CheckM: assessing the quality of microbial genomes recovered from isolates, single cells, and metagenomes. *Genome Res.*, 25, 1043–1055. <http://doi.org/10.1101/gr.186072.114>
- Planet, P. J., Kachlany, S. C., Fine, D. H., DeSalle, R., and Figurski, D. H. (2003). The Widespread Colonization Island of *Actinobacillus actinomycetemcomitans*. *Nature Genet.*, 34(2), 193–198. doi: 10.1038/ng1154
- Pruesse, E., Peplies, J., and Glöckner, F. O. (2012) SINA: Accurate high-throughput multiple sequence alignment of ribosomal RNA genes. *Bioinformatics.*, 28 (14), 1823-1829. doi: 10.1093/bioinformatics/bts252
- Ryjenkov, D.A., Simm, R., Römling, U., and Gomelsky, M. (2006). The PilZ domain is a receptor for the second messenger c-di-GMP: The PilZ domain protein YcgR controls motility in enterobacteria. *J. Biol. Chem.*, 281(41), 30310–30314. doi: 10.1074/jbc.C600179200
- Scott, J. J., Breier, J. A., Luther III, G. W., & Emerson, D. (2015). Microbial Iron Mats at the Mid-Atlantic Ridge and Evidence that Zetaproteobacteria May Be Restricted to Iron-Oxidizing Marine Systems. *PLoS ONE*, 1–19. Singer, E., Chong, L. S., Heidelberg, J. F., & Edwards, K. J. (2015). Similar microbial communities found on two distant seafloor basalts. *Front. Microbiol.*, 6, 1–11. doi: 10.1371/journal.pone.0119284
- Singer, E., Chong, L. S., Heidelberg, J. F., and Edwards, K. J. (2015). Similar microbial communities found on two distant seafloor basalts. *Front. Microbiol.*, 6, 1–11. doi: 10.3389/fmicb.2015.01409
- Singer, E., Emerson, D., Webb, E. A., Barco, R. A., Kuenen, J. G., Nelson, W. C., Chan, C.S., Comolli, L.R., Ferriera, S., Johnson, J., Heidelberg, J.F., and Edwards, K. J. (2011). *Mariprofundus ferrooxydans* PV-1 the first genome of a marine Fe(II) oxidizing *Zetaproteobacterium*. *PLoS ONE*, 6(9). doi: 10.1371/journal.pone.0025386

- Singer, E., Heidelberg, J. F., Dhillon, A., and Edwards, K. J. (2013). Metagenomic insights into the dominant Fe(II) oxidizing Zetaproteobacteria from an iron mat at Lo'ihī, Hawai'i. *Front. Microbiol.*, 4, 1–9. doi: 10.3389/fmicb.2013.00052
- Singer, P. C., and Stumm, W. (1970). Acidic Mine Drainage: The Rate-Determining Step. *Science*, 167(3921), 1121–1123.
- Skerker, J. M., and Shapiro, L. (2000). Identification and cell cycle control of a novel pilus system in *Caulobacter crescentus*. *EMBO J*, 19(13), 3223–3234.
- Stackebrandt, E., and Goebel, B. M. (1994). Taxonomic note: A place for DNA-DNA reassociation and 16S rRNA sequence analysis in the present species definition in bacteriology. *Int. J. Syst. Bacteriol.*, 44(4), 846–849. doi: 10.1099/00207713-44-4-846
- Stamatakis, A. (2014). RAxML version 8: a tool for phylogenetic analysis and post-analysis of large phylogenies. *Bioinformatics*, 30 (9), 1312-1313. doi: 10.1093/bioinformatics/btu033
- Stookey, L. L. (1970). Ferrozine--a new spectrophotometric reagent for iron. *Anal. Chem.*, 42(7), 779–781. doi: 10.1021/ac60289a016
- Sylvan, J. B., Toner, B. M., and Edwards, K. J. (2012). Life and Death of Deep-Sea Vents : Bacterial Diversity and Ecosystem Succession on Inactive Hydrothermal Sulfides. *mBio*, 3(1), 1–10. doi: 10.1128/mBio.00279-11.
- Thiemermann, S., Dervedde, J., Bernhard, M., Schroeder, W., Massanz, C., and Friederich, B. (1996). Carboxyl-terminal processing of the cytoplasmic NAD-reducing hydrogenase of *Alcaligenes eutrophus* requires the *hoxW* gene product. *J. Bacteriol.*, 178(8), 2368-2374.
- Tomich, M., Fine, D. H., and Figurski, D. H. (2006). The TadV protein of *Actinobacillus actinomycetemcomitans* is a novel aspartic acid prepilin peptidase required for maturation of the Flp1 pilin and TadE and TadF pseudopilins. *J. Bacteriol.*, 188(19), 6899–6914. doi: 10.1128/JB.00690-06
- Tomich, M., Planet, P. J., and Figurski, D. H. (2007). The tad locus: postcards from the widespread colonization island. *Nature Rev. Microbiol.*, 5(5), 363–375. doi: 10.1038/nrmicro1636
- Tran-Betcke, A., Warnecke, U., Böcker, C., Zaborosch, C., and Friedrich, B. (1990). Cloning and nucleotide sequences of the genes for the subunits of NAD-reducing hydrogenase. *J. Bacteriol.*, 172(6), 2920-2929.

- van Veen, W. L., Mulder, E. G., & Deinema, M. H. (1978). The Sphaerotilus-Leptothrix Group of Bacteria. *Microbiol. Rev.s*, 42(2), 329–356.
- Vatter, A. E., and Wolfe, R. S. (1956). Electron microscopy of *Gallionella ferruginea*. *J Bacteriol.*, 72, 248–252.
- White, G.F., Edwards M.J., Gomez-Perez, L., Richardson, D.J., Butt, J.N., and Clarke, T.A. (2016) Chapter Three - Mechanisms of Bacterial Extracellular Electron Exchange. In R.K. Poole (Eds.), *Advances in Bacterial Electron Transport Systems and Their Regulation, Volume 68, Advances in Microbial Physiology* (87-138). Cambridge, MA: Academic Press.
- Wilksch, J.J., Yang, J., Clements, A., Gabbe, J.L., Short, K.R., Cao, H., Cavaliere, R., James, C.E., Whitchurch, C.B., Schembri, M.A., Chuah, M.L., Liang, Z.X., Wijburg, O.L., Jenney, A.W., Lithgow, T., and Strugnell, R.A. (2011). MrkH, a novel c-di-GMP-dependent transcriptional activator, controls *Klebsiella pneumoniae* biofilm formation by regulating type 3 fimbriae expression. *PLoS Pathog.*, 7(8). doi: 10.1371/journal.ppat.1002204
- Yoon, S.H., Ha, S.M., Lim, J., Kwon, S., and Chun, J. (2017). A large-scale evaluation of algorithms to calculate average nucleotide identity. *Antonie van Leeuwenhoek*. doi: 10.1007/s10482-017-0844-4

Appendix A

**SUPPLEMENTARY MATERIAL FOR NOVEL PLANKTONIC IRON-
OXIDIZING ZETAPROTEOBACTERIA FROM THE CHESAPEAKE BAY
OXIC-ANOXIC TRANSITION ZONE**

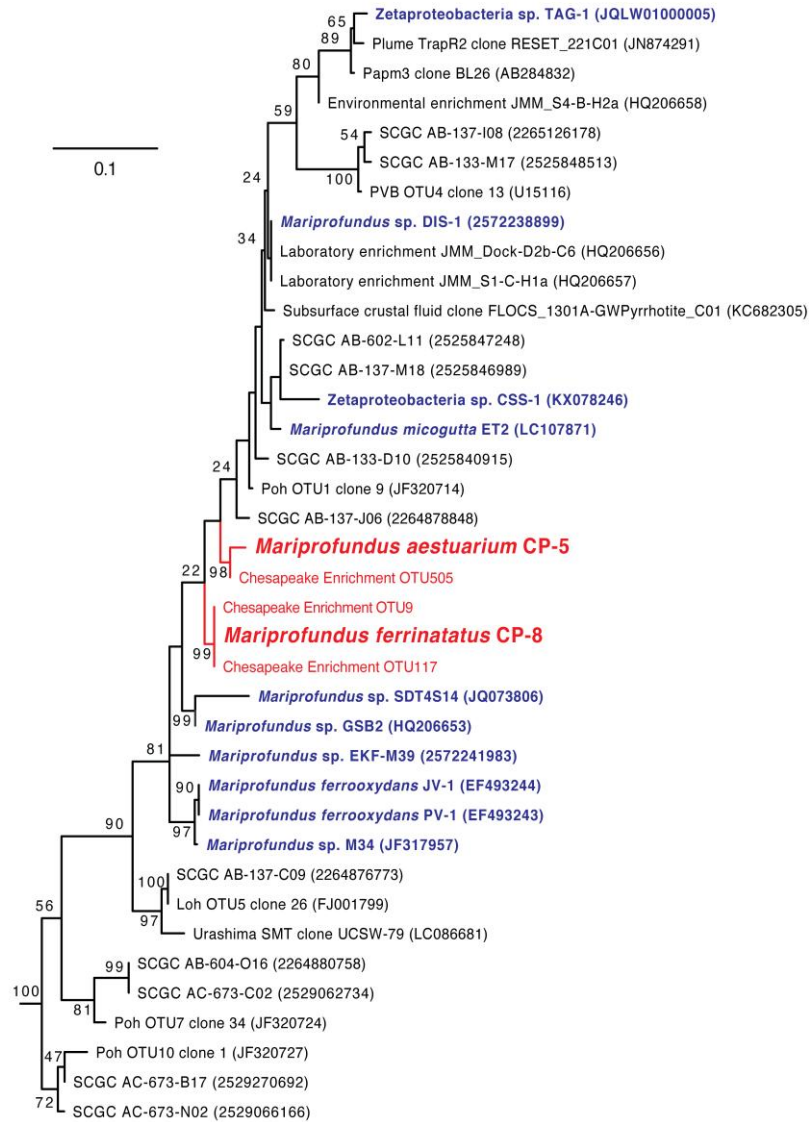


Figure A1: 16S rRNA gene maximum likelihood phylogenetic tree showing that the CP strains cluster with sequences from the original Chesapeake Bay FeOB enrichment (Field *et al.*, 2016), from which the isolates were obtained (Chesapeake sequences highlighted in red). The enrichment sequences represent one partial-length sequence from each of the three detected Zetaproteobacteria OTUs. *Thermotoga maritima* (AJ401021) and *Aquifex pyrophilus* (M83548) were used as the outgroup (not shown). All sequences were masked to 407 bp.

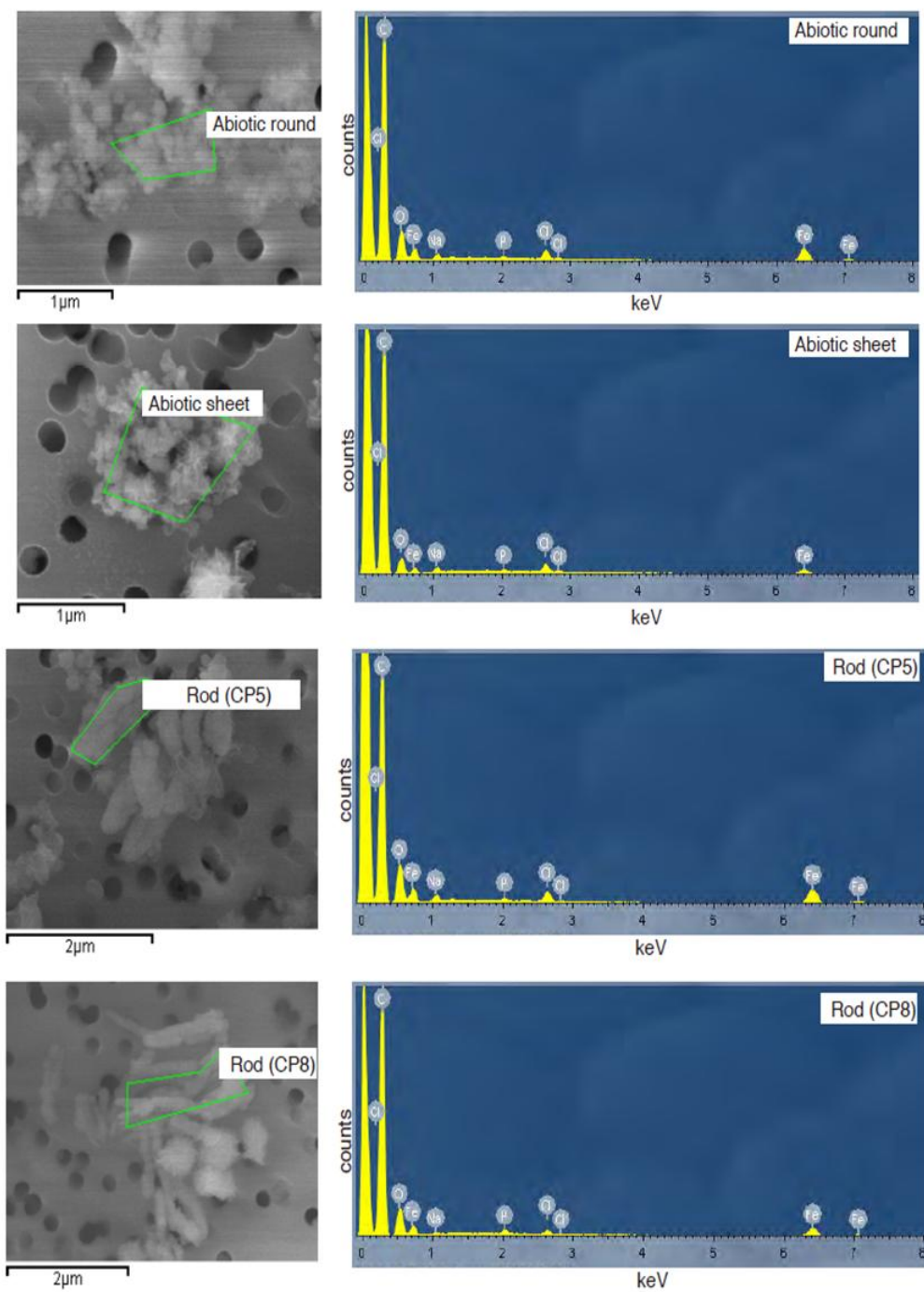


Figure A2: SEM images and corresponding EDX analyses of abiotic iron oxides and CP strain dreads, confirming iron content. Na and Cl are salts from the medium; C is largely from the filter paper substrate.

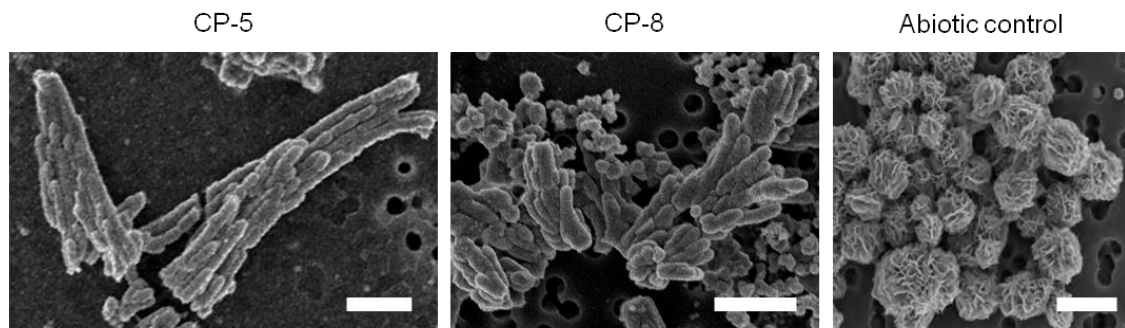


Figure A3: Scanning electron micrographs of iron oxides from strain CP-5, CP-8, and abiotic control cultures. CP strain iron oxides are in the form of dreads, in contrast to the granular iron oxides seen in the abiotic control. Scale bars = 1 μm .

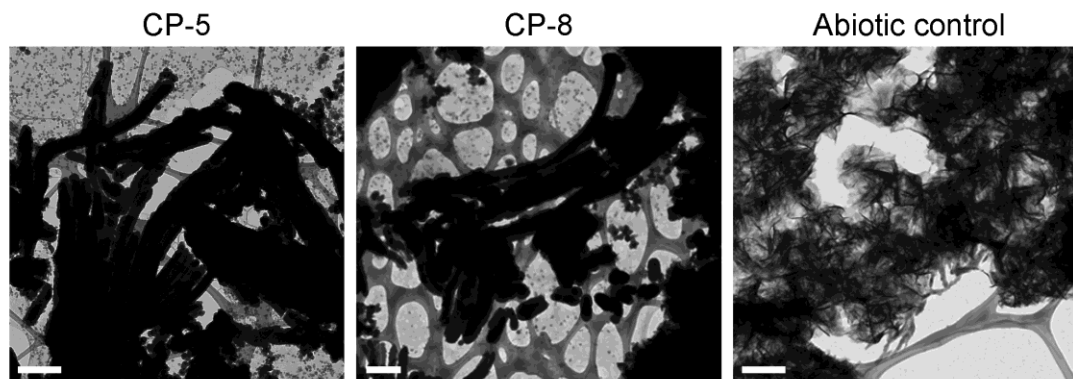


Figure A4: Transmission electron micrographs of iron oxides from strain CP-5, CP-8, and abiotic control cultures. CP strain iron oxides are in the form of dreads in contrast to the more granular iron oxides seen in the abiotic control. Lacey carbon support can be seen in the background. Scale bars = 0.5 μm .

Table A1: Geochemical parameters of the Chesapeake Bay water samples from which strains CP-5 and CP-8 were isolated.

Isolate	Strain CP-5	Strain CP-8
Sampling Profile	CTD12-5	IS8-11.3
Depth (m)	11.4	11.3
Temperature (°C)	25.3	27.1
Salinity (ppt)	17.0	13.6
O ₂ (μM)	0.9	<3
H ₂ S (μM)	<0.2	<0.2
pH	7.4	7.3
Fe(II) Total (μM)	1.36	0.85
Fe(II) Dissolved/ nanoparticulate (μM)	0.41	0
Fe(III) Total (μM)	0.14	0.52
Fe (III) Dissolved/ nanoparticulate (μM)	0.06	0.12

Notes:

Data from Field *et al.*, 2016

Dissolved/nanoparticulate = filtrate through 0.2 μm filter.

Table A2: Comparison of Zetaproteobacteria genome features.

Name	Genome size (Mbp)	Gene count	GC	Protein-coding gene count	IMG genome ID	Genome status (IMG)
<i>Mariprofundus aestuarium</i> CP-5	2.538	2486	51%	2427	2671180110	Finished
<i>Mariprofundus ferrinatatus</i> CP-8	2.302	2288	54%	2237	2671180111	Finished
<i>Mariprofundus micogutta</i> ET2*	2.497	n/a	49%	2417	n/a	n/a
<i>Mariprofundus</i> sp. DIS-1	2.945	2934	49%	2875	2571042359	Permanent Draft
<i>Mariprofundus</i> sp. EKF-M39	2.718	2715	52%	2661	2571042360	Permanent Draft
<i>Mariprofundus ferrooxydans</i> M34	2.736	2733	54%	2684	2513237158	Permanent Draft
<i>Mariprofundus ferrooxydans</i> PV-1	2.867	2920	54%	2866	639857004	Permanent Draft
<i>Mariprofundus ferrooxydans</i> JV-1	2.850	2843	54%	2781	2648501925	Permanent Draft
Zeta proteobacterium SCGC AB-137-I08 (unscreened)	2.049	2392	43%	2340	2265123003	Permanent Draft
Coassembly_Zeta_C09_L23	2.489	2493	48%	2420	2593339174	Permanent Draft
Zetaproteobacteria bacterium TAG-1	2.164	2230	43%	2184	2582580733	Permanent Draft
Zetaproteobacteria bacterium SV108	2.142	2244	43%	2208	2617270712	Draft

*not available on IMG; Genbank genome accession number: BDFD01000059

Table A3: Electron transport genes in the CP strain genomes.

ETC Component	Gene Product Name	CP-5 Locus Tag	CP-8 Locus Tag	e-values against PV-1 sequences
Cyc2	hypothetical protein	Ga0123461_112387		1.00E-73
	hypothetical protein		Ga0123462_112187	4.00E-72
<i>aa₃</i> -type cytochrome <i>c</i> oxidase	cytochrome <i>c</i> oxidase subunit 1	Ga0123461_111687	Ga0123462_11700	
	cytochrome <i>c</i> oxidase subunit 2	Ga0123461_111688	Ga0123462_11699	
	cytochrome <i>c</i> oxidase subunit 3	Ga0123461_111690	Ga0123462_11697	
<i>bc1</i> complex	ubiquinol-cytochrome <i>c</i> reductase cytochrome <i>b</i> subunit	Ga0123461_11969	Ga0123462_111365	
	ubiquinol-cytochrome <i>c</i> reductase cytochrome <i>b/c1</i> subunit/ubiquinol-cytochrome <i>c</i> reductase cytochrome <i>c1</i> subunit	Ga0123461_11970	Ga0123462_111364	
	ubiquinol-cytochrome <i>c</i> reductase iron-sulfur subunit	Ga0123461_11968	Ga0123462_111366	
NADH dehydrogenase	NADH dehydrogenase subunit A	Ga0123461_11443	Ga0123462_111824	
	NADH dehydrogenase subunit B	Ga0123461_11444	Ga0123462_111823	
	NADH dehydrogenase subunit C	Ga0123461_11445	Ga0123462_111822	
	NADH dehydrogenase subunit D	Ga0123461_11446	Ga0123462_111821	
	NADH dehydrogenase subunit E	Ga0123461_11447	Ga0123462_111820	
	NADH dehydrogenase subunit F	Ga0123461_11448	Ga0123462_111819	
	NADH dehydrogenase subunit G	Ga0123461_11449	Ga0123462_111818	
	NADH dehydrogenase subunit H	Ga0123461_11450	Ga0123462_111817	
	NADH dehydrogenase subunit I	Ga0123461_11451	Ga0123462_111816	
	NADH dehydrogenase subunit J	Ga0123461_11452	Ga0123462_111815	
	NADH dehydrogenase subunit K	Ga0123461_11453	Ga0123462_111814	
	NADH dehydrogenase subunit L	Ga0123461_11454	Ga0123462_111813	
	NADH dehydrogenase subunit M	Ga0123461_11455	Ga0123462_111812	
	NADH dehydrogenase subunit N	Ga0123461_11456	Ga0123462_111811	
ATP synthase	ATP synthase F0 subcomplex A subunit	Ga0123461_11512	Ga0123462_111757	
	ATP synthase F0 subcomplex B subunit	Ga0123461_11514	Ga0123462_111755	
	ATP synthase F0 subcomplex C subunit	Ga0123461_11513	Ga0123462_111756	
	ATP synthase F1 subcomplex alpha subunit	Ga0123461_11462	Ga0123462_111805	
	ATP synthase F1 subcomplex beta subunit	Ga0123461_11464	Ga0123462_111803	

Table A3 (cont.): Electron transport genes in the CP strain genomes.

ETC Component	Gene Product Name	CP-5 Locus Tag	CP-8 Locus Tag	e-values against PV-1 sequences
ATP synthase cont.	ATP synthase F1 subcomplex delta subunit	Ga0123461_11461	Ga0123462_111806	
	ATP synthase F1 subcomplex epsilon subunit	Ga0123461_11465	Ga0123462_111802	
ATP synthase cont.	ATP synthase F1 subcomplex gamma subunit	Ga0123461_11463	Ga0123462_111804	
	ATP synthase I chain	Ga0123461_11457	Ga0123462_111810	
Hox NAD-reducing hydrogenase	NAD(P)-dependent nickel-iron dehydrogenase catalytic subunit	Ga0123461_11577	Ga0123462_111691	
	NAD(P)-dependent nickel-iron dehydrogenase flavin-containing subunit	Ga0123461_11580	Ga0123462_111688	
	[NiFe] hydrogenase diaphorase moiety small subunit	Ga0123461_11579	Ga0123462_111689	
	NAD-reducing hydrogenase small subunit hydrogenase maturation protease	Ga0123461_11578 Ga0123461_11576	Ga0123462_111690 Ga0123462_111692	
RNF electron transport complex	electron transport complex protein RnfA	Ga0123461_11559	Ga0123462_111707	
	electron transport complex protein RnfB	Ga0123461_11560	Ga0123462_111706	
	electron transport complex protein RnfC	Ga0123461_11561	Ga0123462_111705	
	electron transport complex protein RnfD	Ga0123461_11562	Ga0123462_111704	
	electron transport complex protein RnfE	Ga0123461_11564	Ga0123462_111702	
	electron transport complex protein RnfG	Ga0123461_11563	Ga0123462_111703	
	cytochrome <i>c</i> peroxidase	cytochrome <i>c</i> peroxidase	Ga0123461_111062	Ga0123462_111273
novel bc complex	Dihaem cytochrome <i>c</i>	Ga0123461_111010	Ga0123462_111321	
	Cytochrome <i>b</i>	Ga0123461_111012	Ga0123462_111319	
Periplasmic cytochrome, potential link between Cyc2 and <i>aa</i> ₃ -type oxidase	cytochrome <i>c</i>	Ga0123461_111656		
	Cytochrome <i>c</i> 2		Ga0123462_111716	

Table A3 (cont.): Electron transport genes in the CP strain genomes.

ETC Component	Gene Product Name	CP-5 Locus Tag	CP-8 Locus Tag	e-values against PV-1 sequences
other genes in neighborhood of a-type cyt <i>c</i> oxidase, including other heme/copper oxidase and other cytochromes	Heme/copper-type cytochrome/quinol oxidase, subunit 1	Ga0123461_111677	Ga0123462_11710	
	Ni,Fe-hydrogenase I cytochrome b subunit	Ga0123461_111678		
	Cytochrome b561		Ga0123462_11709	
Sulfide quinone oxidoreductases	sulfide-quinone oxidoreductase	Ga0123461_111037	Ga0123462_111281	
	sulfide-quinone oxidoreductase		Ga0123462_111295	

Table A4: Carbon-related genes in the CP strain genomes.

Pathway	Gene Product Name	CP-5 Locus Tag	CP-8 Locus Tag
Calvin–Benson– Bassham (CBB) cycle	fructose-bisphosphate aldolase	Ga0123461_111617	Ga0123462_11765
	phosphoglycerate kinase	Ga0123461_111615	Ga0123462_11767
	ribulose 1,5-bisphosphate carboxylase large subunit	Ga0123461_111520	Ga0123462_11892
	ribulose-5-phosphate 3-epimerase	Ga0123461_11967	Ga0123462_111367
	transketolase	Ga0123461_111613	Ga0123462_11769
	fructose-1,6-bisphosphatase II	Ga0123461_111612	Ga0123462_11770
	glyceraldehyde 3-phosphate dehydrogenase	Ga0123461_112433	Ga0123462_112234
	phosphoribulokinase	Ga0123461_112483	Ga0123462_112285
tricarboxylic acid (TCA) cycle	2-oxoglutarate dehydrogenase E1 component	Ga0123461_111820	Ga0123462_11603
	2-oxoglutarate dehydrogenase E2 component	Ga0123461_111819	Ga0123462_11604
	2-oxoglutarate ferredoxin oxidoreductase subunit alpha	Ga0123461_111036	
	2-oxoglutarate ferredoxin oxidoreductase subunit beta	Ga0123461_111035	
	aconitate hydratase	Ga0123461_111667	Ga0123462_11356
	citrate synthase	Ga0123461_112262	Ga0123462_112257
	citrate synthase	Ga0123461_112121	Ga0123462_11258
	dihydrolipoamide dehydrogenase	Ga0123461_112212	Ga0123462_11186
	fumarase, class II	Ga0123461_111540	Ga0123462_11874
	isocitrate dehydrogenase	Ga0123461_111225	Ga0123462_111159
	isocitrate dehydrogenase (NADP)	Ga0123461_111435	Ga0123462_11979
	malate dehydrogenase (NAD)	Ga0123461_111449	Ga0123462_11965
	pyruvate carboxylase subunit A	Ga0123461_11809	Ga0123462_111515
	pyruvate carboxylase subunit B	Ga0123461_11808	Ga0123462_111516
	pyruvate dehydrogenase E1 component alpha subunit	Ga0123461_112215	Ga0123462_11183
	pyruvate dehydrogenase E1 component beta subunit	Ga0123461_112214	Ga0123462_11184
	pyruvate dehydrogenase E2 component (dihydrolipoamide acetyltransferase)	Ga0123461_112213	Ga0123462_11185
	pyruvate ferredoxin oxidoreductase gamma subunit	Ga0123461_11688	Ga0123462_111594
	pyruvate ferredoxin oxidoreductase, alpha subunit	Ga0123461_11687	Ga0123462_111595
	pyruvate ferredoxin oxidoreductase, beta subunit	Ga0123461_11686	Ga0123462_111596
pyruvate-ferredoxin/flavodoxin oxidoreductase	Ga0123461_112208	Ga0123462_11190	
pyruvate-ferredoxin/flavodoxin oxidoreductase	Ga0123461_111567	Ga0123462_11817	
succinate dehydrogenase subunit A	Ga0123461_11963	Ga0123462_111371	

Table A4 (cont.): Carbon-related genes in the CP strain genomes.

Pathway	Gene Product Name	CP-5 Locus Tag	CP-8 Locus Tag
tricarboxylic acid (TCA) cycle cont.	succinate dehydrogenase subunit B	Ga0123461_11964	Ga0123462_111370
	succinate dehydrogenase subunit C	Ga0123461_11961	Ga0123462_111373
	succinate dehydrogenase subunit D	Ga0123461_11962	Ga0123462_111372
	succinyl-CoA synthetase alpha subunit	Ga0123461_111447	Ga0123462_11967
	succinyl-CoA synthetase beta subunit	Ga0123461_111448	Ga0123462_11966
Embden-Meyerhof-Parnas (EMP) pathway	6-phosphofructokinase	Ga0123461_111610	Ga0123462_11772
	enolase	Ga0123461_111980	Ga0123462_11447
	fructose-bisphosphate aldolase	Ga0123461_111617	Ga0123462_11765
	glucokinase	Ga0123461_111602	Ga0123462_11780
	glucose-6-phosphate isomerase	Ga0123461_111600	Ga0123462_11782
	glyceraldehyde 3-phosphate dehydrogenase	Ga0123461_112433	Ga0123462_112234
	phosphoglucomutase	Ga0123461_11991	Ga0123462_111343
	phosphoglycerate kinase	Ga0123461_111615	Ga0123462_11767
	phosphoglycerate mutase	Ga0123461_112097	Ga0123462_11328
pyruvate kinase	Ga0123461_111616	Ga0123462_11766	
Glycogen Metabolism	phosphoglucomutase	Ga0123461_11991	Ga0123462_111343
	glucose-1-phosphate adenylyltransferase	Ga0123461_11990	Ga0123462_111344
	glycogen synthase (ADP-glucose)	Ga0123461_111601	Ga0123462_11781
	1,4-alpha-glucan branching enzyme	Ga0123461_11992	Ga0123462_111342
	glycogen phosphorylase	Ga0123461_111604	Ga0123462_11778
Fermentation Related	pyruvate ferredoxin oxidoreductase, beta subunit	Ga0123461_11686	Ga0123462_111596
	pyruvate ferredoxin oxidoreductase, alpha subunit	Ga0123461_11687	Ga0123462_111595
	pyruvate ferredoxin oxidoreductase gamma subunit	Ga0123461_11688	Ga0123462_111594
	phosphotransacetylase	Ga0123461_11634	Ga0123462_111645
	acetate kinase	Ga0123461_11633	Ga0123462_111646
	Formate C-acetyltransferase	Ga0123461_111184	Ga0123462_111424
	pyruvate formate lyase activating enzyme	Ga0123461_111185	Ga0123462_111425
PTS System Related	Hpr(Ser) kinase/phosphatase	Ga0123461_112342	Ga0123462_11125
	phosphoenolpyruvate--protein phosphotransferase	Ga0123461_112338	Ga0123462_11129
	phosphocarrier protein	Ga0123461_112339	Ga0123462_11128

Table A4 (cont.): Carbon-related genes in the CP strain genomes.

Pathway	Gene Product Name	CP-5 Locus Tag	CP-8 Locus Tag
PTS System Related (cont.)	PTS system, fructose-specific IIC component/PTS system, nitrogen regulatory IIA component	Ga0123461_112343	Ga0123462_11124
	PTS system, mannose-specific IIA component	Ga0123461_112340	Ga0123462_11127

Table A5: Wsp system subunits in the CP strain genomes.

Wsp Subunit	CP-5 Locus Tag	CP-8 Locus Tag
WspA	Ga0123461_11400	Ga0123462_111866
WspB	Ga0123461_11401	Ga0123462_111865
WspC	Ga0123461_11402	Ga0123462_111864
WspD	Ga0123461_11403	Ga0123462_111863
WspE	Ga0123461_11404	Ga0123462_111862
WspF	Ga0123461_11405	Ga0123462_111861
WspR	Ga0123461_11407	Ga0123462_111859
WspR	Ga0123461_11406	Ga0123462_111860

Table A6: WCI genes in the CP strain genomes.

WCI Component	CP-5 Locus Tag	CP-8 Locus Tag
Flp1	Ga0123461_111501	Ga0123462_11910
RcpC	Ga0123461_111502	Ga0123462_11909
RcpB	absent	absent
RcpA	Ga0123461_111503	Ga0123462_11908
TadG	Ga0123461_111505	Ga0123462_11906
TadE	Ga0123461_111506	Ga0123462_11905
TadF?	Ga0123461_111507	Ga0123462_11904
TadZ	Ga0123461_111508	Ga0123462_11903
TadA	Ga0123461_111509	Ga0123462_11902
TadB	Ga0123461_111510	Ga0123462_11901
TadC	Ga0123461_111511	Ga0123462_11900
TadD	Ga0123461_111513	Ga0123462_11898
TadV	absent	absent
Flp2	Ga0123461_111514	absent
PilZ domain-containing protein	Ga0123461_111516	Ga0123462_11896

Appendix B

SUPPLEMENTARY MATERIAL FOR EAST PACIFIC RISE REPORT

B.1 Methods for Trial Fe(II) Oxidation and Expression Experiment with Purified *Riftia* Endosymbionts

The trial Fe(II) oxidation expression experiment was run with only two serum bottles, one inoculated biotic sample and one inoculated abiotic control, set up as described in 4.2.3.3. The trial biotic sample was inoculated with *Riftia* purified endosymbionts just like the actual experiment. The two trial bottles were spiked with ~150 μM FeCl_2 and injected with 4-5 mL filter-sterilized air at intervals between 15-50 minutes over the course of 144 minutes. Every ~30 minutes, 500 μL of 0.22 μm filtered samples from the trial biotic or trial abiotic bottle were taken and transferred into ferrozine tester tubes, which contained ferrozine assay reagents. Qualitative observation for a distinct color difference between samples (indicative of difference in [Fe(II)]) was used to determine an appropriate duration of time for the actual experiment. The trial biotic sample was spiked with RNA preservation medium 1:1 (V:V) at the end of the experiment.

Table B1: Sample Log of all samples retrieved by Alvin on cruise AT37-11 with selected metadata displayed.

Sample name	Dive #	Date (M/D/Y)	Latitude		Longitude		General Location /Site	Alvin collection vessel	E-chem scan #	Alvin video file
			whole degrees	decimal minutes	whole degrees	decimal minutes				
Flocculent_mat_slurp1	4883	4/7/2017	9	50.738	104.000	17.586	Q vent	Slurp	275-277	Stbd AL4883_20170407 165641- 20170407202900
Flocculent_mat_slurp2	4888	4/12/2017	9	50.821	104.000	17.599	M-Vent	Slurp	445-447	Stbd AL4888_20170412 150339- 20170412211940
Flocculent_mat_slurp3	4889	4/13/2017	9	50.275	104.000	17.472	P-Vent	Slurp	485-487	Stbd AL4889_20170413 150807- 2017413151350
Flocculent_mat_slurp4	4890	4/14/2017	9	50.815	104.000	17.597	M Vent	Slurp	540	Port AL4890_20170414 171347- 20170414173018
Flocculent_mat_slurp5	4891	4/15/2017	9	50.178	104.000	17.453	Mkr 28	Slurp	561-565	Stbd AL4891_20170415 144721- 20170415145734
Riftia1	4877	4/1/2017	9	NA	104.000		Bio9	Biobox	--	Stbd AL4877_20170401 192226- 20170401201947
Riftia2	4877	4/1/2017	9	NA	104.000		Bio9	Biobox	--	Stbd AL4877_20170401 192226- 20170401201947
Riftia3	4878	4/2/2017	9	50.400	104.000	17.503	Tica	Biobox	36-44	Stbd AL4878_20170402 190024- 20170402212436
Riftia4	4880	4/4/2017	9	50.293	104.000	17.478	Bio9	Biobox	--	Port AL4880_20170404 151319- 20170404205715
Riftia5	4880	4/4/2017	9	50.961	104.000	17.623	Biovent	Biobox	--	Port AL4880_20170404 151319- 20170404205715

Table B1 (cont.): Sample Log of all samples retrieved by Alvin on cruise AT37-11 with selected metadata displayed.

Sample name	Dive #	Date (M/D/Y)	Latitude		Longitude		General Location /Site	Alvin collection vessel	E-chem scan #	Alvin video file
			whole degrees	decimal minutes	whole degrees	decimal minutes				
Riftia6	4883	4/7/2017	9	50.740	104.000	17.586	Q Vent	Biobox	278	Stbd AL4883_20170407 165641- 20170407202900
Riftia7	4884	4/8/2017	9	50.538	104.000	17.505	Tica	Biobox	341-344	stbd AL4884_20170408 185243- 20170408212151
Riftia8	4889	4/13/2017	9	50.403	104.000	17.490	Tica	Biobox	488-493	Stbd AL4889_20170413 155526- 20170413162815
rock1	4880	4/4/2017	9	50.794	104.000	17.594	Q vent	Crate	--	Port AL4880_20170404 151319- 20170404205715
rock2	4881	4/5/2017	9	50.739	104.000	17.591	Q Vent	?	225-227	Port AL4881_20170405 175838- 20170405181707
rock3	4883	4/7/2017	9	50.738	104.000	17.586	Q Vent	Biobox	275-277	Stbd AL4883_20170407 165641- 20170407202900
rock4	4884	4/8/2017	9	50.743	104.000	17.585	Q-vent	Biobox	321-325	Stbd AL8884_20170408 153922- 20170408185242
rock5	4884	4/8/2017	9	50.743	104.000	17.585	Q-vent	Crate	321-325	Stbd AL8884_20170408 153922- 20170408185242
seawater1	4880	4/4/2017	9	50.956	104.000	17.615	Biovent	Slurp	--	Port AL4880_20170404 151319- 20170404205715
seawater2	4887	4/11/2017	9	50.415	104.000	17.502	Tica	Major	--	AL4887_20170411 145449- 20170411204356

Table B1 (cont.): Sample Log of all samples retrieved by Alvin on cruise AT37-11 with selected metadata displayed.

Sample name	Dive #	Date (M/D/Y)	Latitude		Longitude		General Location /Site	Alvin collection vessel	E-chem scan #	Alvin video file
			whole degrees	decimal minutes	whole degrees	decimal minutes				
seawater3	4888	4/12/2017	9	50.968	104.000	17.615	Biovent	Major	440	Sibd AL4888_20170412 150339- 20170412211940

Table B2: Subsample Log of all subsamples preserved for future analyses with selected metadata displayed.

Sample name	Subsample name	Subsample type	Intended use	Amendment/treatment for preservation	approx. volume (mL)	Storage temp. (°C)
Flocculent_mat_slurp1	S1-4883a	rusty flocculent mat from slurp	DNA_extraction	none	1	-70
Flocculent_mat_slurp1	S1-4883b	rusty flocculent mat from slurp	DNA_extraction	none	1	-70
Flocculent_mat_slurp1	S1-4883-C0a-D	enrichment biomass	DNA_extraction	none	1.5	-70
Flocculent_mat_slurp1	S1-4883-C0a-FeS-D	enrichment biomass	DNA_extraction	none	1.5	-70
Flocculent_mat_slurp2	S1-4888-Da	orange goopy paste caught on slurp filter	DNA_extraction	none	0.1	-70
Flocculent_mat_slurp2	S1-4888-Db	rusty flocculent mat from slurp	DNA_extraction	none	1	-80
Flocculent_mat_slurp2	S1-4888-Dc	rusty flocculent mat from slurp	DNA_extraction	none	1	-70
Flocculent_mat_slurp2	S1-4888-Dd	rusty flocculent mat from slurp	DNA_extraction	none	1	-70
Flocculent_mat_slurp2	S1-4888-CG a	rusty flocculent mat from slurp	enrichment	glycerol-12%	1	-70
Flocculent_mat_slurp2	S1-4888-CGb	rusty flocculent mat from slurp	enrichment	glycerol-12%	1	-70
Flocculent_mat_slurp2	S1-4888-Ra	rusty flocculent mat from slurp	transcriptomics	RNA preservation medium(1:1)	0.5	-70
Flocculent_mat_slurp2	S1-4888-Rb	rusty flocculent mat from slurp	transcriptomics	RNA preservation medium(1:1)	0.5	-70
Flocculent_mat_slurp2	S1-4888-Rc	rusty flocculent mat from slurp	transcriptomics	RNA preservation medium(1:1)	0.5	-70
Flocculent_mat_slurp2	S1-4888-C0a-D	enrichment biomass	DNA_extraction	none	1.5	-70
Flocculent_mat_slurp3	S1-4889-C0a-D	enrichment biomass	DNA_extraction	none	1.5	-70
Flocculent_mat_slurp3	S1-4889- CGa	rusty flocculent mat from slurp	enrichment	glycerol-12%	0.5	-70
Flocculent_mat_slurp3	S1-4889-CGb	rusty flocculent mat from slurp	enrichment	glycerol-12%	0.5	-70
Flocculent_mat_slurp3	S1-4889-Ra	rusty flocculent mat from slurp	transcriptomics	RNA preservation medium(1:1)	1	-70
Flocculent_mat_slurp3	S1-4889-Rb	rusty flocculent mat from slurp	transcriptomics	RNA preservation medium(1:1)	1	-70
Flocculent_mat_slurp3	S1-4889-Da	rusty flocculent mat from slurp	DNA_extraction	none	1	-70
Flocculent_mat_slurp3	S1-4889-Db	rusty flocculent mat from slurp	DNA_extraction	none	1	-70
Flocculent_mat_slurp3	S1-4889-Dc	rusty flocculent mat from slurp	NA	none	NR	4

Table B2 (cont.): Subsample Log of all subsamples preserved for future analyses with selected metadata displayed.

Sample name	Subsample name	Subsample type	Intended use	Amendment/treatment for preservation	approx. volume (mL)	Storage temp. (°C)
Flocculent_mat_slurp4	S1-4890- CGa	rusty flocculent mat from slurp	enrichment	glycerol-12%	1	-70
Flocculent_mat_slurp4	S1-4890-CGb	rusty flocculent mat from slurp	enrichment	glycerol-12%	1	-70
Flocculent_mat_slurp4	S1-4890-Ra	rusty flocculent mat from slurp	transcriptomics	RNA preservation medium(1:1)	1	-70
Flocculent_mat_slurp4	S1-4890-Rb	rusty flocculent mat from slurp	transcriptomics	RNA preservation medium(1:1)	1	-70
Flocculent_mat_slurp4	S1-4890-Da	rusty flocculent mat from slurp	DNA_extraction	none	1.2	-70
Flocculent_mat_slurp4	S1-4890-Db	rusty flocculent mat from slurp	DNA_extraction	none	1.2	-70
Flocculent_mat_slurp4	S1-4890-C0b-FeS-D	enrichment biomass	DNA_extraction	none	1.5	-70
Flocculent_mat_slurp4	S1-4890-C0c-FeS-D	enrichment biomass	DNA_extraction	none	1.5	-70
Flocculent_mat_slurp4	S1-4890-C0d-FeS-D	enrichment biomass	DNA_extraction	none	1.5	-70
Flocculent_mat_slurp5	S1-4891- CGa	rusty flocculent mat from slurp	enrichment	glycerol-12%	1	-70
Flocculent_mat_slurp5	S1-4891 -CGb	rusty flocculent mat from slurp	enrichment	glycerol-12%	1	-70
Flocculent_mat_slurp5	S1-4891-Ra	rusty flocculent mat from slurp	transcriptomics	RNA preservation medium(1:1)	1	-70
Flocculent_mat_slurp5	S1-4891-Rb	rusty flocculent mat from slurp	transcriptomics	RNA preservation medium(1:1)	1	-70
Flocculent_mat_slurp5	S1-4891-Da	orange goopy paste caught on slurp filter	DNA_extraction	none	1.5	-70
Flocculent_mat_slurp5	S1-4891-Db	orange goopy paste caught on slurp filter	DNA_extraction	none	1.5	-70
Flocculent_mat_slurp5	S1-4891-Dc	rusty flocculent mat from slurp	DNA_extraction	none	1.3	-80
Flocculent_mat_slurp5	S1-4891-Dd	rusty flocculent mat from slurp	DNA_extraction	none	1.3	-70
Flocculent_mat_slurp5	S1-4891-C0a-D	enrichment biomass	DNA_extraction	none	1.5	-70
Riftia1	P1-4877-D	purified endosymbionts	DNA_extraction	none	0.2	-70
Riftia1	W1-4877a	whole trophosome	NA	NA	NR	-70
Riftia1	W1-4877b	whole trophosome	NA	NA	NR	-70
Riftia2	R2-4877-BLOOD	blood, Riftia	NA	NA	20	-70
Riftia2	P2-4877-D	purified endosymbionts	DNA_extraction	none	0.5	-70

Table B2 (cont.): Subsample Log of all subsamples preserved for future analyses with selected metadata displayed.

Sample name	Subsample name	Subsample type	Intended use	Amendment/treatment for preservation	approx. volume (mL)	Storage temp. (°C)
Riftia2	W2-4877a	whole trophosome	NA	NA	NR	-70
Riftia2	W2-4877b	whole trophosome	NA	NA	7	-70
Riftia3	W1-4878	whole trophosome	NA	NA	NR	-70
Riftia3	R2-4878-BLOOD	blood, Riftia	NA	NA	20	-70
Riftia3	P1-4878a-P	purified endosymbionts	proteomics	TE-buffer-washed	1.25	-70
Riftia3	P1-4878b-P	purified endosymbionts	proteomics	TE-buffer-washed	1.8	-70
Riftia3	P1-4878-C0-campy-CG	enrichment biomass	enrichment	glycerol-12%	0.1	-70
Riftia3	P1-4878-C0-campy-D	enrichment biomass	DNA_extraction	none	NR	-70
Riftia3	P1-4878-C0-anaerobic CG	enrichment biomass	enrichment	glycerol-12%	0.1	-70
Riftia3	P1-4878-C0-anaerobic-D	enrichment biomass	DNA_extraction	none	NR	-80
Riftia3	P1-4878-C1b-D	enrichment biomass	DNA_extraction	none	1.5	-70
Riftia4	E1-4880	rusty chitin tube, Riftia	NA	NA	NA	-70
Riftia4	E1-4880	rusty chitin tube scraping, Riftia	DNA_extraction	none	0.5	-70
Riftia4	E1-4880-C0a-D	enrichment biomass	DNA_extraction	none	1.5	-70
Riftia5	P2-4880a-P	purified endosymbionts	proteomics	TE-buffer-washed	0.75	-70
Riftia5	P2-4880b-P	purified endosymbionts	proteomics	TE-buffer-washed	0.75	-70
Riftia5	W2-4880	whole trophosome	NA	NA	4.5	-70
Riftia5	P2-4880-C0d-extra fridge aliquot	enrichment biomass	NA	none	NR	4
Riftia5	P2-4880-C0a-FeS-D	enrichment biomass	DNA_extraction	none	1.5	-70
Riftia5	P2-4880-C1a-D	enrichment biomass	DNA_extraction	none	1.5	-70
Riftia5	P2-4880-C1f-D	enrichment biomass	DNA_extraction	none	1.5	-70
Riftia5	P2-4880-C1a-FeS-D	enrichment biomass	DNA_extraction	none	1.5	-70
Riftia5	P2-4880-C2f-D	enrichment biomass	DNA_extraction	none	1.5	-70
Riftia5	P2-4880-C0-CGa	enrichment biomass	enrichment	glycerol-12%	0.3	-70
Riftia5	P2-4880-C0-CGb	enrichment biomass	enrichment	glycerol-12%	0.3	-70

Table B2 (cont.): Subsample Log of all subsamples preserved for future analyses with selected metadata displayed.

Sample name	Subsample name	Subsample type	Intended use	Amendment/treatment for preservation	approx. volume (mL)	Storage temp. (°C)
Riftia5	P2-4880-C0-Da	enrichment biomass	DNA_extraction	none	0.3	-80
Riftia5	P2-4880-C0-Db	enrichment biomass	DNA_extraction	none	0.3	-70
Riftia5	P2-4880-C0f-Dc	enrichment biomass	DNA_extraction	none	0.1	-70
Riftia5	E2-4880	rusty chitin tube scrapinng, Riftia	DNA_extraction	none	0.1	-70
Riftia5	E2-4880-C0a-D	enrichment biomass	DNA_extraction	none	1.5	-70
Riftia6	E1-4883	rusty chitin tube, Riftia	NA	NA	NA	-70
Riftia6	E1-4883a	rusty chitin tube scrapinng, Riftia	DNA_extraction	none	1	-70
Riftia6	E1-4883b	rusty chitin tube scrapinng, Riftia	DNA_extraction	none	0.5	-80
Riftia6	E1-4883-C0a-D	enrichment biomass	DNA_extraction	none	1.5	-70
Riftia7	W1-4884	whole trophosome	NA	NA	NR	-70
Riftia8	W1-4889	whole trophosome	NA	NA	NR	-70
Riftia8	R1-4889-BLOOD	blood, Riftia	NA	NA	7	-70
Riftia8	R1-4889-Vestimentum	vestimentum, Riftia	DNA_extraction	none	NA	-70
Riftia8	P1-4889-Da	purified endosymbionts	DNA_extraction	none	0.5	-80
Riftia8	P1-4889-Db	purified endosymbionts	DNA_extraction	none	0.5	-70
Riftia8	P1-4889-C0a-Ra	enrichment biomass	transcriptomics	RNA preservation medium(1:1)	0.6	-70
Riftia8	P1-4889-C0b-Rb	enrichment biomass	transcriptomics	RNA preservation medium(1:1)	0.2	-70
Riftia8	P1-4889-C0- no Fe(0)-D	enrichment biomass	DNA_extraction	none	1.5	-70
Riftia8	P1-4889 TRIAL_a	Fe oxidation kinetics experiment	transcriptomics	RNA preservation medium(1:1)	30	-70
Riftia8	P1-4889 TRIAL_b	Fe oxidation kinetics experiment	transcriptomics	RNA preservation medium(1:1)	30	-70
Riftia8	P1-4889 TRIAL_c	Fe oxidation kinetics experiment	transcriptomics	RNA preservation medium(1:1)	30	-70
Riftia8	P1-4889 Set 1A_a	Fe oxidation kinetics experiment	transcriptomics	RNA preservation medium(1:1)	30	-70
Riftia8	P1-4889 Set 1A_b	Fe oxidation kinetics experiment	transcriptomics	RNA preservation medium(1:1)	30	-70
Riftia8	P1-4889 Set 1A_c	Fe oxidation kinetics experiment	transcriptomics	RNA preservation medium(1:1)	8	-70

Table B2 (cont.): Subsample Log of all subsamples preserved for future analyses with selected metadata displayed.

Sample name	Subsample name	Subsample type	Intended use	Amendment/treatment for preservation	approx. volume (mL)	Storage temp. (°C)
Riftia8	P1-4889 Set 1A_d	Fe oxidation kinetics experiment	transcriptomics	RNA preservation medium(1:1)	8	-70
Riftia8	P1-4889 Set 1A_e	Fe oxidation kinetics experiment	transcriptomics	RNA preservation medium(1:1)	8	-70
Riftia8	P1-4889 Set 1B_a	Fe oxidation kinetics experiment	transcriptomics	RNA preservation medium(1:1)	30	-70
Riftia8	P1-4889 Set 1B_b	Fe oxidation kinetics experiment	transcriptomics	RNA preservation medium(1:1)	30	-70
Riftia8	P1-4889 Set 1B_c	Fe oxidation kinetics experiment	transcriptomics	RNA preservation medium(1:1)	8	-70
Riftia8	P1-4889 Set 1B_d	Fe oxidation kinetics experiment	transcriptomics	RNA preservation medium(1:1)	8	-70
Riftia8	P1-4889 Set 1B_e	Fe oxidation kinetics experiment	transcriptomics	RNA preservation medium(1:1)	8	-70
Riftia8	P1-4889 Set 2A_a	Fe oxidation kinetics experiment	transcriptomics	RNA preservation medium(1:1)	30	-70
Riftia8	P1-4889 Set 2A_b	Fe oxidation kinetics experiment	transcriptomics	RNA preservation medium(1:1)	30	-70
Riftia8	P1-4889 Set 2A_c	Fe oxidation kinetics experiment	transcriptomics	RNA preservation medium(1:1)	8	-70
Riftia8	P1-4889 Set 2B_a	Fe oxidation kinetics experiment	transcriptomics	RNA preservation medium(1:1)	30	-70
Riftia8	P1-4889 Set 2B_b	Fe oxidation kinetics experiment	transcriptomics	RNA preservation medium(1:1)	30	-70
Riftia8	P1-4889 Set 2B_c	Fe oxidation kinetics experiment	transcriptomics	RNA preservation medium(1:1)	8	-70
Rock1	B1-4880a	rusty mat scraping from rock	DNA_extraction	none	1	-70
Rock1	B1-4880b	rusty mat scraping from rock	DNA_extraction	none	1	-70
Rock1	B1-4880-C0a-D	enrichment biomass	DNA_extraction	none	1.5	-70
Rock2	B1-4881a	rusty mat scraping from rock	DNA_extraction	none	1	-80
Rock2	B1-4881-refrigerator	rusty mat scraping from rock	NA	none	NR	4
Rock2	B1-4881-C0a-D	enrichment biomass	DNA_extraction	none	1.5	-70
Rock2	B1-4881b	rusty mat scraping from rock	DNA_extraction	none	0.5	-70
Rock3	B1-4883a	rusty mat scraping from rock	DNA_extraction	none	1	-80
Rock3	B1-4883b	rusty mat scraping from rock	DNA_extraction	none	1	-70

Table B2 (cont.): Subsample Log of all subsamples preserved for future analyses with selected metadata displayed.

Sample name	Subsample name	Subsample type	Intended use	Amendment/treatment for preservation	approx. volume (mL)	Storage temp. (°C)
Rock3	B1-4883b-refrigerator	rusty mat scraping from rock	NA	none	NR	4
Rock3	B1-4883-C0a-D	enrichment biomass	DNA_extraction	none	1.5	-70
Rock4	B1-4884	rusty mat scraping from rock	DNA_extraction	none	1	-70
Rock5	B2-4884	rusty mat scraping from rock	DNA_extraction	none	1	-70
Seawater1	S1-4880	filter with DNA	DNA_extraction	none	NA	-70
Seawater2	S1-4887-D	filter with DNA	DNA_extraction	none	NA	-70
Seawater3	S2-4888-D	filter with DNA	DNA_extraction	none	NA	-70

NA - not applicable

NR - not recorded

Table B3: Enrichment Log of all enrichments performed aboard the cruise with selected metadata displayed.

Sample name	Inoculum		Details of seawater medium used										Potential signs of growth?	Subsample of culture preserved?
	Enrichment culture name	Type	volume (uL)	Culture type	Fe source	CTD sample	2 mM NaHCO3?	10 mM MES?	Vitamins and minerals (1 uL/mL each)?	pH	Control type	Gaspak type for incubation		
Riftia3	P1-4878-C0a-anaerobic	Purified endosymbionts	15	Liquid plate	ZVI	CTD1	yes	yes	no	6	NA	anaerobic with needle prick	floc	yes
Riftia3	P1-4878-C0b-anaerobic	Purified endosymbionts	10	Liquid plate	ZVI	CTD1	yes	yes	no	6	NA	anaerobic with needle prick	floc	yes
Riftia3	P1-4878-C0a-campy	Purified endosymbionts	15	Liquid plate	ZVI	CTD1	yes	yes	no	6	NA	campy	floc	yes
Riftia3	P1-4878-C0b-campy	Purified endosymbionts	10	Liquid plate	ZVI	CTD1	yes	yes	no	6	NA	campy	floc	yes
Riftia3	P1-4878-C0a-anaerobic-formaldehyde killed	Purified endosymbionts	15	Liquid plate	ZVI	CTD1	yes	yes	no	6	formaldehyde 1.4%	anaerobic with needle prick	floc	no
Riftia3	P1-4878-C0a-campy formaldehyde killed	Purified endosymbionts	15	Liquid plate	ZVI	CTD1	yes	yes	no	6	formaldehyde 1.4%	campy	floc	no
Riftia3	P1-4878-C1a	Transfer of purified endosymbiont flocc	50	Liquid plate	ZVI	CTD1	yes	yes	no	6	NA	anaerobic with needle prick	NA	no

Table B3 (cont.): Enrichment Log of all enrichments performed aboard the cruise with selected metadata displayed.

Sample name	Inoculum			Details of seawater medium used										
	Enrichment culture name	Type	volume (uL)	Culture type	Fe source	CTD sample	2 mM NaHCO3?	10 mM MES?	Vitamins and minerals (1 uL/mL each)?	pH	Control type	Gaspak type for incubation	Potential signs of growth?	Subsample of culture preserved?
Riftia3	P1-4878-C1b	Transfer of purified endosymbiont flocc	50	Liquid plate	ZVI	CTD1	yes	yes	no	6	NA	anaerobic with needle prick	NA	yes
Riftia3	P1-4878-C1-formaldehyde killed	Transfer of purified endosymbiont flocc	50	Liquid plate	ZVI	CTD1	yes	yes	no	6	formaldehyde 4%	anaerobic with needle prick	NA	no
Riftia4	E1-4880-C0a	Rusty Riftia tube scrapings	60	Liquid plate	ZVI	CTD1	yes	yes	no	6	NA	campy	NA	yes
Riftia5	P2-4880-C0a	Purified endosymbionts	25	Liquid plate	ZVI	CTD1	yes	yes	no	6	NA	anaerobic with needle prick	floc	yes
Riftia5	P2-4880-C0b	Purified endosymbionts	25	Liquid plate	ZVI	CTD1	yes	yes	no	6	NA	anaerobic with needle prick	floc	yes
Riftia5	P2-4880-C0-formaldehyde killed	Purified endosymbionts	25	Liquid plate	ZVI	CTD1	yes	yes	no	6	formaldehyde 4%	anaerobic with needle prick	floc	no
Riftia5	P2-4880-C0c	Purified endosymbionts	40	Liquid plate	ZVI	CTD1	yes	yes	no	6	NA	anaerobic with needle prick	floc	yes

Table B3 (cont.): Enrichment Log of all enrichments performed aboard the cruise with selected metadata displayed.

Sample name	Inoculum		Details of seawater medium used										Subsample of culture preserved?	
	Enrichment culture name	Type	volume (uL)	Culture type	Fe source	CTD sample	2 mM NaHCO ₃ ?	10 mM MES?	Vitamins and minerals (1 uL/mL each)?	pH	Control type	Gaspak type for incubation		Potential signs of growth?
Riftia5	P2-4880-C0d	Purified endosymbionts	40	Liquid plate	ZVI	CTD1	yes	yes	no	6	NA	anaerobic with needle prick	floc	yes
Riftia5	P2-4880-C0e	Purified endosymbionts	40	Liquid plate	ZVI	CTD1	yes	yes	no	6	NA	anaerobic with needle prick	floc	yes
Riftia5	P2-4880-C0f	Purified endosymbionts	40	Liquid plate	ZVI	CTD1	yes	yes	no	7	NA	anaerobic with needle prick	floc	yes
Riftia5	P2-4880-C0-no Fe(0)-2	Purified endosymbionts	40	Liquid plate	NA	CTD1	yes	yes	no	6	no ZVI	anaerobic with needle prick	floc	no
Riftia5	P2-4880-C0-no Fe(0)-2	Purified endosymbionts	40	Liquid plate	NA	CTD1	yes	yes	no	7	no ZVI	anaerobic with needle prick	floc	no
Riftia5	P2-4880-C0a-FeS	Purified endosymbionts	3	Liquid gradient tube	FeS	CTD1	yes	yes	no	7	NA	NA	NA	yes
Riftia5	P2-4880-C1a	Transfer of purified endosymbiont flocc	40	Liquid plate	ZVI	CTD1	yes	yes	no	7	NA	anaerobic with needle prick	NA	yes

Table B3 (cont.): Enrichment Log of all enrichments performed aboard the cruise with selected metadata displayed.

Sample name	Enrichment culture name	Inoculum		Details of seawater medium used										Subsample of culture preserved?
		Type	volume (uL)	Culture type	Fe source	CTD sample	2 mM NaHCO3?	10 mM MES?	Vitamins and minerals (1 uL/mL each)?	pH	Control type	Gaspak type for incubation	Potential signs of growth?	
Riftia5	P2-4880-C1f	Transfer of purified endosymbiont flocc	50	Liquid plate	ZVI	CTD1	yes	yes	yes	7	NA	anaerobic	NA	yes
Riftia5	P2-4880-C1a-FeS	Transfer of purified endosymbiont flocc	3	Liquid gradient tube	FeS	CTD1	yes	yes	no	7	NA	NA	NA	yes
Riftia5	P2-4880-C1b-FeS	Transfer of purified endosymbiont flocc	8	Liquid gradient tube	FeS	CTD1	yes	yes	no	7	NA	NA	NA	no
Riftia5	P2-4880-C2f	Transfer of purified endosymbiont flocc	20	Liquid plate	ZVI	CTD3	yes	yes	yes	7	NA	anaerobic with needle prick	NA	yes
Riftia5	E2-4880-C0a	Rusty Riftia tube scrapings	60	Liquid plate	ZVI	CTD1	yes	yes	no	6	NA	campy	NA	yes
Rock1	B1-4880-C0a	Rock mat/crust	40	Liquid plate	ZVI	CTD1	yes	yes	no	6	NA	campy	NA	yes
Rock2	B1-4881-C0a	Rock mat/crust	40	Liquid plate	ZVI	CTD1	yes	yes	no	6	NA	anaerobic with needle prick	NA	no

Table B3 (cont.): Enrichment Log of all enrichments performed aboard the cruise with selected metadata displayed.

Inoculum		Details of seawater medium used												
Sample name	Enrichment culture name	Type	volume (uL)	Culture type	Fe source	CTD sample	2 mM NaHCO3?	10 mM MES?	Vitamins and minerals (1 uL/mL each)?	pH	Control type	Gaspak type for incubation	Potential signs of growth?	Subsample of culture preserved?
Rock2	B1-4881-C0b	Rock mat/crust	40	Liquid plate	ZVI	CTD1	yes	yes	no	6	NA	anaerobic with needle prick	NA	yes
Rock2	B1-4881-C0c	Rock mat/crust	50	Liquid plate	ZVI	CTD1	yes	yes	no	7	NA	anaerobic	NA	no
Rock2	B1-4881-C0a-FeS	Rock mat/crust	2	Liquid gradient tube	FeS	CTD1	yes	yes	no	7	NA	NA	NA	no
Rock3	B1-4883-C0a	Rock mat/crust	50	Liquid plate	ZVI	CTD1	yes	yes	no	7	NA	anaerobic	NA	yes
Riftia6	E1-4883-C0a	Rusty Riftia tube scrapings	40	Liquid plate	ZVI	CTD1	yes	yes	no	7	NA	anaerobic	NA	yes
Flocculent_mat_slurp1	S1-4883-C0a	Slurp flocculent mat	10	Liquid plate	ZVI	CTD1	yes	yes	yes	7	NA	anaerobic	NA	yes
Flocculent_mat_slurp1	S1-4883-C0a-FeS	Slurp flocculent mat	4	Liquid gradient tube	FeS	CTD1	yes	yes	no	7	NA	NA	NA	yes
Flocculent_mat_slurp2	S1-4888-C0a	Slurp flocculent mat	250	Liquid plate	ZVI	CTD3	yes	yes	yes	6	NA	anaerobic with needle prick	NA	yes
Flocculent_mat_slurp2	S1-4888-C0b	Slurp flocculent mat	250	Liquid plate	ZVI	CTD3	yes	yes	yes	6	NA	anaerobic with needle prick	NA	no

Table B3 (cont.): Enrichment Log of all enrichments performed aboard the cruise with selected metadata displayed.

Sample name	Enrichment culture name	Type	volume (uL)	Culture type	Fe source	CTD sample	2 mM NaHCO3?	10 mM MES?	Details of seawater medium used			Gaspak type for incubation	Potential signs of growth?	Subsample of culture preserved?
									CTD3	yes	yes			
Flocculent_m at_slurp2	S1-4888-C0c	Slurp flocculent mat	250	Liquid plate	ZVI	CTD3	yes	yes	yes	6	NA	anaerobic with needle prick	NA	no
Riftia8	P1-4889-C0a	Purified endosymbionts	60	Liquid plate	ZVI	CTD3	yes	yes	yes	7	NA	anaerobic with needle prick	floc	yes
Riftia8	P1-4889-C0b	Purified endosymbionts	60	Liquid plate	ZVI	CTD7	yes	yes	yes	7	NA	anaerobic with needle prick	floc	yes
Riftia8	P1-4889-C0c	Purified endosymbionts	60	Liquid plate	ZVI	CTD3	yes	yes	yes	7	NA	anaerobic with needle prick	floc	yes
Riftia8	P1-4889-C0-no Fe(0)	Purified endosymbionts	60	Liquid plate	NA	CTD3	yes	yes	yes	7	no ZVI	anaerobic with needle prick	floc	yes
Riftia8	P1-4889-C0-formaldehyde killed	Purified endosymbionts	60	Liquid plate	ZVI	CTD3	yes	yes	yes	7	formaldehyde 4%	anaerobic with needle prick	floc	no
Riftia8	P1-4889-C0-sodium azide	Purified endosymbionts	60	Liquid plate	ZVI	CTD3	yes	yes	yes	7	sodium azide 3 mM	anaerobic with needle prick	floc	no

Table B3 (cont.): Enrichment Log of all enrichments performed aboard the cruise with selected metadata displayed.

Inoculum		Details of seawater medium used												
Sample name	Enrichment culture name	Type	volume (uL)	Culture type	Fe source	CTD sample	2 mM NaHCO3?	10 mM MES?	Vitamins and minerals (uL/mL each)?	pH	Control type	Gaspak type for incubation	Potential signs of growth?	Subsample of culture preserved?
Flocculent_m at_slurp3	S1-4889-C0a	Slurp flocculent mat	250	Liquid plate	ZVI	CTD3	yes	yes	yes	7	NA	campy	NA	yes
Flocculent_m at_slurp3	S1-4889-C0b	Slurp flocculent mat	250	Liquid plate	ZVI	CTD3	yes	yes	yes	7	NA	campy	NA	no
Flocculent_m at_slurp3	S1-4889-C0c	Slurp flocculent mat	250	Liquid plate	ZVI	CTD3	yes	yes	yes	7	NA	campy	NA	no
Flocculent_m at_slurp4	S1-4890-C0a-FeS	Slurp flocculent mat	8	Liquid gradient tube	FeS	CTD5	yes	yes	yes	7	NA	NA	NA	no
Flocculent_m at_slurp4	S1-4890-C0b-FeS	Slurp flocculent mat	8	Liquid gradient tube	FeS	CTD5	yes	yes	yes	7	NA	NA	NA	yes
Flocculent_m at_slurp4	S1-4890-C0c-FeS	Slurp flocculent mat	80	Liquid gradient tube	FeS	CTD5	yes	yes	yes	7	NA	NA	hazy white material	yes
Flocculent_m at_slurp4	S1-4890-C0d-FeS	Slurp flocculent mat	80	Liquid gradient tube	FeS	CTD5	yes	yes	yes	7	NA	NA	hazy white material	yes
Flocculent_m at_slurp5	S1-4891-C0a	Slurp flocculent mat	25	Liquid plate	ZVI	CTD3	yes	no	yes	8	NA	campy	NA	yes
Flocculent_m at_slurp5	S1-4891-C0b	Slurp flocculent mat	25	Liquid plate	ZVI	CTD3	yes	no	yes	8	NA	campy	NA	no